PEOPLE'S DEMOCTRATIC REPUBLIC OF ALGERIA

الجمهورية الجزائرية الديمقراطية

MINISTRY OF HIGHER EDUCATION AND SCIENTIFIC RESEARCH

وزارة التعليم العالي والبحث العلمي

UNIVERSITY OF AMAR TELIDJI LAGHOUAT

جامعة عمار ثليجي بالأغواط

FACULTY OF SCIENCES

كلية العلوم

DEPARTEMENT OF BIOLOGIY

قسم البيولوجيا

In partial fulfillment of the requirements for the

Degree of MASTER

Field: Biological Sciences

Option: Applied Biochemistry

TITLE

In silico study of anti-cancer activity (neuroblastoma) of some metabolites of marine sponges

Presented by:

BENSENOUCI Sabrina & BEN LAHBIB Hafsa

By the committee consisting of:

President	**Dr. BOUKAROUIS Djoudi**
Reviewer	**Dr. BOU-SALAH Leila**
Supervisor	**Pr. BENAROUS Khedidja**
Co-supervisor	**Dr. LINANI Abderahmane**

2022/2023

AKNOWLEDGMENTS

First of all, we would like to thank our supervisor, ***Pr. Khedidja BENAROUS*** *for giving us the opportunity to work on our master's thesis under her guidance, and to become a part in the investigation about Neuroblastoma that truly motivates us to know more about, by introducing us to the world of bioinformatics. She provided us with a lot of advice, encouragement, feedback and suggestions throughout our studies, all of which were very helpful to our research. We have developed the knowledge and abilities necessary to conduct the scientific research under her supervision. God bless her.*

To our co-supervisor, ***Dr. Abderahmane LINANI****, who has our sincere gratitude and admiration for his openness to devote his time and expertise to us as well as for his precise advice, encouraging direction, and creative suggestions. Deep thanks to you for being the sympatic teacher that we could ask for over these three years of study and for helping us to accomplish this thesis.*

Our appreciation also extends to ***Pr. Rachid CHAIBI****, the head of the biology department, and his team, who were situated next to us throughout the academic year.*

To the jury members, ***Dr. BOUKAROUIS*** *and* ***Dr. BOU-SALAH,*** *thank you for your time, attention and careful consideration for this thesis, we are honored to have presented this work in front of you, with all our respect, we dedicate this work to you.*

Finally, we want to say that we are really proud of ourselves, the hard work we've put in over the past eight months, as well as all of our passion and patience.

DEDICATION

With Almighty God's blessing, this work is dedicated:

*To the spirit of my grandfathers **SACI YAHIA** and **BENSENOUCI AEK**, who taught me the value of hard work and kindness, your legacy lives on in me, I am sure that you are going to be proud of me for this achievement. May you rest in peace.*

*To my dear father **Mr. RACHID** for having supported me morally and materially to this day, for his love and encouragement. Your guidance and wisdom have been invaluable in shaping me into the person I am today. May this work be for you with love and gratitude and may ALLAH the Almighty preserve you, grant you health, happiness and protect you from all evil.*

*To my dearest mother **Mrs. SOUAD**, as many sentences as expressive as they are, they cannot show the degree of love and affection I feel for you, your unwavering belief in me and your tireless efforts to support my dreams have been a constant source of inspiration, you have always encouraged me throughout the years of my studies. May ALLAH protect you and give you health, happiness and long life.*

*To my dear sisters **SARA** and **IMANE,** thank you for being my cheerleaders, you have been driving force behind my success, thank you for your little word and support since the first day. To my dearest aunt Doctor **SACI SAMIA**, my second mother who helped me with everything in this domain, I thank you very much, God bless you to me.*

*to my dear bestfriend **SEDIK**, for his presence and patience full of support all throughout five years of university studies, many thanks to you.*

*Especially to my partner **HAFSA** a bigger sister, my bestfriend who has been by my side all through these years and has shared with me many things in this journey, thank you for your hard work and for sharing with me this beautiful achievement. God bless you.*

To you dear readers.

BENSENOUCI SABRINA.

DEDICATION

*My dear father **Toufik BEN LAHBIB**, who has guarded me throughout my life. I want to thank you for your love, support, and care during my life and academic career. I pray that I made you proud of me, and I wish you health and happiness in life. God bless you.*

*My beloved mother **Khadidja HADJARI**. My guardian angel and strong supporter in life. Since you were my first teacher in life before the academic one, I sincerely appreciate everything you have done for me and continue to do. There are not enough words to express my love and gratitude for you. I hope to be able to repay some of your favors, but since I'll never be able to do that, all I can say is "thank you," and I hope it expresses how I feel. I send you my best wishes for health and happiness. God bless you.*

*To my darling sister **SABRINE**, who has been my friend and has experienced both my joyful and sad moments with me. I appreciate all of your help and support throughout my life and profession.*

*To my younger brother **MOUHAMED**. My little star, who stands by my side and encourages me morally, by pushing me further to make him proud.*

*To my grandparents, and the spirit of my grandfather **MAHMOUD HADJARI**, who were my biggest inspiration in life, I thank you for everything and your presence in my life was the best thing I could ever ask for.*

To all my family members aunts, uncles and cousins who were there for me and very excited to see me graduated.

*Thank you to my loyal sisters and friends **SOUHILA** and **HAFSA** for sharing five years with me that were full of love, care, joy, and support, as well as for all the memories you gave me. God bless you, and best wishes for a successful profession and life.*

*To my beautiful, sweet sister and bestfriend **SABRINA**, who has been my greatest supporter. I appreciate all of the memories you gave me, and I will hold them close to my heart and mind forever. You were there for me and traveled with me during this wonderful trip, and you cared the same time, thoughts and memories. I wish you the best of luck in your work and will always be there for you if you need me.*

BEN LAHBIB HAFSA.

Abstract

Neuroblastoma (NB) is the most frequent malignant solid tumor in children derived from primordial neural crest cells and accounts for 15% of childhood cancer mortality. Several clinical trials are still underway to identify specific drugs for the treatment of this exceptional cancer. *Agelas sp.* has proven to serve as a biochemical storage for secondary metabolites such as alkaloids including pyrrole-imidazole alkaloids (PIAs) which constitute a highly diverse and densely functionalized subclass of marine natural products with an intense biologic activity. The present study aimed to examinate *in silico* the ability of five *Agelas sp.* alkaloids, such as Ageladine A (Mol1), Oroidin (Mol2), Strepoxazine A (Mol3), Cyclooroidin (Mol4), and Taurodispacamide A (Mol5) in order to inhibit six neuroblastoma targets including; the focal adhesion kinase 1 (FAK), the caspase-3, the phosphatidylinositol 4,5-bisphosphate 3-kinase catalytic subunit gamma isoform (PI3K), the telomerase reverse transcriptase (TERT), the osm-9-like TRP channel 1 (TRPV1), and the RAC-alpha serine/threonine-protein kinase (AKT1). Molecular docking (Md) analysis was performed using AutoDock Vina (ADV) and Auto Dock Tools (ADT), Md results were further analyzed with Discovery Studio Visualizer (DSV) v2017, and then a pharmacokinetic (pK) study was performed to verify the inhibitors safety, using SwissADME and pre-ADMET servers. The results show that all compounds displayed significant inhibition towards neuroblastoma targets compared with their controls. Mol3 was ranked as the best inhibitor among the five inhibitors based on its binding energy of -9.5 kcal/mol, in addition to having an appropriate pK profile; its toxicity was adequate and ranked it first in this context. The other compounds were moderate; their binding energy ranged from -6.9 kcal to -8.8 kcal/mol with a moderate pK profile, indicating their strict use as their toxicity was significant. These results are promising, although the efficacy of these inhibitors needs to be confirmed *in vitro* and *in vivo*.

Keywords: Neuroblastoma, *Agelas sp.*, pyrrole-imidazole alkaloids, Md, ADMET, Strepoxazine A.

ملخص

إن الورم الأرومي العصبي هو الورم الصلب الخبيث الأكثر شيوعا لدى الأطفال المشتق من الخلايا العصبية البدائية ويمثل15% من وفيات سرطان الأطفال.

لا تزال هناك العديد من التجارب السريرية الحالية لتحديد أدوية محددة لعلاج هذا السرطان الاستثنائي. أثبت حيوان الاسفنج البحري وبالتحديد نوع الاسفنج الطبيعي انه بمثابة مخزن كيميائي حيوي لمختلف المركبات الكيميائية مثلا القلويدات بما في ذلك قلويدات البيرول إيميدازول التي تشكل مجموعة فريدة بسبب كثرة تنوع هذه الجزيئات بالإضافة إلى نشاطها البيولوجي المتنوع وكثافة الوظائف من المنتجات الطبيعية البحرية. تهدف هذه الدراسة إلى فحص قدرة خمس قلويدات معرفة في نوع الاسفنج الطبيعي مثل: أجيلادين أ (جزيئة1) وأوروادين (جزيئة2) وستريبوكسازين أ (جزيئة3) وسيكلوأوروادين (جزيئة4) وتوروديسباكاميد أ (جزيئة5) من أجل تثبيط ست بروتينات منها إنزيمات ومستقبلات غشائية من الورم الأرومي العصبي مثل بروتين كيناز الالتصاق البؤري، إنزيم البروتياز الموجه بالأسبارتات المعتمد على السيستين، إنزيم فوسفينوسيتايد 3-كينازات، إنزيم النسخ العكسي للتيلوميراز، المستقبل للآلية الخاصة بالشم رقم 9 وأخيرا الإنزيم المرتبط بالسيرين/الثريونين من نوع بروتين كيناز. قمنا بدراسة الإرساء الجزيئي باستخدام برنامج أوتدوك فينا، ثم حللنا النتائج المتحصل عليها باستخدام ديسكفري ستوديو فيزوا ليزر نسخة2017، قمنا بإجراء دراسة الحركية الدوائية للتحقق من سلامة المثبطات باستعمال الموقع سويس أدمي وبري أدميت. أظهرت النتائج أن جميع المركبات ثبطت بنسبة كبيرة البروتينات المدروسة وذلك مقارنة بالأدوية المستخدمة. لقد وجدنا أن الجزيئة 3 هي أفضل مثبط بين كل المثبطات المدروسة اعتمادا على طاقة الارتباط البالغة بـ 9.5- سعرة حرارية/مول، وكانت سميته قليلة وصنف على هذا الأساس في المرتبة الأولى. أما المركبات الأخرى فقد وجدنا انها كانت معتدلة حيث تراوحت طاقتها من 6.9- سعرة حرارية/مول إلى 8.8- سعرة حرارية/مول مع خاصية حركية دوائية معتدلة، كما لا يمكن استخدامها بسبب أن سميتها كبيرة. لقد وجدنا من هذه الدراسة أن هذه النتائج هي واعدة وتحتاج الى دراسة مخبرية ودراسة في الحيوان حتى نتأكد من فعالية هذه المثبطات.

كلمات مفتاحية: ورم أرومي عصبي، اسفنج طبيعي، قلويدات، إرساء جزيئي، حركية دوائية، ستريبوكسازين أ.

Résumé

Le neuroblastome (NB) est la tumeur solide maligne la plus fréquente chez les enfants qui provient de cellules primitives de la crête neurale et représente 15 % de la mortalité par cancer pédiatrique. Plusieurs essais cliniques sont encore en cours pour identifier des médicaments spécifiques pour le traitement de ce cancer exceptionnel. *Agelas sp.* a prouvé qu'il sert comme réservoir naturel des métabolites secondaires comme les alcaloïdes, y compris les alcaloïdes pyrrole-imidazole (API), qui constituent une sous-classe de produits naturels marins ayant une activité biologique intense. La présente étude visait à examiner *in silico* la capacité de cinq alcaloïdes d'*Agelas sp.* comme l'Ageladine A (Mol1), Oroidin (Mol2), la Strepoxazine A (Mol3), la Cyclooroidine (Mol4) et la Taurodispacamide A (Mol5) afin d'inhiber six cibles de neuroblastome, y compris l'adhésion focale kinase 1 (FAK), la caspase-3, le phosphatidylinositol 4,5-bisphosphate 3-kinase (sous-unité catalytique isoforme) gamma (PI3K), la transcriptase inverse de télomérase (TERT), le canal 1 de TRP de type osm-9 (TRPV1) et la kinase de RAC-alpha sérine/thréonine-protéine (AKT1). L'analyse de l'amarrage moléculaire (AM) a été effectuée à l'aide d'AutoDock Vina (ADV), les résultats de AM ont été analysés avec Discovery Studio Visualizer (DSV) v2017, puis une étude pharmacocinétique (PC) a été réalisée pour vérifier la sécurité des inhibiteurs, en utilisant SwissADME et pre-Serveurs ADMET. Les résultats montrent que tous les composés ont montré une inhibition significative vers les cibles de neuroblastome par rapport à leurs témoins. Mol3 a été classé comme le meilleur inhibiteur parmi les cinq inhibiteurs en raison de son énergie de liaison de -9.5 kcal/mol, en plus d'avoir un profil PC approprié ; sa toxicité était adéquate et le classait au premier rang dans ce contexte. Les autres composés étaient modérés ; leur énergie de liaison allait de -6.9 kcal à -8.8 Kcal/mol avec un profil PC modéré, indiquant leur utilisation stricte car leur toxicité était significative. Ces résultats sont prometteurs, bien que l'efficacité de ces inhibiteurs doit être confirmée *in vitro* et *in vivo.*

Mots clés : Neuroblastome, *Agelas sp.*, alcaloïdes pyrrole-imidazole, AM, ADMET, Strepoxazine A.

List of Abbreviations

A	L
ACCO: **American childhood cancer organization** ADP: **Adenosine di-phosphate** ADT: **AutoDock Tools** ADMET: **Absorption, Distribution, Metabolism and Toxicity** ADV: **AutoDock Vina** ALK: **Anaplastic lymphoma kinase** ASCT: **Autologous Stem Cell Transplantation** ATP: **Adenosine tri-phosphate**	**L-MYC:** Lung myelocytomatosis viral oncogene homolog
B	**M**
BBB : **Blood–brain barrier**	**Md:** Molecular Docking **MRI:** Magnetic resonance imaging **MYCN:** v-myc myelocytomatosis viral related oncogene, neuroblastoma derived (avian) **mAb :** monoclonal antibody
C	**N**
C-MYC: **Cellular myelocytomatosis oncogene** CNS: **Central nervous system** CT: **Computed tomography** CYPs: **Cytochromes P**	**NB:** Neuroblastoma **NC:** Neural crest **NCBI:** National Center for Biotechnology Information **NCCs:** Neural crest cells **NGF:** Nerve Growth Factor **NIH:** National Institutes of Health **NLM:** National Library of Medicine **N-Type :** Neuroblastic type
D	**O**
ΔG Affinity : **Binding energy affinity** DNA: **Deoxyribonucleic Acid** DSV : **Discovery studio visualizer**	**Osm-9:** osmotic avoidance abnormal family member9
E	**P**
EMTs: **Epithelial-mesenchymal transitions** E SOL: **Estimated SOLubility**	**PDB:** Protein Data Bank **PDBj:** Protein Data Bank Japan **PDBe:** Protein Data Bank Europe **PDBQT:** Protein Data Bank, Partial Charge (**Q**), Atom Type (**T**) **P-gp :** P-glycoprotein **PIAs :** Pyrrole-imidazole alkaloids **PK :** Protein Kinase**,** **PKB :** Protein Kinase B
F	**R**
FAK: **Focal Adhesion Kinase** FDG-PET: **Fluorodeoxyglucose-Positron emission tomography**	**RNA:** Ribonucleic acid **RR:** Repetition rate **RO5:** Rule of 5
G	**S**
G2D : **Anti-disialoganglioside**	**SAR:** Structure-activity relation **SBT345:** *Streptomyces sp.* SBT345 **SDF:** Structure-data file **SH-SY5Y:** human neuroblastoma cell line **S-Type:** Substrate adherent type **SPECT: Single** Photon Emission Computed Tomography
H	**T**
HDC: **High dose chemotherapy** HERG: **Human ether related gene** HIA : **Human intestinal absorption**	**TERT :** Telomerase reverse transcriptase **TRPV :** The Transient receptor potential vanilloid **TPSA** : Topological Polar Surface Area
I	**V**
IC: **Induction chemotherapy** INSS: **The International Neuroblastoma Staging System** INPN : **Inventaire national du patrimoine naturel** I-Type : **Intermediate type**	**VMA :** Vanillylmandelic acid
K	
KD: **KiloDalton** Ki: **Inhibition constant** Kp: **Skin permeability constant**	

List of figures

List of tables

Table of content

Table of content

Appendices

Introduction

Cancer is one of the main causes of mortality, with an estimated 18.1 million new cases worldwide **[1]**. Furthermore, the malignant tumors are one of the leading causes of death in the world. It has grown into a dangerous illness that seriously jeopardizes human health and life, as well as limiting social and economic advancement **[2]**.

Neuroblastoma (NB) is the most common extracranial tumor among children with an average age of 17 months. It is a tumor of the autonomic nervous system originating from embryonic neural crest cells in which the pathogenesis of this malignancy is characterized by a block of differentiation **[3]**. NB accounts for close to 10% of all cancer cases in children but disproportionately leads to 15% of cancer-related deaths in this population of patients, equating to 1 in every 7000 live births **[4]**. Even in patients with generally favorable outcome profiles, MYCN (v-myc myelocytomatosis viral related oncogene, neuroblastoma derived (avian)) amplification is one of the major markers of the consequences, which is associated with a survival rate of 15 to 35% **[5]**. Furthermore, the site of presentation of this cancer varies from the abdomen, chest, neck, and pelvis, while over half of the patients will show metastasis to sites including the lymph nodes, bone, and bone marrow at the time of diagnosis. It is likely to relapse and develop acquired drug resistance, posing a challenge in treatment **[6]**.

In the past three decades, secondary metabolites with marine origin have become an important source of bioactive compounds. Among the marine organisms explored **[7]**. Marine sponges such as *Agelas sp.* wich are sessile invertebrates that can be found in temperate, polar and tropical regions **[8]** have proved to be a prolific source of unique bioactive secondary metabolites, among which the alkaloids occupy a special place in terms of unprecedented structures and outstanding biological activities **[9]**.

A massive class of interesting natural chemicals known as pyrrole-imidazole alkaloids (PIAs), which are strictly isolated from marine sponges, are structurally characterized by distinctive pyrrole-2-carboxamide and 2-aminoimidazole (or derivatives thereof) moieties **[10]**. We investigated the effectiveness of PIAs in treating neuroblastoma in the current study because of their wide range of biologic functions.

The data and molecular modeling reported in this study are new and original, and we confirm that no previous work has been done until nowadays. The main goal of this work is to find new drugs to treat neuroblastoma by inhibiting specific targets remated to this cancer. It is situated in the field of bio-informatic technology and makes use of molecular modeling methods, which is known as "Molecular Docking (MD)", applied with the use of software such as "Auto dockVina (ADV)," "Discovery Studio Visualizer (DSV)," and "AutoDockTools-1.5.7. (ADT)".

In order to speed up the search for new treatments for specific illnesses, it is important to recognize that developing new drugs is a costly and time-consuming endeavor. Fortunately, these issues can be decreased by using bioinformatics tools.

We investigated how five compounds from the marine sponges *Agelas oroides* S. and *Agelas nakamurai* H., including alkaloids, affected the inhibition of six neuroblastoma targets. This manuscript is divided into four parts:

- The first part is dedicated to a bibliographic synthesis, which summarizes essential information on neuroblastoma and a description of the marine sponges *Agelas oroides* S. and *Agelas nakamurai* H.
- In the second part, we cited the materials and methods used in this study.
- Then the third part consists in presenting the results and their discussion.
- Finally, we finished our work with a conclusion and outlook.

Literature review

I. Neuroblastoma

1. History

One of the earliest descriptions of neuroblastoma is believed to be from Rudolf Virchow in the 1860s, who described this pediatric intra-abdominal mass as an "abdominal glioma". In the early 1900s, neuroblastoma was better characterized by William Pepper, Robert Hutchison, and James Homer Wright. In 1901, Pepper published a series of cases of Philadelphia infants who died after presenting with adrenal tumors and extensive hepatic infiltration, but without evidence of bone metastases. In 1907, Hutchison reported a series of pediatric patients in London with adrenal tumors and bone metastases in the skull and orbit **[11].**

In 1910, Wright, a pathologist at Massachusetts General Hospital, after reviewing the results of Hutchison and Pepper, published a case series of patients with adrenal tumors and disseminated liver involvement and/or bone metastases. Although Pepper and Hutchison described these tumors as sarcomas, Wright found that microscopic "rosettes" of adrenal tumor tissue resembled fetal adrenal tissue. He concluded that these adrenal tumors arose from primitive nerves and described them as "Neuroblastomas" **[11]**.

2. Definition

Neuroblastoma (NB) is the most frequent solid tumor in infancy that arises from neural crest cells, which mature and develop into other cell types such as melanocytes, cranial neurons and glia, cartilage, bone, connective tissue as well as peripheral sympathetic neurons and Schwann cells. It is a type of cancer that usually develops in the adrenal medulla and affects the peripheral sympathetic nervous system. Additionally, it is present in the sympathetic nerve ganglia, which are situated in the neck, chest, abdomen, and pelvis along the sympathetic nervous system. Children are most commonly affected with NB, which is the most prevalent extracranial solid tumor in this population **[12]**.

Approximately 5–10% of all cases of pediatric cancer are neuroblastoma (**Appendix1**). NB affects 11 to 13 children per million who are under the age of 15, with incidence rates ranging from 1 per million for children aged 10 to 14 to 65 per million for infants. More than 90% of all cases of neuroblastoma are discovered before the age of ten, and it frequently arises as an early childhood tumor. 19 months is the typical diagnostic age **[13]**.

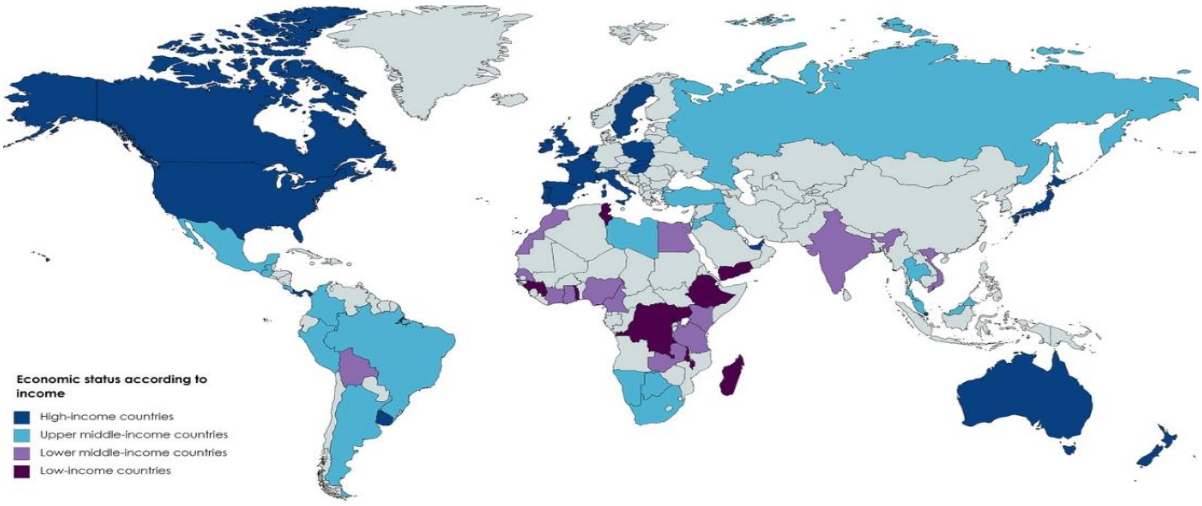

Figure 1: Neuroblastoma distribution graph around the world **[14]**.

NB distribution varies by geographic region (**Figure1**), with the highest rates reported in Europe and North America, Asia and Africa. According to the American Cancer Society, the incidence of NB is higher in developed countries like the United States, Canada, Australia, Japan, and European countries compared to developing countries (**Table1**). The reasons for this may include differences in screening and diagnostic methods, environmental factors, and genetic factors **[15]**.

Table 1. Incidence rate of NB in children and adolescents (Per 1 million person-years).

		Children (0-14 years old) (%)	Adolescents (15-19 years old) (%)	Reference
Asia	**Japan**	15.8%	0.7%	**[15]**
Africa	**Egypt**	10.4%	0.9%	
	Uganda	0.8%	0.0%	
America (Latin and Carribbean)	**Brazil**	8.8%	0.7%	
	Colombia	4.1%	0.6%	
America (North)	**USA**	12.5%	0.8%	
	Canada	14.0%	0.7%	
Europe	**UK**	9.7%	0.9%	
	France	14.4%	0.9%	
	Germany	12.4%	0.7%	
	Australia	11.8%	0.6%	
	New Zealand	11.5%	1.0%	

3. International neuroblastoma staging system

The stages of neuroblastoma are used to describe the extent or spread of the cancer in the body. The stages of neuroblastoma are as follows:

Table 2. International neuroblastoma staging system.

Stage	Definition
1	The cancer is confined to one area and has not spread. Surgery may be enough to remove the cancer.
2	The cancer has spread to nearby lymph nodes but is still only on one side of the body. Surgery and/or chemotherapy may be needed.
2A	Uncompleted surgical surgury of a localized tumor; typical dorsal tissue lymph nodes microscopically free of cancer **[16]**.
2B	Dorsal lymph nodes that are positive for the tumor, a localized tumor, and huge opposing lymph nodes that must be microscopically negative **[16]**.
3	The cancer has spread to the other side of the body or to distant lymph nodes. Surgery, chemotherapy, and radiation therapy may be needed.
4	The cancer has spread to distant sites, such as the bone, liver, or lungs. Chemotherapy and radiation therapy may be needed. Any primary tumor with dissemination to distant lymph nodes, bone, bone marrow, liver, skin, or other organs (except as defined for stage 4S) **[16]**.
4S	This stage is only seen in infants less than 1 year of age. The cancer is confined to certain areas of the body, such as the liver, skin, and/or bone marrow. Chemotherapy may be needed, but the outlook is generally favorable. Localized primary tumor (as defined for stage 2A, or 2B) with dissemination limited to skin, liver, or bone marrow (limited to infants <1 year of age) **[16]**.

*The neuroblastoma stage aids doctors in selecting the best method of treatment and predicting the child's prognosis.

4. Origin

The exact origin of neuroblastoma is not fully understood, but it is believed to arise from the neural crest cells (NCCs). This population of cells is restricted to vertebrates, The neural crest arises from the embryonic ectoderm and develops from the neural tube after its closure. The differentiation of neural crest cells into a wide range of cell types contributes to the emergence of diverse anatomical structures and occurs due to the epithelial-to-mesenchymal transition (EMT) **[17]**.

4.1. Neural crest cells

The neural crest, also known as the fourth germ layer, is a multi-potent embryonic population of progenitors that develops into a wide variety of cell types. The general developmental repertoire of the neural crest lineage has been extensively established since the discovery of the future mapping methods. Melanocytes, peripheral sensory neurons, derivatives of the autonomic nervous system like parasympathetic and sympathetic neurons, chromaffin cells of the adrenal medulla, enteric neurons, peripheral glia, and other nerve-associated cells (Schwann cells, satellite and enteric glial cells, endo-neurial fibroblasts) are included in this lengthy list.

In addition to this profound spectrum, the cranial neural crest gives rise to ectomesenchymal derivatives in the face, neck and teeth (mesenchymal cells, chondrocytes, osteoblasts, dermal fibro-blasts, adipocytes, myocytes, odontoblasts, pulp cells **[18]**.

In the early embryo NCCs originate from the border of the neuroectoderm approximately at the time of neural tube closure. These cells undergo epithelial-to mesenchymal transition (also known as delamination in this context) to exit the epithelial layer and temporarily acquire mesenchymal properties necessary for migration. On their way, NCCs follow specific navigational clues and become exposed to an array of factors directing their future fate **[19]**.

4.2. Epithelial-mesenchymal transitions (EMTs)

The acquisition of mesenchymal features from epithelial cells, occur during some biological processes and are classified into three types: The first type happens when an embryo develops, the second type is related to adult tissue regeneration, and the final type happens as cancer develops. While gastrulation, kidney development, and the formation of the neural crest are all highly regulated processes throughout embryonic development, EMT occurring during embryonic development in gastrulation, renal development, and the origin and fate of the neural crest is a highly regulated process, while EMT occurring during tumor progressions highly deregulated **[20]**. NCCs originate from four major segments of the neural tube to form cranial (or cephalic), vagal, trunk, and sacral NCCs (**Figure2**) **[21].**

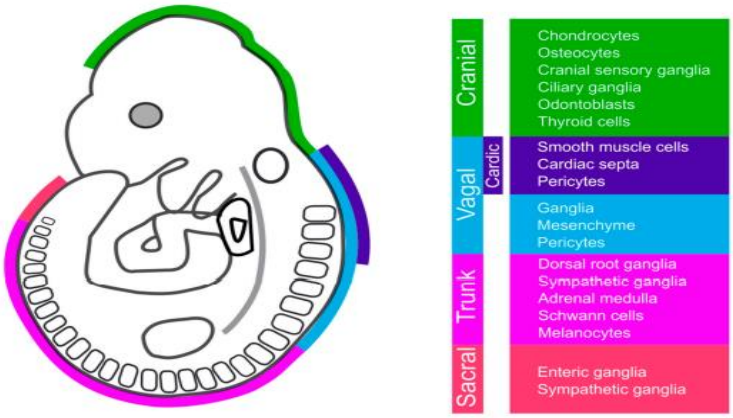

Figure 2 : Anatomically distinct NCCs population and their major derivates **[21]**.

4.3. Development of neuroblastoma cells from neural crest cells

NB is thought to arise when NCCs fail to differentiate properly and instead continue to divide and form masses of immature neuroblasts. These masses, or tumors, can grow and spread to other parts of the body. Mutations in **p53** can lead to loss of its tumor suppressor function, resulting in uncontrolled cell growth and an increased risk of cancer. **NGF** (Nerve Growth Factor) appears to play a role in the growth, development, survival and progression of neuroblastoma. **MYCN** Amplification promotes the proliferation of neuroblastoma cells and inhibits their differentiation into functional neurons. **ALK** mutation leads to the proliferation of neuroblastoma cells and their resistance to therapy (**Figure3**) **[17]**.

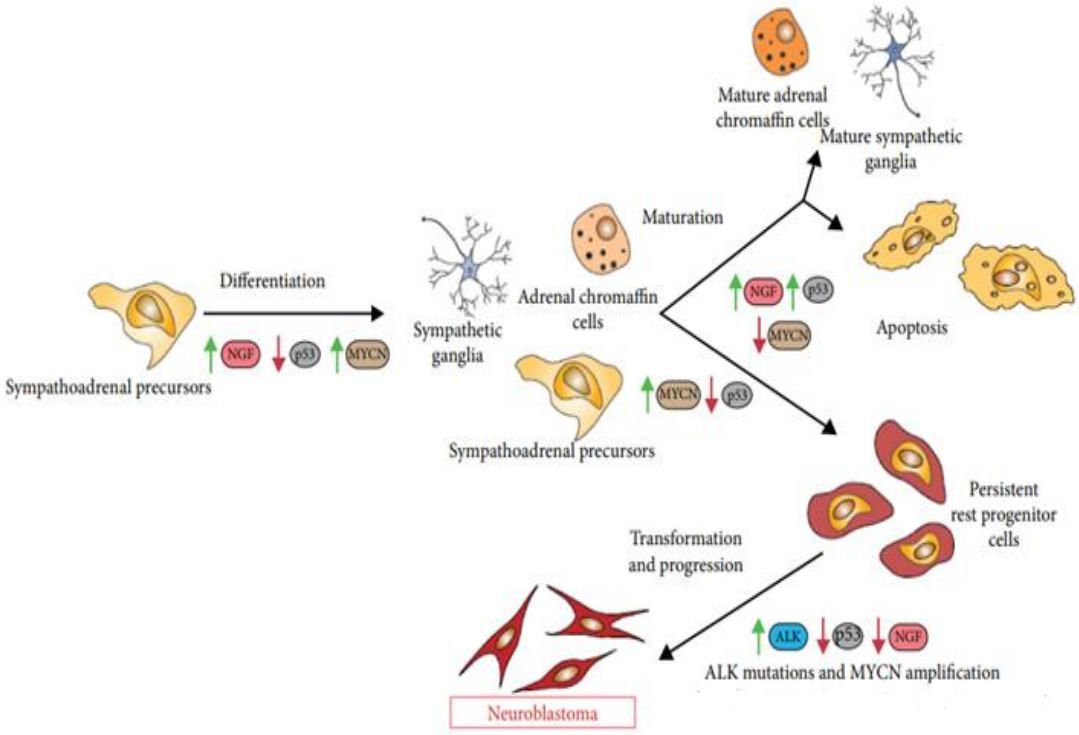

Figure 3 : The transformation of NCCs into NB cells **[17]**.

4.4. Neuroblastoma genetic alterations

MYCN is a member of a small gene family that also includes the genes C-Myc and L-Myc, which are closely linked to MYCN (or N-Myc). MYC proteins are master regulators of cell fate and part of a network of interacting transcription factors. Together, these transcription factors control the expression of numerous genes involved in cell development, differentiation, apoptosis, senescence, and metabolism. More specifically, MYC proteins change transcription mediated by all three RNA polymerases and affect the expression of more than 15% of all genes in a cell when they bind to active promoters and enhancers (**Figure4**) **[22]**.

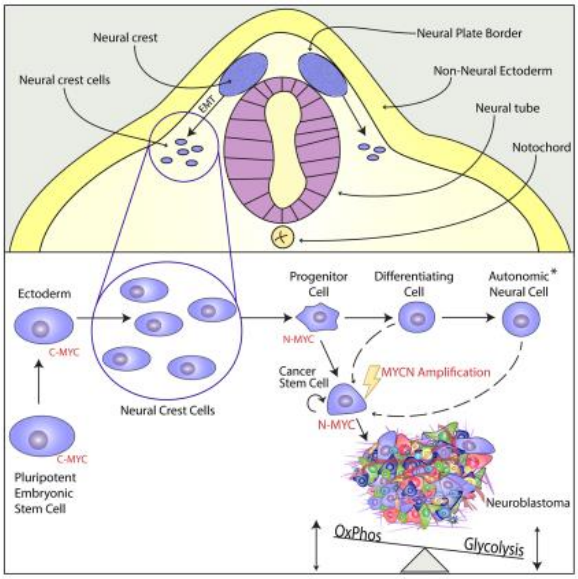

Figure 4 : MYCN acts as a cancer stem cell factor in the developing neural crest and promotes tumorigenesis in NB **[22].**

5. Neuroblastoma cell lineages phenotypes

It has been determined that there are at least three different NB cellular phenotypes: neuroblastic (N-type), flat or substrate adherent (S-type), and intermediate (I-type), each of which has distinctive characteristics that can be determined by unique molecular markers. The first and most widely recognized theory contends that NB cells are capable of interconverting spontaneously from one phenotype to another and is referred to as the transdifferentiation theory. This theory states that I-type cells that have not undergone differentiation give rise to S-type and N-type cells **[23]**.

- **N-type cells:** are characterized as immature nerve cells, precursors to the neural crest sympathoadrenal lineage.
- **S-type cells:** are multipotent precursors to melanocytes, Schwann, and central nervous system glial cells that represent the neural crest non-neuronal components.
- **I-type cells:** firstly, described as an intermediate phenotype, have been recently described as a progenitor of the N-types and S-type cells, capable of self-renewal and bidirectional differentiation.

The SH-SY5Y cell line and its parental line, SK-N-SH, represent the most frequently cited NB cell lines. SK-N-SH represents an I-type cell line used to subclone a few different cell lines in 1978 by Biedler, including SH-SY5Y and SH-EP. The SH-SH5Y is an N-type cell line, although some studies demonstrate that it is also composed of S-type cells, while the SH-EP represents a predominant S-type lineage. The SH-SY5Y and SK-N-SH are extensively used for the study of neuronal diseases **[24]**.

6. Neuroblastoma's most attacked organs

NB affects mainly the adrenal glands, which are located on top of the kidneys. It can also affect other organs such as the brain, the neck (paraspinal cord), the chest (heart and lung), the liver, which can cause an abdominal pain. A pelvic NB can cause some difficulty in walking or standing, it also spreads to the bone marrow causing anemia and an increased risk of infection. However, it can induce some pains in the large joints like the knees (**Figure5**).

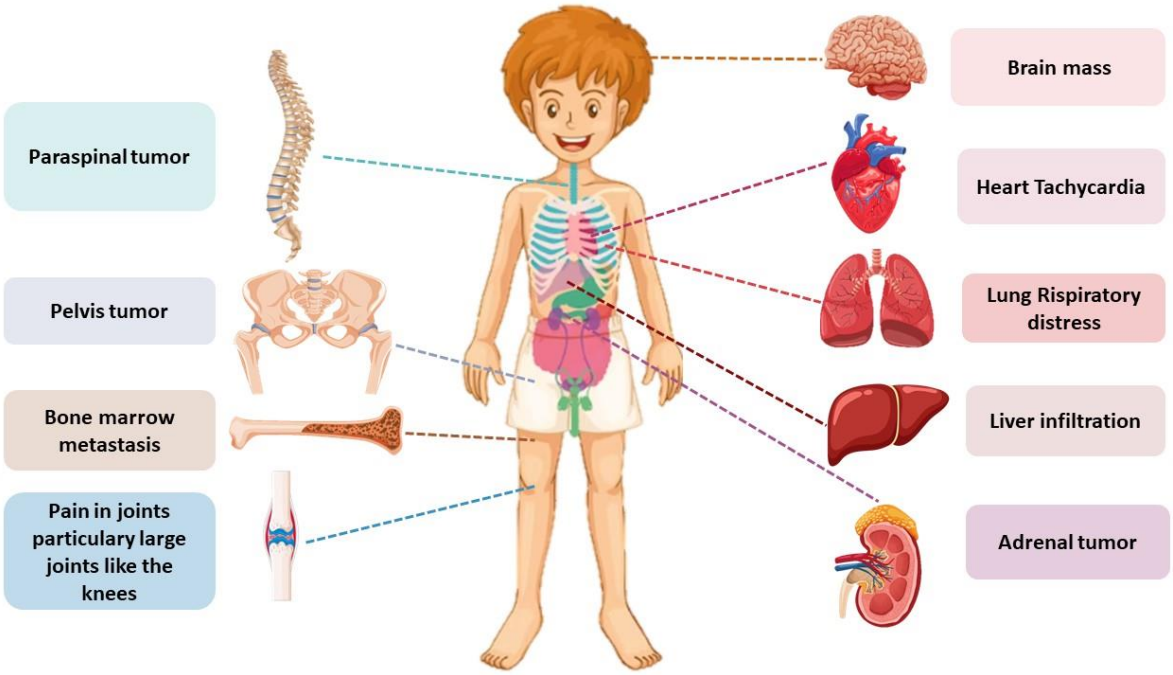

Figure 5 : Most attacked organs by NB **[25].**

7. Clinical presentation of neuroblastoma

The clinical appearance of a patient is influenced by a number of variables, including the location, size, degree of invasion, effects of catecholamine secretion, and symptoms associated with paraneoplastic syndromes. Around half of abdominal tumors, which represent close to 65% of all malignancies, are located in the medulla of the adrenal gland. However, 1% of patients have no identifiable primary, 5% of patients have a pelvic tumor, 20% of patients have a chest tumor, and 5% of patients have a neck tumor. Despite the fact that many individuals are asymptomatic, others may exhibit constitutional symptoms (malaise, fevers, and weight loss), an expanding mass, pain, abdominal distension, lymphadenopathy, or respiratory distress brought on by compression or hepatomegaly. While thoracic involvement might result in dysphagia, dyspnea, or infrequently, thoracic outlet syndrome, pelvic tumors may induce constipation or trouble urinating. For cervical tumors, a patient may develop Horner's syndrome (**Figure6**), and in up to 15% of patients, epidural extension may result in neurological deficits

such as progressive paralysis. Numerous syndromes, including the following, can arise from NB: Horner syndrome, Hutchison syndrome, Pepper syndrome, Spinal cord compression (Back pain, weakness) **[26].**

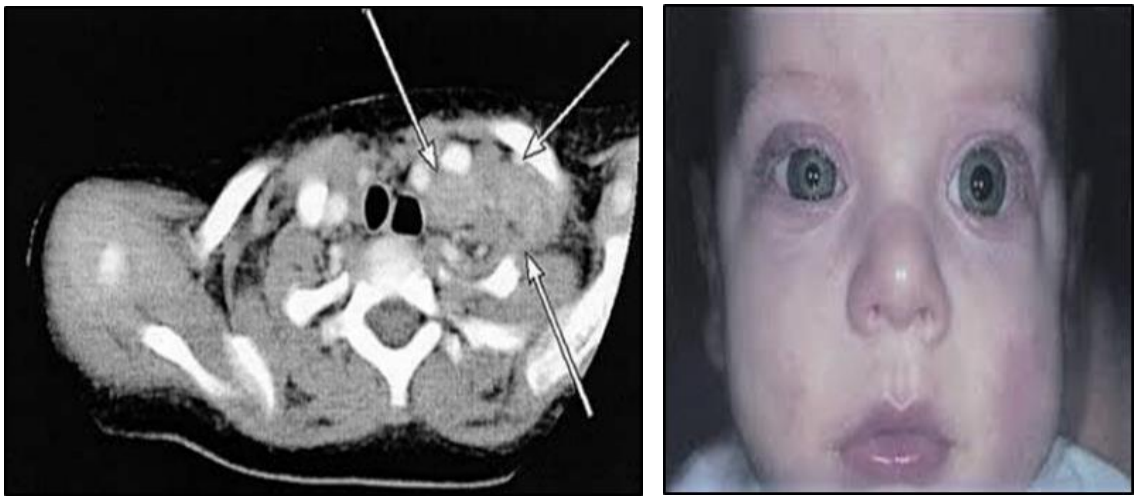

Figure 6 : Computed tomography scan of an apical paraspinal NB in a child who presented with **Horner's Syndrome [27].**

8. Neuroblastoma Diagnosis

To confirm the diagnosis and staging of neuroblastoma, a number of laboratory tests, imaging scans, and pathologic examinations are necessary. The first set of tests to take include a complete blood count, Prothrombin time, Partial thromboplastin time, Uric acid, Electrolytes, Creatinine, Liver function tests, Ferritin, Lactate dehydrogenase **[28]**.

Urine should also be tested for dopamine, homovanillic acid, and vanillylmandelic acid (VMA). These catecholamines and catecholamine metabolites are present in 90% of children with NB **[28]**.

For staging, tumor characterization, and surgical planning, extensive imaging are necessary. Ultrasound is an accessible way without requiring sedation to confirm the presence and location of a mass. However, cross-sectional imaging with either computed tomography (CT) or magnetic resonance imaging (MRI) is necessary for accurate localization and characterization **[28]** (**Figure7**).

Figure 7 : Computed tomography (CT) and Magnetic resonance imaging (MRI) **[29]**.

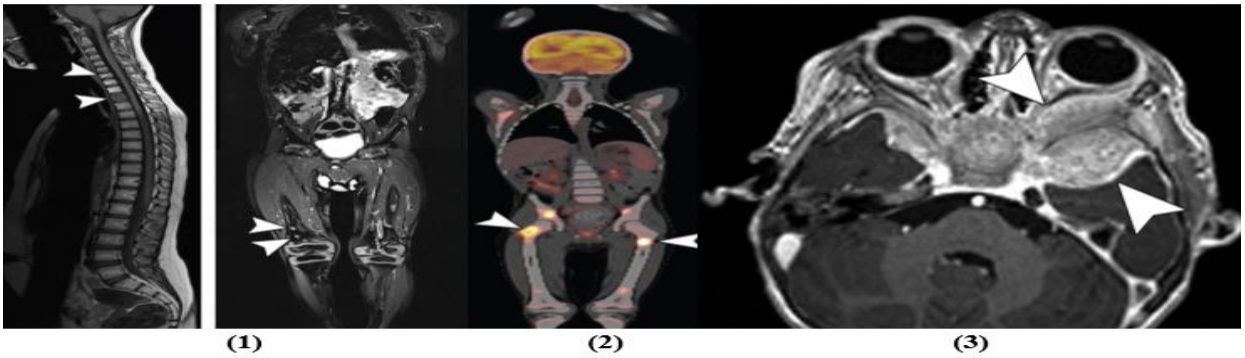

Figure 8 : (**1**) : FDG PET/CT and PET maximum intensity projection, (**2**) : Whole-body MR images show multifocal osseous lesions with sagittal T1-weighted and coronal short inversion time inversion-recovery, (**3**) : Axial postcontrast T1-weighted MR image reveals infiltration of the intraorbital extraconal space with associated mass effect and proptosis (arrowheads) **[30]**.

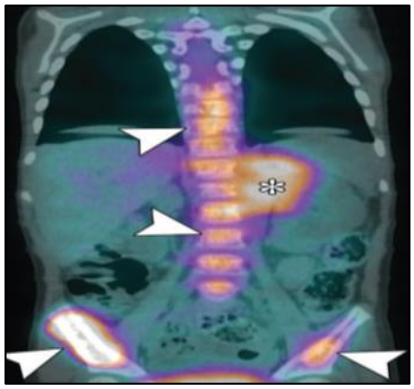

Figure 9 : SPECT/CT image shows superior anatomic detail for characterization of sites of tumor involvement **[30].**

9. Neuroblastoma studied targets

9.1. Focal Adhesion Kinase 1 (FAK)

Focal Adhesion Kinase (FAK), a hydrolase cytoplasmic protein kinase with a molecular weight of 125 kD with 1052 amino acids, including Lys454, Val436, Ile428, Ala452, Met499, Glu500, Arg550, Glu506, Leu553, Cys502, Asp564, Glu471, Phe565, Asn551, Gln432, Lys454, Phe433 that have been linked to the catalytic activity of the active site. FAK is activated by autophosphorylation at Tyr397 and connected to a number of cellular processes. It occurs by extracellular matrix adhesion and plays an essential role in controlling how the actin cytoskeleton is organized as well as in the survival of various cellular types that depend on adhesion **[31]**. It has an important role in the development of several human cancers, including neuroblastoma. FAK is involved in the growth, migration, survival, and death of tumor cells **[32]**. This protein is an attractive molecular target for cancer therapy.

FAK's catalytic activity:

ATP + L-tyrosyl-[protein] = ADP + H^+ + O-phospho-L-tyrosyl-[protein] [33], [34], [35].

9.2. Caspase-3

Caspases are a class of cysteinyl-specific proteases that cleave an aspartate residue through their substrates and cause irreversible cell death **[36]**. Caspase-3 is a transferase and hydrolase that contains 277 amino acids including Leu168, Thr166 and Ocs163 that have been involved in the active site's catalytic activity, Caspase-3 is generated as an invisible proenzyme (p32), which is made up of a large and small subunits. **[37]**. Its catalytic activity is tightly regulated by various mechanisms, including protein-protein interactions, post-translational modifications, and subcellular localization. Its dysregulation is implicated in various diseases, including cancer such as neuroblastoma, it is an attractive therapeutic target for treatment of diseases involving dysregulated apoptosis **[38]**.

9.3. Gamma isoform of the catalytic subunit of phosphatidylinositol 4,5-bisphosphate 3-kinase (PI3K)

PI3K is an intracellular lipid kinase is a transferase that contains 1044 amino acids including ; Met953, Met804, Ile963, Ile831, Val882, Tyr867, Asp964 and Ile879, that have been identified in the catalytic activity of the active site, it is activated by growth factors and cytokine receptors through a tyrosine-kinase-dependent mechanism **[39]**. It controls cell metabolism, growth, survival, and proliferation **[40]**. The mutations and amplification of PI3K are the most occurring events in cancer, and abnormal PI3K activity is a transforming event in the disease process **[41]**.

It plays an essential role through intracellular signaling in tumors and is connected to oncogenic transformation, cancer metastasis, and cancer progression **[42]**.

PI3K's catalytic activity:

1,2-diacyl-sn-glycero-3-phospho-(1D-myo-inositol-4,5-bisphosphate) + ATP = a 1,2-diacyl-sn-glycero-3-phospho-(1D-myo-inositol-3,4,5-trisphosphate) + ADP + H^+ [43].

9.4. Telomerase reverse transcriptase (TERT)

Telomerase reverse transcriptase, or TERT, is an enzyme that has also a transferase, which contains 1132 amino acids including; Gly309, Asp251 and Asp343, that have been implicated in the active site's catalytic activity. In most eukaryotes, the replication of chromosomal termini depends on the ribonucleoprotein enzyme telomerase **[44]**. It can take telomere DNA (TTAGGG) into the end of chromosome to shorten telomere, making TERT mutation a critical study hotspot in the etiology of tumor since it was first identified since 2013 **[45].** Numerous biological processes, such as embryonic development, tissue repair, and immune system operation, depend on TERT activation. As increased telomerase activity allows cancer cells to maintain their telomeres and continue to divide uncontrollably, it is also an essential stage in the growth of cancer.

TERT's catalytic activity:

2'-deoxyribonucleoside 5'-triphosphate + DNA(n) = diphosphate + DNA(n+1) [46], [47].

9.5. Osm-9-like TRP channel 1 (The Transient receptor potential vanilloid) (TRPV1)

The Transient receptor potential vanilloid (TRPV) family of ligand gated ion channels represents a group of non-selective cation channels which are involved in sensory perception. **[48]** TRPV1 has 839 amino acids involving Leu555, Ala568, Leu576, Leu517, Tyr513, Val520, Ser514, Asn553, Arg559, Thr552 and Met549, being associated in the active site's cavity. In TRP channel family, from the *Caenorhabditis elegans*, first identified TRP channel of the TRPV family was OSM-9 (osmotic avoidance abnormal family member 9). OSM-9 is specifically involved in the worm's ability to detect osmotic changes in its environment, such as changes in salt concentration **[48].**

TRPV1 doesn't have catalytic activity in the conventional sense. Instead, it serves as a molecular sensor that opens in response to diverse stimuling including heat, acid, and certain chemicals in order to let cations enter the cell.

9.6. RAC-alpha serine/threonine-protein kinase (AKT1)

PK, or protein kinase AKT, also known as RAC-alpha serine/threonine-protein kinase (RAC-PK), is a Transferase, one of the most significant protein kinases, playing a significant role in several important biological functions including cell survival and immunoregulation. It has 480 amino acids, those who are implicated in the active site's catalytic reaction are flowing: Glu228, Ala230, Glu234, Lys276, Val164, Ala177, Asp292, Met281, Phe161 and Thr291. The vertebrate AKT family has three members who are closely related to one another: AKT1 (PKB), AKT2 (PKB), and AKT3 (PKB). AKT1 is one of them and is considered to play a role in cell activities such cell proliferation, migration, and penetration **[49].** A variety of downstream substrates are phosphorylated on serine and/or threonine to control this **[50].**

AKT1's catalytic activity:

ATP + L-seryl-[protein] = ADP + H^+ + O-phospho-L-seryl-[protein] [51], [52].

*Each one of the targets is represented in the ***Appendix*** section.

10. Treatment strategies for neuroblastoma

NB patients are classified into four pre-treatment risk groups: very-low, low, intermediate, and high-risk, which is mostly based on clinical and molecular characteristics such age group, disease stage (INSS staging system), histological class, the degree of tumor differentiation, DNA ploidy, and MYCN amplification status (non-amplified vs. amplified), among others **[53].**

Patients with low-risk NB have a favorable prognosis and a 5-year survival rate of more than 90.9% However, 60% of patients have high-risk NB, and the prognosis of treatment in such patients remains poor. Patients categorized as having low-risk NB are typically provided minimal therapy, and some children are curatively treated by surgery alone, or may experience spontaneous tumor regression **[54]**. Milder chemotherapy is administered to patients in the intermediate-risk group, and they may also be treated by removing the remaining tumor mass. The current standard treatment for high-risk NB includes three treatment blocks; (i) induction, (ii) consolidation, and (iii) maintenance Induction chemotherapy (IC) aims to reduce the tumor by shrinking it and also reducing the risk of metastasis via chemotherapy and surgery. The consolidation block involves the administration of HDC (high dose chemotherapy) accompanied by ASCT (autologous stem cell transplantation) and radiotherapy. Maintenance involves immunotherapy using anti-disialoganglioside (GD2) monoclonal antibody (mAb) with cytokines and differentiation therapy using 11-cis retinol. Approximately half of high-risk patients do not respond to the first-line therapy protocol or relapse in the first 2 years after

treatment. The outcome for high-risk NB patients is very poor, with a 5-year survival rate of less than 50% **[54]**.

11. Natural metabolites in treating Neuroblastoma

Traditional medicine has used natural metabolites from a variety of sources, including bacteria, animals, minerals, and plants, to treat a variety of human diseases, including cancer. The recent advancements in spectroscopic and analytical technology, as well as high-throughput screening, have greatly accelerated the identification of natural pharmaceuticals, particularly marine-based drugs. According to reports from several marine creatures, including sponges, the marine environment provides a rich source of a large group of structurally unique metabolites with a variety of pharmacological activities. These metabolites have an increasing effect on the pharmaceutical sector. They have been discovered to exhibit a variety of biological properties, with the main ones being antibacterial, immunosuppressive, antifouling, anticancer, anthelmintic, antiprotozoal, neuroprotective, antiviral, and anti-inflammatory **[55].** Moreover, the metabolites isolated from marine sponges have been identified as an essential source for developing new drugs for the treatment of NB.

II. Marine sponges

The ocean is the source of all life and is a vast natural resource for screening natural products. It is also rich in biological resources. So far, researchers have found>300,000 species of marine organisms in the ocean, and more than a one million new species are expect to remain undiscovered **[54]**.

1. Definition

Marine sponges (Porifera), the most primitive multicellular metazoan animals, are sessile organisms that efficiently filter feed organisms from the surrounding water. They live in a high-salinity, high-pressure, light-avoiding, anoxic and oligotrophic environment **[56]**. Sponge development can be extremely changeable in response to environmental conditions presenting various sizes, ranging from 0.1 to 50 μm **[57]** and can take on a variety of forms, including encrusting, rope, ball, tube, barrel, and vase, as well as colors, including white, yellow, red, orange, green, blue, purple, brown, and black **[58].** Marine sponges have been studied as potential sources of lead compounds for biomedical uses **[59].**

The Mediterranean basin has been ranked among the 25 "biodiversity hotspots" on earth on the basis of its high species richness and endemism. It is the ideal hotspot for biodiversity due to its semi-closed environment, continual enrichment of Red Sea and Atlantic waters (and species) through the Suez Canal, and warm climate. Furthermore, the biodiversity of its sponges on the seafloor is unexplored due to the seabed's abundance of caves and deep canyons. More than 600 species of Mediterranean sponges with a high endemicity value are included among the major marine species. The high biodiversity rate of Mediterranean sponges at the taxonomic level is reflected in the wide range of bioactive extracts, fractions, and compounds that have been discovered and endowed with pharmacological potential (**Figure10**) **[60].**

As one of the most common marine sponges in tropical and subtropical oceans, the sponges of the genus *Agelas*, have emerged as unique and yet under-investigated pools for discovery of natural products with fabulous molecular diversity and myriad interesting biological activities **[61].**

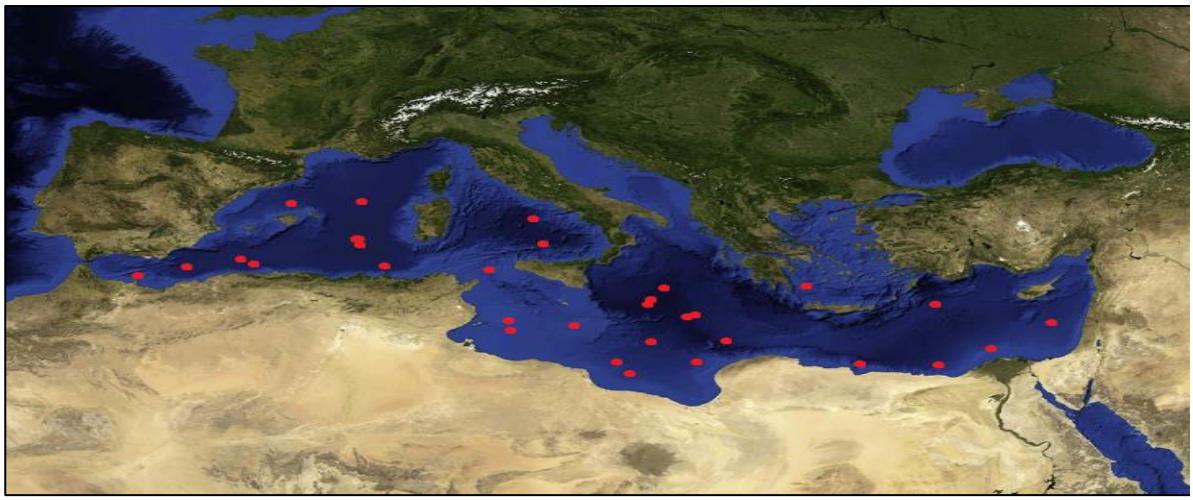

Figure 10 : Marine sponges distibution in the Mediterranean basin **[62]**.

2. The marine sponge *Agelas sp.*

The sponge *Agelas* sp. (Order: Agelasida, Family: Agelasidae) has a smooth surface. Sponges are solid, flexible, and compact. The skeleton is made of thick, reticulate fibers and has a rough texture (**Figure11**). Primary fibres cored and echinated by verticillate spined acanthostyles **[63].**

Figure 11 : Marine sponge *Agelas sp.* **[64]**

The marine sponge Agelas (Porifera, Demospongiae, Agelasida, Agelasidae) is widely distributed in the marine eco-system and includes at least 19 species: A. *axifera*, A. *cerebrum*, A. *ceylonica*, A. *citrina*, A. *clathrodes*, A. *conifera*, A. *dendromorpha*, A. *dispar*, A. *gracilis*, A. *linnaei*, A. *longissima*, A. *mauritiana*, A. *nakamurai*, A. *nemoechinata*, A. *oroides*, A. *sceptrum*, A. *schmidtii*, A. *sventres*, and A. *wiedenmayeri*. Since the beginning of the 1970s, many research groups around the world have carried out chemical investigation on *Agelas sp*., resulting in fruitful achievements. Their research showed that Agelas sponges contain a variety

of bioactive secondary metabolites, including terpenoids, glycosphingolipids, carotenoids, fatty acids, alkaloids (particularly bromopyrrole derivatives), and meroterpenoids. These natural compounds' extensive chemodiversity and interesting biological activity make them a desirable resource for therapeutic possibilities **[65].**

2.1.Taxonomy [66]

Basing on our research, we found the taxonomy of these two species in **INPN** database **[67]**, below is the detailed taxonomy:

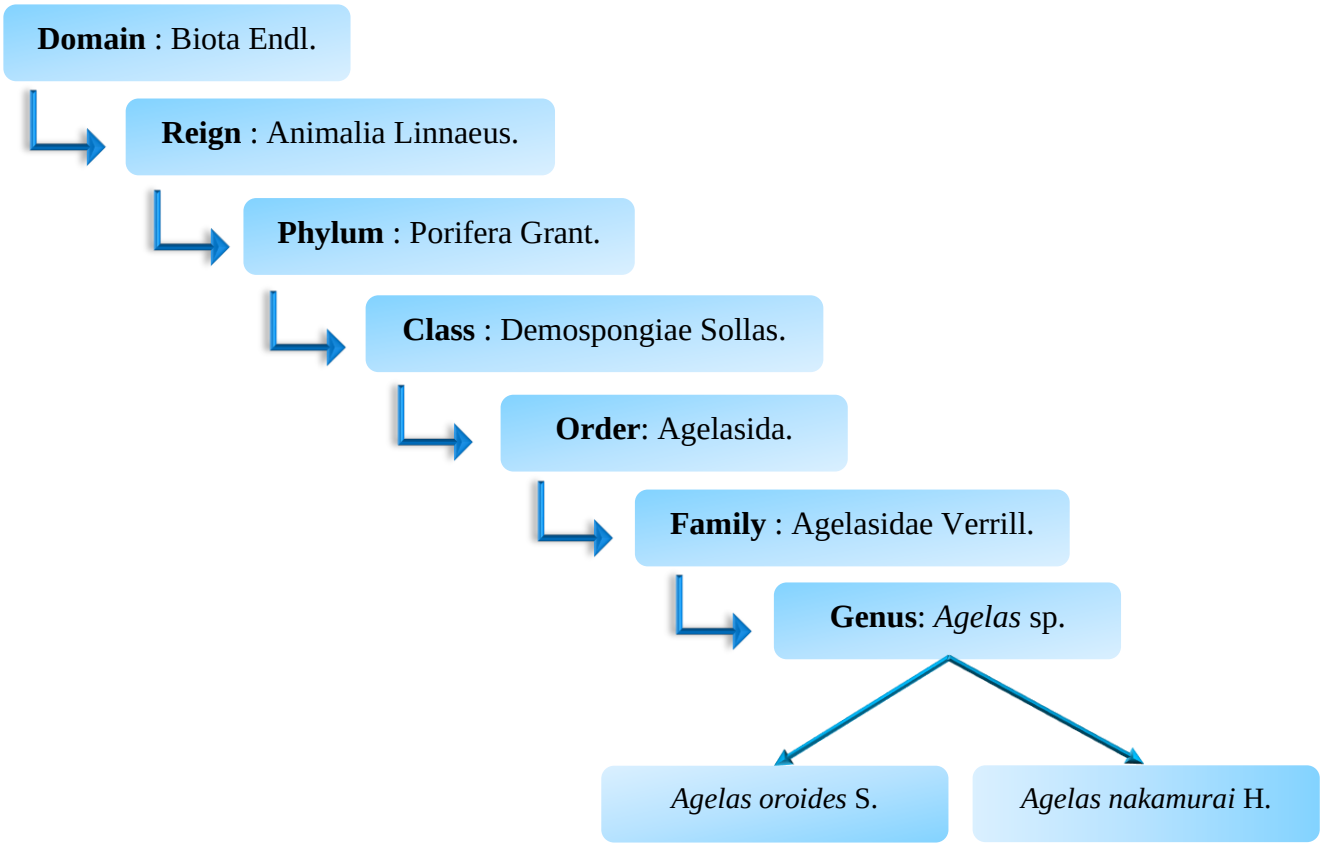

2.2.*Agelas oroides* S.

Agelas oroides is a large, variably lobate-digitate sponge that often stands 5 to 25 meters tall. Individuals of this species are often bright orange in color, although those that live in low light conditions tend to be paler. The surface is Conulose, and the tissue is hard but elastic **[68]** is a sponge that can be found across the Mediterranean Sea, both at shallow levels (40 m) and mesophotic levels (40–150 m). It lives in protected areas with limited light, such as cave openings, fissures, or mesophotic environments. By enhancing the structural complexity of its surrounds and so creating a home for the invertebrates and fish that live in and on it, it plays a significant ecological role. *A. oroides* S. has also shown to be a significant source of numerous novel natural compounds, some of which have bioactivity that has been shown, such as oroidin **[69].**

Figure 12 : *Agelas oroides* S. **[70]**

2.3.*Agelas nakamurai* H.

Agelas nakamurai has a number of bioactive chemicals that have shown interest in treating a number of diseases, and these substances have led to research into therapeutic benefits. It has been discovered to have anti-inflammatory, antioxidant, and anticancer properties, for instance. The medicinal characteristics of *Agelas nakamurai* H. have been the subject of interesting research, but much more has to be done to determine its safety and efficacy in humans **[68].**

Figure 13 : *Agelas nakamurai* H. **[64]**

3. Marine sponges of the genus Agelas as a source of Secondary metabolites

Secondary metabolites isolated from marine sponges of the genus Agelas (Class: Demospongiae, Order: Agelasida, Family: Agelasidae) display an amazing structural diversity of bromopyrrole and diterpene alkaloids. To this date, 36 species of the *Agelas* genus have been identified. Structurally, pyrrole alkaloids generally have a bromoor dibromopyrrole-2-carboxamide core attached to a variety of side chains, either linear or cyclic. Apart from their structural diversity, this class of compounds has shown a wide range of biological activity, including antiparasitic and antimalarial, antihistaminic, antimicrobial, antifouling, and inhibitory action towards voltage-gated K + channels **[7].**

Alkaloids are nitrogen-containing organic substances (natural products) with substantial biological effects. Typically, they match bases in terms of their chemical characteristics. Despite not being alkaline, several nitrogenous plant chemicals may still be classified as alkaloids because to their apparent biological activity. Alkaloids are found in a wide variety of creatures in nature, including plants, animals, microbial organisms, and marine organisms **[54].**

Pyrrole-imidazole alkaloids (PIAs) and simple pyrrole alkaloids represent a specific structural class of compounds isolated from sponges including those from the genus *Agelas* PIAs can be divided into monomeric and polymeric groups. Currently, although hundreds of PIAs have been discovered from sponges, the structural diversity of this alkaloid family, especially for the monomeric ones, is relatively conservative **[71].**

In this study we were interested by this serie of alkaloids that is represented in **table3**:

Table 3. Definition of the studied Marine Alkaloids.

Molecules	Definition
Ageladine A	**-Ageladine A** belongs to the pyrrole-imidazole alkaloids family. It is a brominated pyrrole–imidazole alkaloid .it was first reported in 2003 by Fusetani et al. and isolated from the hydrophilic extract of the marine sponge *Agelas nakamurai* H. using a bioassay-guided fractionation **[7].** -The alkaloid showed biological effects such as the inhibition of matrix metallo-proteinases and the inhibition of cell migration of bovine endothelial cells **[72].**
Oroidin	- Oroidin was isolated in 1971 from the marine sponge *Agelas oroides* S. It is the simplest among bromopyrrole-imidazole alkaloids and it has a linear structure characterized by a bromopyrrole carboxamide and an amino-imidazole moiety linked through a propenyl chain. It might be considered a biogenetic precursor of the other alkaloids **[73] .**Oroidin is a chemical defense for sponges of the genus Agelas against predation by the reef fish *Thalassomia bifasciatum* **[73].** Oroidin has a good antihistaminic activity **[74].**
Strepoxazine A	-Strepoxazine A, a new cytotoxic phenoxazine analogue isolated from the solid culture of sponge-associated *Streptomyces sp.* SBT345, which had earlier been isolated from the Mediterranean sponge *A. oroides* S. **[75].** The alkaloid Strepoxazine A has antihistaminic activity **[68].**
Cyclooroidin	-In 2000, Fattorusso et al. isolated a new alkaloid belonging to the pyrroleimidazole alkaloid family from the Mediterranean sponge *Agelas oroides* S. **[76].** Cyclooroidin has a antihistaminic activity.
Taurodispacamide A	-Is a novel pyrrole-imidazole alkaloids. isolates from the Mediterranean sponge *Agelas oroides* S. **[77].** Taurodispacamide A exhibited a good antihistaminic activity **[77].**

Materials and methods

III. Materials and methods

1. Softwares, Databases and Web servers

In this study, we employed the different softwares such as Discovery Studio Visualizer (DSV) v2017, AutoDock Tools-1.5.7 (ADT), AutoDock Vina (ADV) and different databases and webservers.

1.1.Softwares

- Discovery Studio Visualizer (DSV) v2017: is suit of software that is developed and distributed by Dassault system BIOVIA (formerly Accelerys) for stimulating small molecule and macromolecule system **[78]**.
- AutoDock Tools-1.5.7 (ADT) : is a software made by the AutoDock team that prepares and analyzes molecular structures for use with the AutoDock software. it is a graphical user interface which, among other functions, aids in determining which bonds in the ligand will be treated as flexible **[79].**
- AutoDock Vina (ADV): is a molecular docking software that is applied to predict the binding affinities and mechanisms of small compounds to protein targets **[79].**

1.2. Databases

- **PubChem**

PubChem BioAssay (https://pubchem.ncbi.nlm.nih.gov/) is an open access database hosted by the National Center for Biotechnology Information (NCBI), National Library of Medicine (NLM), National Institutes of Health (NIH). Since around 2004, it has served as a public archive for data resulting from studies in functional genomics, medicinal chemistry, and chemogenomics. The public has free access to the database's total collection of data for exploring and downloading. Almost 80 organizations (data sources) across the world have presently contributed 230 000 000 bioactivity results to the PubChem BioAssay database, reaching over one million records **[80].**

- **Protein Data Bank (PDB)**

The Protein Data Bank (PDB), the first open-access digital resource in the biological sciences, was founded in 1971. It is the sole global database of experimentally defined 3D structures of biological macromolecules and their complexes. There are currently 130,000 items in the PDB archive (May 2017). The RCSB Protein Data Bank (https://www.rcsb.org/), the Protein Data Bank Japan (PDBj; pdbj.org), the Protein Data Bank in Europe (PDBe; pdbe.org) , and

BioMagResBank (BMRB; www.bmrb.wisc.edu). are all managed by the Worldwide Protein Data Bank organization (wwPDB;wwpdb.org) **[81].**

- **PDBsum**

PDBsum, (http://www.ebi.ac.uk/pdbsum) offers multiple visual evaluations of each Protein Data Bank entry. It shows all of the proteins, DNA, and ligands in the entry's structural characteristics and their interactions. Annotation of human protein sequences with their naturally occurring amino acid variants, dynamic graphs illustrating the relationships between related protein domain configurations, assessments of ligand binding clusters across various experimental determinations of the same protein, evaluations of tunnels in proteins, and new search options among the most recent features, which are described here **[82].**

- **Molinspiration**

Several bioinformatic professionals in both academia and business utilize Molinspiration (https://www.molinspiration.com/) to produce high-quality study results. Google Scholar reports that its tools have been referenced more than 4500 times.

1.3. Web servers used for ADMET study

The ability to anticipate ADMET properties has considerably improved during the past several years. The majority of them are now predictable. Predicted ADMET characteristics are increasingly exploited and play a significant part in drug development because to their benefits (speed and cost). Theoretical calculations of the ADMET (Absorption, Distribution, Metabolism, Excretion, and Toxicity) were examined using the SwissADME server (http://www.swissadme.ch/) and PreADMET server (https://preadmet.webservice.bmdrc.org/). To determine the ADMET parameters, the canonical SMILES of the compounds were retrieved from the PubChem Database **[83].**

2. Structure-activity relation (SAR)

To understand the main functions of the examined enzymes in relation to their substrates and inhibitors. First, the crystal structures of the enzymes : Focal Adhesion Kinase 1 (FAK) (PDB ID : 2IJM), Caspase-3 (PDB ID : 3DEI), Phosphatidylinositol 4,5-bisphosphate 3-kinase catalytic subunit gamma isoform (PI3K) (PDB ID : 4FA6), Telomerase reverse transcriptase (TERT) (PDB ID : 6USR), Osm-9-like TRP channel 1 (TRPV1) (PDB ID : 7LQZ), RAC-alpha serine/threonine-protein kinase (AKT1) (PDB ID : 4EKK) ; were obtained from the PDB and designated as receptors. Then, we chose five ligands, including alkaloides of the marine sponge *Agelas sp.* :

- Ageladine A ;
- Oroidin ;
- Strepoxazine A ;
- Cyclooroidin ;
- Taurodispacamide A.

2.1. Molecular docking preparation

2.1.1. Protein preparation

The crystal structures of our proteins were obtained from the PDB. Before the MD, the targets 3D structure and the ligands should be prepared, this preparation consists of three steps.

- The first one includes elimination of all unnecessary molecules such as ; water molecules, heteroatomes and any ligands or cocrystallized solvent.
- The second step is to add polar hydrogens and partial charges using ADT. After defining the grid box, the molecular docking was performed by ADV program. We must cite that all parameters are used by default, except that the number of output conformations was set to 1.
- The final step involves adjusting the size and center of the grid box and showing it using ADT (x,y and z).

A total of 60 docking runs were planned. 60 conformations constitute the total number of solutions **[83].**

2.1.2. Ligand preparation

The 3D structures of the ligands (Mol1, Mol2, Mol3, Mol4, and Mol5) were downloaded from the PubChem data source (https://pubchem.ncbi.nlm.nih.gov/) as SDF files, and then converted to PDB files using the *Discovery Studio Visualizer* v2017 software. Following that, the PDB files were converted into PDBQT format using ADT to get the molecules ready for MD. The 2D and 3D structures are represented in **Appendices 8 and 9**, while **table4** represents the chemical properties and the sources of the investigated ligands.

Table 4. chemical properties of the studied ligands and their sources.

Code	Pubchem ID	Name	Formula	Molecular weight (g/mol)	Source	Refrence
Mol1	10089677	Ageladine A	$C_{10}H_7Br_2N_5$	357.00	*Agelas nakamurai* H.	**[7]**
Mol2	6312649	Oroidin	$C_{11}H_{11}Br_2N_5O$	389.05	*Agelas oroides* S.	**[8]**
Mol3	132526082	Strepoxazine A	$C_{17}H_{14}N_2O_6$	342.30	*Agelas oroides* S.	**[9]**
Mol4	10739060	Cyclooroidin	$C_{11}H_{11}Br_2N_5O$	389.05	*Agelas oroides* S.	
Mol5	135501141	Taurodispacamide A	$C_{13}H_{16}Br_2N_6O_4S$	512.18	*Agelas oroides* S.	**[77]**

3. Molecular Docking study

MD is a software method which allows to simulate the optimal conformation according to the complementarity and pre-organization, which could predict and obtain the binding affinity and interactive mode between ligand and receptor **[84].** It is realized by ADV which provides the ligand with complete flexibility, as represented in **figure14**.

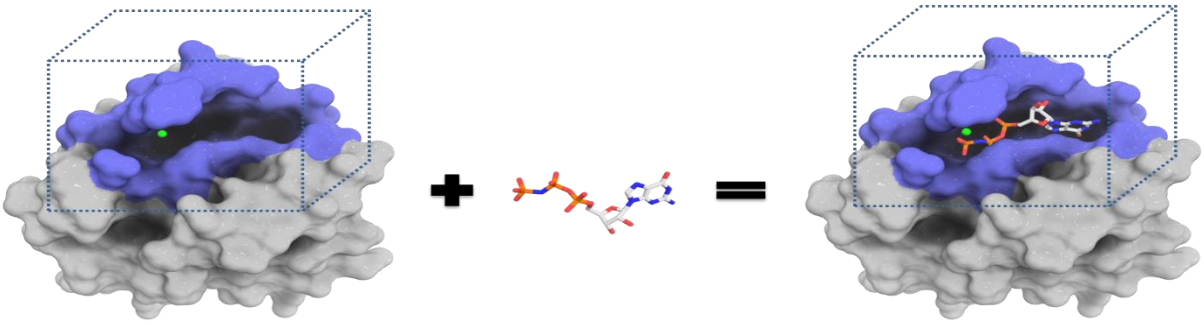

Figure 14 : Schematic representation of the basic molecular docking concept **[85]**.

ADT is used to determine and display grid Box's center and size respectively, for exemple the receptor (PDB ID : 6USR) is presented by the next values (x=28.056, y=-12.649, z=-19.577) and (x=14, y=18, z=14) (**Figure15**). According to the lowest energy value (Kcal/mol), the best molecular position for each receptor-ligand complex is selected, with a maximum repetition rate in percent (%).

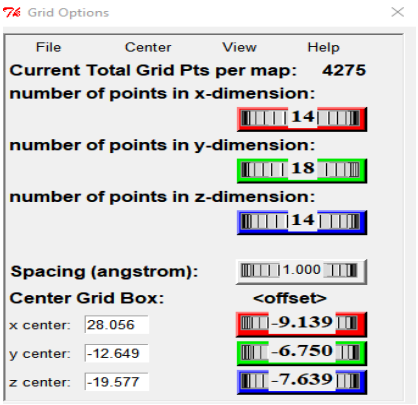

Figure 15 : 6USR's Grid Box configurations.

The results of the MD were applied to 10 of the obtained solutions in order to identify the amino acids and interactions types (Hydrogen bonding, electrostatic interactions, or hydrophobic interactions) between inhibitors and receptors in this study. The different parameters and targets names are shown in **table5**.

Table 5. Investigated targets with docking parameters.

PDB ID	Enzyme	Number of water Molecules	x*y*z Center of Grid Box	x*y*z Size of Grid Box
2IJM	Focal Adhesion Kinase 1 (FAK)	HOH210	2.636*7.006*5.92	14*16*14
3DEI	Caspase-3	-	-45.991*13.444*-22.289	16*12*12
4FA6	Phosphatidylinositol 4,5-bisphosphate 3-kinase catalytic subunit gamma isoform (PI3K)	HOH301	43.858*13.729*31.015	16*14*12
6USR	Telomerase reverse transcriptase (TERT)	HOH702, HOH704	28.056*-12.649*-19.577	14*18*14
7LQZ	Osm-9-like TRP channel 1 (TRPV1)	-	143.813*119.67*126.842	18*14*18
4EKK	RAC-alpha serine/threonine protein kinase (AKT1)	HOH633	14.088*2.086*18.286	14*16*14

4. ADMET Analysis

ADMET properties of a compound deal with its Absorption, Distribution, Metabolism, Excretion, and Toxicity and through the human body, which constitutes the pharmacokinetic profile of a drug molecule, is very essential in evaluating its pharmacodynamic activities. Today a lot of online tools and offline software programs are available which helps us in predicting this behaviour of the drug candidate **[86].**

We evaluated ADMET and the pharmacokenitics prediction of the major obtained compounds using SwissADME (http://www.swissadme.ch/) and Pre-ADMET (https://preadmet.webservice.bmdrc.org/toxicity/) webservers. The canonical SMILES of the compounds were obtained from PubChem Database to calculate ADMET properties **[87].**

In our study, we used the online Pre-ADMET server that is available on the website (https://preadmet.webservice.bmdrc.org/toxicity/). Based on the following parameters, the ADMET profile was chosen :

4.1.Drug ability

4.1.1. Lipinski Rule

Also know as the rule of five (RO5) is a general guideline used to analyze a chemical compound's druglikeness (**Figure16**), or to identify if that contains chemical and physical characteristics that would likely make it an orally active drug in humans and has a particular pharmacological or biological activity **[88], [89].**

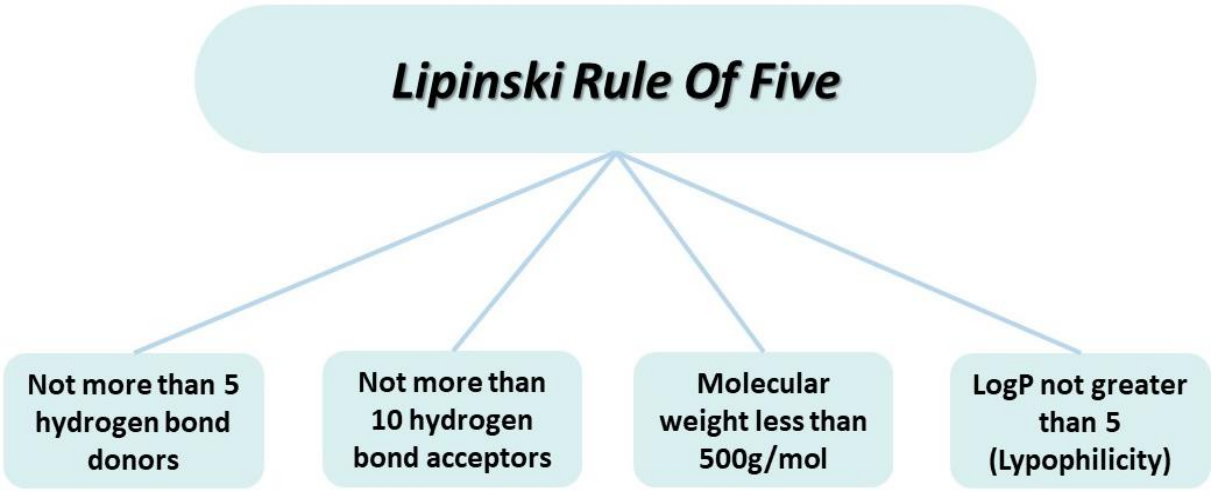

Figure 16 : Lipinski rule physicochemical properties **[90]**.

4.2. Absorption

It is the process of movement of a drug from an extravascular site of administration into the systemic circulation **[91]**. We used as parameter :

4.2.1. Human Intestinal Absorption (HIA)

It is one of the most important ADME properties. Utilization of drugs in the human body is such a complicated process that it can hardly be analyzed precisely by statistical models. HIA is also one of the key steps during the drugs'transporting to their targets. It is considered as one of the important components which influence bioavailability, so a lot of effort has been made for accurate prediction of HIA **[92].**

4.2.2. Caco-2 cell permeability

It is used to measure drug absorption. Expert Opinion on Drug Metabolism & Toxicology **[93].**

4.3. Distribution

It is the distribution of the compound throughout different compartments within the body **[91].** We used as parameters :

4.3.1. Blood-Brain-Barrier (BBB)

The blood–brain barrier (BBB) is a complex multicellular structure separating the central nervous system (CNS) from the systemic circulation. BBB is perhaps the most selective and tightly controlled of the barriers, reflecting the brain's critical roles in cognition, regulating metabolism and co-ordinating the functions of peripheral organs **[94].**

4.3.2. LogKp (Skin Permeation)

The greatest rate of dermal absorption from a pharmaceutical during saturation condition is quantified by a drug's skin permeability, which is a major element in dermatological risk assessment **[95].**

4.3.3. P-glycoprotein (P-gp) Substrate

Drug molecules are transported from the gastroenteric tract to the blood circle and permeate the gastroenteric membrane by various mechanisms. The primary mechanism is passive diffusion caused by a concentration gradient. P-gp is a common carrier in drugs intestinal penetration, which caused efflux process **[92]**.

4.4. Metabolism

is the biotransformation of drugs to facilitate their excretion **[91].** We were interested by :

4.4.1. CYP450

More than 80% of therapeutically used medicines are metabolized by these enzymes :

- ✓ Cytochromes P1A2
- ✓ Cytochromes P2C19
- ✓ Cytochromes P2C9
- ✓ Cytochromes P2D6
- ✓ Cytochromes P3A4

4.5.Toxicity

It is still one of the main causes of failed late-stage drug development since it determines how much a molecule may damage an organism or its components, including cells and organs **[91]** We used as parameters :

4.5.1. Ames test

Ames test is an assay to analyze a chemical's or drug's capacity to cause DNA mutations, this assay can be modeled *in silico* by using structure activity relationship **[96].**

4.5.2. Carcinogenecity (Mouse/Rat)

The Cancerogenicity is defined as a substance's ability to cause cancer **[96].**

4.5.3. hERG Inhibition

(human Ether-a-go-go-Related Gene), is a potassium (K+)-selective voltage-gated ion channel expressed in several organs and cell types. Since it is particularly abundant in the heart, it is essential for maintaining the cardiac action potential. The evaluation of the hERG inhibition of a compound at an early stage is quite important in the drug discovery process **[97].**

Results and discussion

IV. Results and Discussion

1. Results

1.1.Structure-activity relation (SAR)

We docked each of the five test ligands, namely, Ageladine A, Oroidin, Strepoxazine A, Cyclooroidin and Taurodispacamide A with our six targets separately. We found the following best results with each of the tested ligands**.**

The main parameter produced as a result of molecular docking is binding energy. It provides knowledge about the nature, strength, and affinities of the ligand-receptor interaction. The MD results represented by the values of the interaction energies for the five ligands, these values were observed in the range of: (PDB ID: 2IJM; -6.9 to -8.1 Kcal/mol), (PDB ID: 3DEI; -6.5 to -7.4 Kcal/mol), (PDB ID: 4FA6; -6.5 to -7.7 Kcal/mol), (PDB ID: 6USR ; -7.1 to -9.5 Kcal/mol) (PDB ID : 7LQZ ; -6.0 to -7.1 Kcal/mol), (PDB ID : 4EKK ; -7.2 to -8.8 Kcal/mol), respectively. These values are revealed in **table6**.

The values of the Repetition Rate (RR) (%) and the different interactions, including hydrophobic interactions and hydrogen bonds, formed between the inhibitor and the various amino acids present in the active sites of the six targets accompanied by values for the hydrogen bond distance.

Table 6. Binding energy values of the tested ligands.

Target PDB ID	Binding energy values and ranking of docked molecules
2IJM	**Mol3**<Mol5<Mol4<Mol2<Mol1 -8.1<-8.0<-7.3<-7.0<-6.9
3DEI	**Mol3**<Mol5<Mol1<Mol2<Mol4 -7.7<-7.4<-6.5<-6.4<-6.2
4FA6	**Mol3**<Mol2<Mol4<Mol1<Mol5 -7.7<-7.0<-6.7<-6.6<-6.5
6USR	**Mol3**<Mol1, Mol5<Mol2<Mol4 -9.5<-8.3, -8.3<-7.4<-7.1
7LQZ	**Mol3**=Mol1<Mol5<Mol2<Mol4 -7.1= -7.1<-6.9<-6.2<-6.0
4EKK	**Mol5**<**Mol3**<Mol4<Mol2<Mol1 -8.8<-8.7<-7.6<-7.3<-7.2

According to the results of molecular docking ranked by the tested ligand's binding energy value, all the ligands have a good binding affinity towards the receptor in different ways.

Mol3 is the best inhibitor among the other studied ligands based on the minimal energy values, RR %, and the number of hydrogen bonds, while **Mol4** is the last ranked inhibitor model

for the most of the six targets with the minimum served criteria comparing to the control. All the results are revealed in **table7**.

Based on its low energy value and RR%, **Mol5** is regarded as the best 4EKK inhibitor, additionally, to the total number of ten hydrogen bonds which are represented in **table7**.

Table 7. Molecular docking analysis of the five *Agelas oroides* S. and *Agelas nakamurai* H. compounds against the six NB targets.

Molecule	ΔG Affinity (kcal/mol)	Ki (μM)	RR%	Closest residues	Hydrogen bonds/ Length(Å)	Hydrophobic Interactions	Favorable/ Unfavorable Bond
Target PDB: 3DEI							
rxb	-8.0	1.34	100	PHE256 PHE256 LEU168 THR166 LEU168	THR166(2.45) LEU168(1.81)	Π-Π T-shaped Π-alkyl	6/0
Mol1	-6.5	16.9	90	PHE256 LEU168 THR166	THR166(2.90)	Π-Π T-shaped Π-Sigma	4/2
Mol2	-6.4	20.1	100	GLY122 GLU123 OCS163 PHE256 LEU168 THR166	THR166(2.21) GLY122(2.44) GLU123(2.37) OCS163(2.38)	Π-Sulfur Π-alkyl Π-Π T-shaped	7/2
Mol3	-7.7	2.23	100	PHE256 PHE256 THR166 LEU168	LEU168 (2.31)	Π-Π T-shaped Π-Sigma	6/0
Mol4	-6.2	28.2	100	THR166 THR166 PHE256 LEU168	LEU168(1.77) THR166(2.79) THR166(2.13)	Π-Π T-shaped	4/2
Mol5	-7.4	3.71	100	PHE256 LUE168 LYS259 THR166 GLY122 OCS163	THR166(2.18) OCS163(2.63) GLY122(2.44)	Π-Π T-shaped Π-Alkyl Charge - Charge	6/2

Target PDB: 4FA6							
0TA	-9.4	0.126	100	MET953 MET804 PHE961 ILE963 ILE831 ILE879 VAL882 TYR867	VAL882(2.30; 2.15)	Π-Sulfur, Π-alkyl Alkyl	14/0
Mol1	-6.6	14.3	80	MET953 ILE831 ILE963 ILE879 ASP964	ASP964(2.59)	Π-alkyl Π-Sigma	10/2
Mol2	-7.0	7.29	80	MET804 LYS890 ILE963 ILE879 ASP841	ASP841(2.49)	Π-Sulfur Π-Cation Π-alkyl	5/2
Mol3	-7.7	2.23	100	MET953 SER806, ILE831 ILE881 ILE879 ILE963 VAL882	VAL882(2.42)	Π-Sulfur, Π-Sigma Carbon Π-alkyl,	11/0
Mol4	-6.7	12.1	60	MET804 ILE963 ILE879 ILE831 ASP964 ASP841 TYR867	ASP964(2.50; 2.45) ASP841(2.41)	Π-Sulfur Π-alkyl Π-Sigma Acceptor- Acceptor	8/3
Mol5	-6.5	16.9	60	MET953 ILE963 ASP950 LYS890	ASP950(1.92; 2.02) LYS890(2.53; 2.73)	Π-Sigma, Π-Sulfur Π-alkyl	9/2

Target PDB: 6USR							
G2P	-10.5	0.0197	100	GLY309 U2 ARG194 C1 ASN369 ASP251 ALA255 LYS198 ARG253 ASP343 DA15	ALA255(2.37) ASN369(2.45) ARG194(2.79; 2.34) C1(2.0; 2.12)	Donor-Donor ∏-∏ stacked ∏-cation, ∏-donor; ∏-cation Charge-Charge Positive-Positive ; Charge –Charge; Carbon Carbon	36/4
Mol1	-8.3	0.811	100	ARG194 DA15 C1; U2	DA15(2.74) C1(2.44; 2.93) ARG194(1.97)	∏-cation, ∏-donor ∏-∏ stacked	10/2
Mol2	-7.4	3.71	90	ARG194 DC14 DT13 DA15 C1	DC14(2.56) DT13(2.59)	∏-cation, ∏-donor ∏-∏ T- shaped ∏-∏ stacked Donor-Donor	8/3
Mol3	-9.5	0.106	100	ARG194 ASP310 TYR256 ALA255 GLY309 DA15 C1; U2	GLY309(1.78) ASP310(3.07) C1(2.43) TYR256(1.96)	∏-cation; ∏-cation ∏-donor Carbon ∏-∏ T- shaped Π-alkyl ∏-∏ stacked,	22/0
Mol4	-7.1	6.16	90	ASP343 ALA255 ARG194 GLN308 DA15 C1	ALA255(2.13) GLN308(2.67) C1(2.18)	∏-Anoin Donor-Donor ∏-∏ stacked, Carbon	7/5
Mol5	-8.3	0.811	90	ARG194 LYS189 ASP251 DA15	LYS189(2.96)	Charge-Charge; ∏-cation Carbon ∏-Anoin ∏stacked; Nigative – Nigative	17/5

Target PDB: 7LQZ							
6EU	-8.7	0.41	100	LEU555, ALA568, LEU576, LEU517, TYR513, VAL520	TYR513(2.15)	Π-alkyl Alkyl Acceptor-Acceptor	8/1
Mol1	-7.1	6.16	100	LEU555, LEU517, ALA568 ASN553, TYR513, SER514,	SER514(2.20) ASN553(3.01)	Π-alkyl Carbon Π-Π T-shaped, Π-Π Stacked	10/2
Mol2	-6.2	28.5	100	ILE575, ASN553, TYR513, LEU517, SER514,	SER514(2.67; 2.79) ASN553(2.78)	Π-alkyl Π-Π T-shaped	7/2
Mol3	-7.1	6.16	100	ILE571, LEU517, THR552, ARG559, ASN553, TYR513,	ASN553(2.95; 2.78) ARG559(2.13) TYR513(2.37)	Π-alkyl Π-Sigma	8/0
Mol4	-6.0	39.5	90	ILE575, LEU517, ASN553, THR552, SER514	SER514(2.60; 3.05)	Π-alkyl Π-Sigma Carbon	6/2
Mol5	-6.9	8.64	60	MET549, ASN553, LEU517, ARG559, SER514, TYR513	SER514(2.85) ARG559(2.23) ASN553(2.57)	Π-alkyl Salt Bridge; Charge-Charge Π-Sulfur Carbon Π-Anion	9/2

Target PDB: 2IJM							
ATP	-8.3	0.811	95	LYS454, VAL436, ILE428, ALA452, MET499, GLU500, ARG550, GLU506, LEU553, CYS502,	LYS454(2.91 ; 2.43) MET499(2.40) CYS502(1.94) GLU506(3.10) ARG550(2.23) GLU500(1.85)	Salt Bridge; Charge-Charge Charge-Charge Π-alkyl Π-Sigma Carbon	23/0
Mol1	-6.9	8.64	90	LEU553, GLU506, ASP564, ARG550	GLU506(2.25) ARG550(2.91)	Π-alkyl Π-Anion	4/2
Mol2	-7.0	7.2	95	GLU471 PHE565 LYS454 VAL436 ASN551 LEU553	GLU471(2.42) PHE565(2.61; 2.82)	Π-alkyl Π-Cation, Π-Donor Π-Sigma Carbon	7/2
Mol3	-8.1	1.13	100	LEU553, ASN551, ASP564, GLN432, ALA452, VAL436, MET499, LYS454	ASN551(2.21) ASP564(2.39) LYS454(2.18)	Π-alkyl Donor-Donor Π-Sigma Π-Sulfur Carbon	12/1
Mol4	-7.3	4.39	50	LEU553, ARG550, ASN551, GLU506, LYS454, ILE428, MET499	ILE428(2.40) ASN551(2.18) ARG550(2.68; 2.70)	Π-alkyl Π-Sulfur Π-Cation Π-Anion	8/2
Mol5	-8.0	1.34	90	LEU553, GLU506, ASN551, ARG550, LYS454, VAL436, PHE433,	ARG550(2.70; 2.76; 2.80) ASN551(3.03) GLU506(2.68)	Π-Sulfur Charhe-Charge Π-alkyl Donor-Donor Π-Sigma	10/3

Target PDB: 4EKK							
AMP-PNP	-9.7	0.076	90	THR160 GLU228 ALA230 GLU234 LYS276 VAL164 ALA177 ASP292 ARG4 MET281 LEU156	THR160(1.97) GLU228(2.52) ALA230(1.91) GLU234(1.99) LYS276(2.89; 2.55) ARG4(2.23)	Donor-Donor Charge-Charge Salt Bridge: Charge-Charge ∏-Alkyl Carbon ∏-Sulfur	23/1
Mol1	-7.2	5.20	100	LEU295 ASP292 GLU198 LYS179 PHE161	GLU198(2.37) ASP292(3.08) LYS179(2.55)	∏-∏ T shaped Donor-Donor ∏ -Alkyl ∏ -Anoin	11/3
Mol2	-7.3	4.39	90	THR291, MET281 ALA177 VAL164 ARG4 THR5	THR291(2.41; 1.98) ARG4(2.38) THR5(1.94)	∏-Cation ∏-Alkyl ∏-Sigma	8/2
Mol3	-8.7	0.412	100	GLU198 LYS179 PHE161 ASP292 SER7 THR5 LYS272 ARG4	LYS179(2.55) ASP292(2.83; 1.98) ARG4(2.94) SER7(2.11) LYS272(2.14)	∏-∏ T Shaped ∏ Cation - ∏Donor Carbon	14/0
Mol4	-7.6	2.64	100	LYS276 ASN279 ASP292 THR291 VAL164	ASN279(2.57) THR291(2.83; 2.10) ASP292(2.74; 2.24)	∏- Sigma Donor-Donor	7/3
Mol5	-8.8	0.348	100	VAL164 MET281 ARG4 LYS276 SER7 THR160 ASP292 THR291 LYS179 PHE161	THR160(2.01) SER7(2.40; 2.36; 2.51) THR291(2.03; 2.35) ASP292(3.09) ARG4(2.71) LYS276(2.27) LYS179(2.90)	∏-Sigma ∏-Alkyl ∏-∏ T Shaped Donor-Donor Salt Bridg: Charge-Charge	16/3

1.2. ADMET Analysis

A drug's success is influenced by both its effectiveness and its ADMET profile, in addition to its efficacy. With availability of large variety of medium- and high-throughput in vitro ADMET screens, it might be helpful to be able to predict some of these qualities, previously. It is now understood that using computational ADMET together with *in vivo* and *in vitro* predictions as early as possible in the drug discovery process helps in reducing the amount of safety issues **[98].**

The transformation of a medication in the body after administration is typically described as a series of pharmacokinetic steps, including absorption, distribution, metabolism, and excretion. Each of these steps requires the active principle to pass via cellular interfaces, whether it is to enter the bloodstream from the site of administration (the gastrointestinal tract, the skin, the ears, etc.) or to transfer blood to the targeted tissues or organs involved in its excretion. **[99].**

HIA and access to the central nervous system (CNS) by penetration into the BBB is useful for drug discovery and development. Through human intestinal absorption, orally administered drugs are absorbed from the gastrointestinal system into the bloodstream. The BBB can be considered as a shield protecting the brain, while P-gp is responsible for the efflux of substrates from inside to outside the cell. Although active transport is important, passive diffusion is the major route for drugs to access the brain from the bloodstream **[100].**

CYP450 is a superfamily of isoenzymes, which plays a crucial role in drug elimination through metabolic biotransformation. Drugs can be metabolized through oxidative reactions (phase I) and conjugative reactions (phase II). From the 57 CYP isoforms (phase I enzymes), five isoenzymes; 1A2, 2C9, 2C19, 2D6, and 3A4 are responsible for the metabolism of >80% of clinically used drugs. The examination of the interactions of CYPs with potential drugs is one of the important steps in drug design **[100].**

The ADMET parameters were determined and verified for quantification with their standard ranges, then represented in **table8**.

Table 8. ADMET results of the five studied molecules

Parameters		Mol1	Mol2	Mol3	Mol4	Mol5
Physicochemical Properties	Formula	$C_{10}H_7Br_2N_5$	$C_{11}H_{11}Br_2N_5O$	$C_{17}H_{14}N_2O_6$	$C_{11}H_{11}Br_2N_5O$	$C_{13}H_{16}Br_2N_6O_4S$
	Molecular weight	357.00 g/mol	389.05 g/mol	342.30 g/mol	389.05 g/mol	512.18 g/mol
	Num. rotatable bonds	1	5	4	2	8
	Num. H-bond acceptors	2	2	6	2	6
	Num. H-bond donors	3	4	4	3	5
	TPSA	83.38 Å²	99.59 Å²	131.11 Å²	88.73 Å²	170.41 Å²
Lipophilicity	Log $P_{o/w}$ (iLOGP)	1.56	1.26	1.93	1.18	0.80
	Log $P_{o/w}$ (XLOGP3)	2.27	2.00	2.39	1.52	0.20
	Log $P_{o/w}$ (WLOGP)	3.07	2.19	2.21	1.47	1.07
	Log *S* (ESOL)	-4.03	-3.57	-3.56	-3.47	-2.76
Absorption	Human Intestinal Absorption (HIA%) 80 to 100%	0.9943 (High)	0.9753 (High)	0.7865 (High)	0.9867 (High)	0.6218 (Low)
	Caco-2 Cell permeability (nm/sec)>20	0.6152	0.6328	0.8006	0.5526	0.9022
	Water Solubility(mg/l)	Moderately soluble	Soluble	Soluble	Soluble	Soluble
Distribution	Blood-Brain Barrier >2(C.brain/C.blood) cross the BBB easily	0.5250 (No)	0.7250 (No)	0.7429 (No)	0.6750 (No)	0.5750 (No)
	Log Kp (Skin permeation) <-2.5 considered high Permeable	-6.87 cm/s	-7.25 cm/s	-6.69 cm/s	-7.59 cm/s	-9.28 cm/s
	Plasma protein binding (%) 80 to 100% (high), 50 to 80% (moderate), <50% (low)	0.768 Moderate	0.746 Moderate	0.793 Moderate	0.691 Moderate	0.616 Moderate
	P-gp Substrate	Yes	No	Yes	Yes	Yes
	P-glycoprotein inhibitior	0.9465	0.9360	0.8290	0.5106	0.7058
Metabolism	Cytochrome P450 CYP1A2 inhibitor	Yes	Yes	Yes	Yes	No
	CYP2C19 inhibitor	No	No	No	Yes	Yes
	CYP2C9 inhibitor	No	No	No	No	No
	CYP2D6 inhibitor	Yes	No	No	No	No
	CYP3A4 inhibitor	Yes	Yes	No	Yes	No
	Lipinski Rule	Yes; 0 violation	Yes; 0 violation	Yes; 0 violation	Yes; 0 violation	Yes ; 1 violation
Toxicity	algae_at	0.0337963	0.0225075	0.0575396	0.0658392	0.0141849
	Ames_test	Mutagen	Mutagen	Mutagen	Mutagen	Mutagen
	Carcino_Mouse	Positive	Positive	Negative	Positive	Positive
	Carcino_Rat	Positive	Positive	Positive	Positive	Positive
	hERG_inhibition	Medium_risk	Medium_risk	Medium_risk	Medium_risk	High_risk

HERG: Human ether related gene channel, **Caco-2**: Human colorectal carcinoma, **Kp**: skin permeability constant **Green**: high, **Red**: low, **Orange**: medium.

2. Discussion

2.1. Structure activity relation SAR

2.1.1. Focal Adhesion Kinase 1 (FAK) (PDB ID: 2IJM)

- **ATP ($C_{10}H_{16}N_5O_{13}P_3$)** also named **ATP-gamma-32P.** In biochemical and molecular biology research, [gamma-32P]-ATP is a radioactive isotope of adenosine triphosphate (ATP). The third phosphate group of ATP contains the radioactive isotope of phosphorus, which is where the term "gamma" refers to. It is a binding compound for the FAK protein. According the MD results, it has a RR of 95% and an energy value of -8.3 Kcal/mol (**Table7**). ATP takes a triangular shape and is directed to the upper part of the active site cavity (**Appendix2**). It forms numerous hydrophobic types such as Pi-Alkyl, Pi-Sigma, Pi-Sulfur, Carbon hydrogen bond, Attractive charge and a salt bridge interaction, in addition hydrogen bonds with the binding site's amino acids (**Figure17**). In a total 23 favorable interactions, 10 of which were formed with the Purine function (main function) which shows the preferred orientation of ATP to FAK.

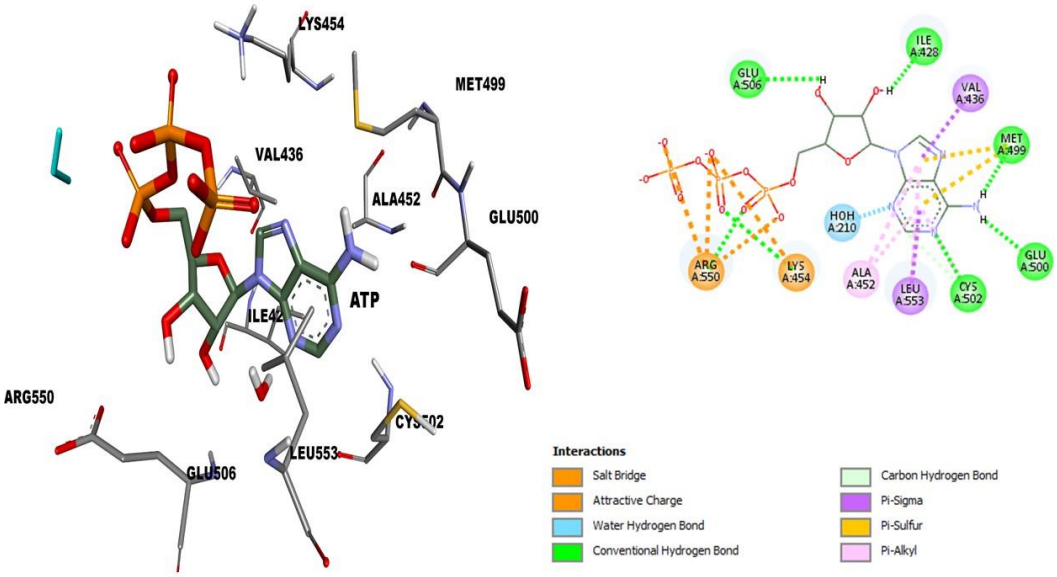

Figure 17 : Best 2D and 3D docking pose of ATP with FAK enzyme.

The predicted MD results show significant inhibition by the used marine alkaloids inside the active site with 55.26% hydrophobic interactions.

- **Mol1**

Ageladine A is a pyrrole-imidazole alkaloid identified as 1H-imidazo[4,5-c]pyridin-2-amine, whose structure shows the presence of an aromatic ring skeleton. Mol1 is substituted with a

4,5-dibromo-1H-pyrrol-2-yl group at position 4 and acts as a matrix metalloproteinase inhibitor **[72]**. MD results show that the best pose of Mol1 takes a horizontal shape and prefers the side chains of the pyridine and pyrrole rings as the first to enter deeply into the active site, which explains its affinity with an RR value of 90% and its stability with an energy of -6.9 kcal/mol (**Table7**) was ranked the 5th among all inhibitors (**Table6**) in comparison to ATP ligand. Mol1 forms hydrogen bonds and hydrophobic interactions with four different amino acids such as Leu553, Asp564, Glu506 and Arg550 (**Table7**). The pyridine and pyrrole side chains react with the amino acids of the binding site such as Leu553 and Asp564, forming Pi-Alkyl and Pi-Anion types of hydrophobic interactions, wherein Leu553 and Asp564 play an important role in stabilizing the pyridine and pyrrole rings. In addition, imidazole hydroxyl groups react with Glu506 and Arg550 and form a conventional hydrogen bond (**Figure18**).

In total, four favorable interactions were formed. Md shows that the preferred orientation of Mol1 to FAK was close to the nonpolar amino acid Leu553.

- **Mol2**

Oroidin is the simplest bromopyrrole-imidazole alkaloid, it is also known as N-[(E)-3-(2-amino-1H-imidazol-5-yl)prop-2-enyl]-4,5-dibromo-1H-pyrrole-2-carboxamide. It has a linear structure characterized by a bromopyrrole carboxamide and an amino-imidazole group linked by a propenyl chain. Structurally, Mol2 was docked in a triangular shape and the pyrrole ring side is the first side that penetrates deep into the active site according to MD results, which explains its affinity for FAK, its RR value was 95% with an energy value of -7.0 kcal/mol considerably lower than mol1 (**Table7**) ranked the 4th among other inhibitors (**Table6**) compared to the ATP ligand. Mol2 forms a total of seven hydrogen bonds and one hydrophobic interaction with six different amino acids such as Val436, Asn551, Leu553, Phe565, Glu471 and Lys454. The pyrrole ring shows two hydrophobic interactions type Pi-Sigma and Pi-Alkyl with Leu553 and Val436, respectively, the propenyl chain forms a carbon hydrogen bond with Asn551. Meanwhile, the imidazole ring shows four interactions, including a Pi-Cation hydrophobic interaction with Lys454 and three hydrogen bonds, including two with Phe565 and one with Glu471 (**Figure18**).

A total of seven favorable interactions, 4 of which are formed with the pyrrole ring backbone, which was responsible for the best orientation inside the active site cavity.

- **Mol3**

Strepoxazine A is a cytotoxic phenoxazine analog identified as 9-(1-amino-2-hydroxy-3-methoxy-3-oxoprop-1-enyl)-10H-phenoxazine-4-carboxylic acid isolated from solid culture of *Streptomyces sp*. SBT345 associated with sponge **[75]**. MD results show that the best pose of

Mol3 is vertical and the side chain of the benzene ring is the first to penetrate deep into the binding site, which explains its high affinity to FAK, its RR value was 100% this shows that all positions on the active site were located and its energy was -8.1 kcal/mol. These two results are the highest among the other compounds (**Table7**) as compared to ATP ligand, it has to be the best inhibitor for FAK enzyme. Mol3 forms a total of eight hydrogen bonds and hydrophobic interactions with amino acids namely Gln432, Lys454, Asp564, Asn551, Leu553, Val463, Met499, and Ala452. In addition, one formed interaction with a water molecule.

The benzene ring of Mol3 was directed to the upper part of the active site and formed Pi-Sigma, Pi-Sulfur, and Pi-Alkyl hydrophobic interactions with amino acids such as Ala452; Met499, Val463, Lys454, and Leu553 which play an important role in stabilizing Mol3. The piperidine ring formed Pi-Alkyl hydrophobic interactions with Val463 and Leu553. However, the amine function saved two conventional hydrogen bonds with Asn551 and Asp564, and the two-hydroxyl functions formed hydrophobic interactions with Gln432 and with a water molecule (**Figure18**). A total of 12 interactions were favorable, 5 of which were formed with the backbone of the benzene ring, this ring being responsible for the best preferred orientation within the active site. Therefore, Mol3 is centralized alongside Ala452, Met499, Val436, Leu553, and Lys454 as the preferred type due to their nonpolar nature.

- **Mol4**

Cyclooroidin is a pyrrole-imidazole alkaloid known as (4S)-4-[(2-amino-1H-imidazol-5-yl)methyl]-6,7-dibromo-3,4-dihydro-2H-pyrrolo[1,2 a]pyrazin-1-one. MD results show that Mol4 takes a triangular shape like Mol2 as the preferred pose and the imidazole ringside is the first to penetrate into the binding site, which explains its affinity for FAK protein, its RR value was lower than all other inhibitors (50%), and its energy value was -7.3 kcal/mol (**Table7**). As instead of ATP ligand, it was ranked the 3rd among other inhibitors (**Table6**).

The imidazole ring of Mol4 binds to the active site by forming a hydrophobic; Pi-Cation type interaction with Glu506 and a hydrogen bond with Ile428. In addition, the piperidine ring forms two hydrogen bonds with Arg550 and Asn551. The pyrrole ring forms three hydrophobic interactions; type Pi-Sulfur, Pi-Alkyl, and Pi-Anion with Met499, Leu553, and Lys454, respectively (**Figure18**), the latter being essential for the stabilization and orientation of Mol4. The pyrrole function is considered the most reactive function in the studied molecule; it is responsible for three of the eight favorable interactions. The piperidine ring saved no interaction with the studied protein.

- **Mol5**

Taurodispacamide A is the fourth tested pyrrole-imidazole alkaloid, identified as N-[3-[2-Imino-4-[(2-sulfoethyl)amino]-1H-imidazole-5(2H)-ylidene]propyl]-4,5-dibromo-1H-pyrrole-2-carboxamide. MD results show a RR value of 90% and an energy of -8.0 kcal/mol (**Table7**) ranked the 2nd among other inhibitors (**Table6**) as compared with ATP ligand, it is one of the greatest FAK inhibitors. Which explains its affinity with this protein, the best orientation of mol5 takes a triangular shape like Mol2 and Mol4. The pyrrole ringside was the first to approach the active site. Mol5 recorded numerous interactions with amino acids such as Phe433, Arg550, Asn551, Lys454, Glu506, Val436, and Leu553 also with a water molecule. In addition, Phe433 and Lys454 form hydrophobic interaction type Pi-Sulfur with the sulfonate function of Mol5, Arg550 and Asn551 form three hydrogen bonds with the imidazole ring. However, the carbonyl function forms a hydrogen bond with Glu506 and the water molecule. Val436 and Leu553 form two hydrophobic interactions type Pi-Alkyl and Pi-Sigma with the Mol5 pyrrole ring (**Figure18**). Both, Val436 and Leu553, could strongly participate in the stability of Mol5. With 10 favorable interactions, two of them are formed with the pyrrole ring (main reactive function); Mol5 was centralized alongside hydrophobic amino acids as the preferred type due to its non-polarity.

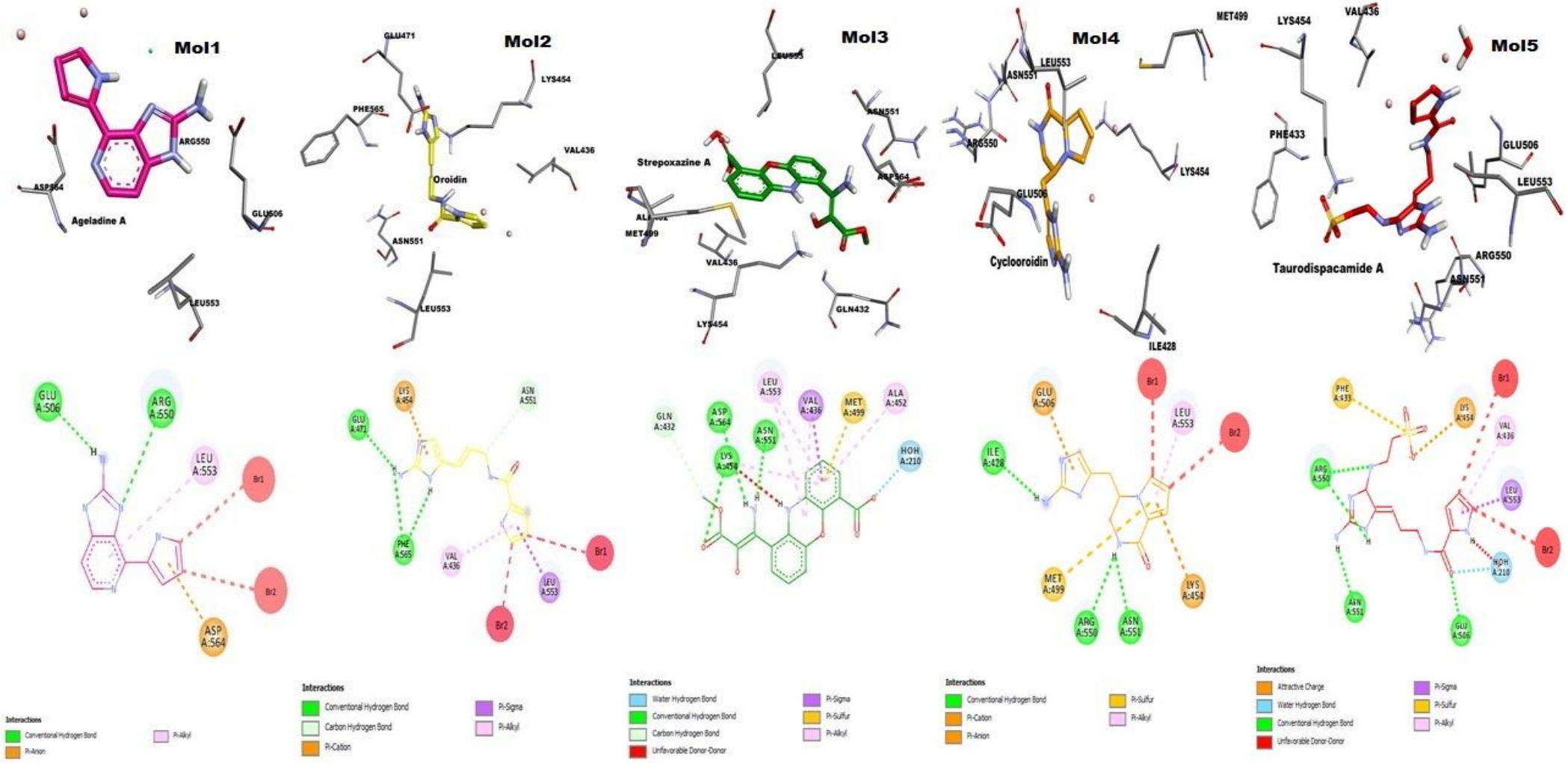

Figure 18 : 2D and 3D best docking poses of the fives ligands with FAK enzyme.

2.1.2. Caspase-3 protein (PDB ID: 3DEI)

- **Rxb ($C_{19}H_{14}N_2O_6$)** also named **(1S)-2-oxo-1-phenyl-2-[(1,3,4-trioxo-1,2,3,4-tetrahydroisoquinolin-5-yl)amino]ethyl acetate.** It is used in the study of apoptosis and in the creation of treatments for diseases like cancer and neurodegenerative disorders where abnormal apoptosis is involved. It serves as the protein caspase-3's inhibitor. It has a RR of 100% and an energy value of -8.0 Kcal/mol, according to the MD findings (**Table7**). It enters deep inside the active site cavity, with a triangular shape (**Appendix3**). With the amino acids at the binding site, specifically Phe256, Phe256, Leu168, Thr166, and The168, it forms two hydrogen bonds as well as hydrophobic types such as Pi-Pi T-shaped and Pi-Alkyl interactions (**Figure19**). Six favorable interactions were observed, four of which were associated with the Piperidine function (main function), demonstrating rxb's preferential orientation to caspase-3.

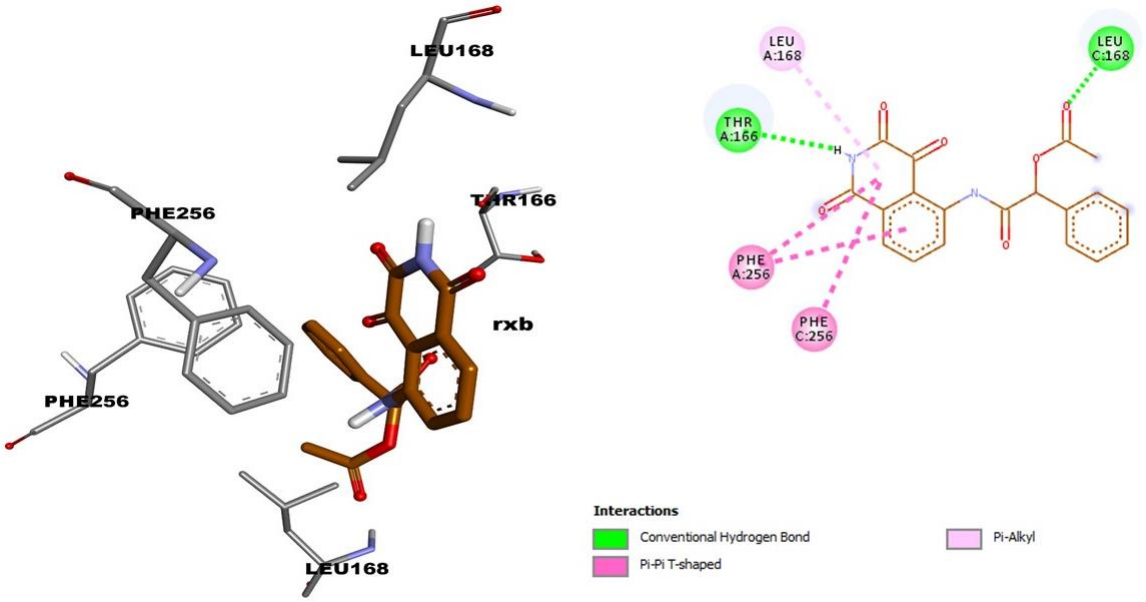

Figure 19 : Best 2D and 3D docking pose of rxb with caspase-3 enzyme.

The predicted MD results show significant inhibition by the used marine alkaloids inside the active site with 47.82% hydrophobic interactions.

- **Mol1**

The structure and the function of Ageladine A was already described in the previous part. according the MD, the best pose of Mol1 takes a vertical shape and prefers the side chains of the pyrrole ring as the first to enter deeply into the active site, which explains its affinity with a RR value of 90% and its stability with an energy of -6.5 kcal/mol (**Table7**) ranked the 3rd among

other inhibitors (**Table6**) instead of rxb inhibitor. Mol1 forms hydrogen bonds and hydrophobic interactions with four different amino acids such as Phe256, Phe256, Leu168 and Thr166 (**Table7**).

The pyridine and pyrrole side chains react with the amino acids of the binding site such as Leu168 and Phe256, forming Pi-Sigma and Pi-Pi T-shaped types of hydrophobic interactions, the pyrrole hydroxyl group reacts with Thr166 and forms a conventional hydrogen bond. Wherein Leu168 and Phe256 play an important role in stabilizing the pyridine and pyrrole rings. In addition, imidazole reacts with Phe256 and form a Pi-Pi T-shaped interaction (**Figure20**).

In total, four favorable interactions were formed. MD shows that the preferred orientation of Mol1 to caspase was close to the nonpolar amino acid Phe256.

- **Mol2**

Mol2 was docked in a triangular shape and the imidazole ring side is the first side that penetrates deep into the active site according to MD results, which explains its affinity for caspase-3, its RR value was 100% with an energy value of -6.4 kcal/mol considerably higher than mol1 (**Table7**) and ranked the 4th among other inhibitors (**Table6**) contrasted with rxb. Mol2 forms a total of four hydrogen bonds and two hydrophobic interactions with six different amino acids such as Gly122, Glu123, Ocs163, Thr166, Leu168 and Phe256. The pyrrole ring shows two hydrophobic interactions type Pi-Pi T-shaped and Pi-Alkyl with Phe256 and Leu168 respectively, the hydroxyl group reacts with Thr166 and forms a conventional hydrogen bond. Meanwhile, the imidazole ring shows three hydrogen bonds, including Gly122, Glu123 and Ocs163 (**Figure20**). A total of seven favorable interactions, 3 of which are formed with the pyrrole ring backbone, which was responsible for the best orientation inside the active site cavity.

- **Mol3**

MD results show that the best pose of Mol3 is horizontal and the side chain of the benzene ring is the first to penetrate deep into the binding site, which explains its high affinity to caspase-3, its RR value was 100% and its energy was -7.7 kcal/mol. These two results are the highest among the other compounds (**Table7**), which is able to be the best inhibitor for this studied enzyme. Mol3 forms a total of five hydrogen bond and hydrophobic interactions with amino acids namely Leu168, Phe256, Phe256 and Thr166.

The benzene ring of Mol3 was directed to the upper part of the active site and formed Pi-Sigma hydrophobic interaction with Thr166. The piperidine ring formed two Pi-Pi T-shaped

with the Phe256 of the two different protein chains. The other benzene ring forms as well a Pi-Pi T-shaped interaction with Phe256. However, the carbonyl function saved one conventional hydrogen bond with Leu168 (**Figure20**). A total of 6 interactions were favorable, 2 of which were formed with the backbone of the piperidine ring, this ring being responsible for the best preferred orientation within the active site. Therefore, Mol3 is centralized alongside Phe256 as the preferred type due to its nonpolar nature.

- **Mol4**

MD results show that Mol4 takes a triangular shape like Mol2 as the preferred pose and the imidazole ringside is the first to penetrate into the binding site, which explains its affinity for caspase-3 protein, its RR value was 100%, and its energy value was -6.2 kcal/mol higher than all the other inhibitors (**Table7**) as contrasted to rxb ligand.

The imidazole ring of Mol4 binds to the active site by forming a hydrophobic; Pi-pi T-shaped type interaction with Phe256 and a hydrogen bond with Thr166. In addition, the piperidine ring forms two hydrogen bonds with Thr166 and Leu168 (**Figure20**). The imidazole ring was essential for the stabilization and orientation of Mol4, which is considered as the most reactive function in the studied molecule; it is responsible for the two of the four favorable interactions.

- **Mol5**

MD results show a RR value of 100% and an energy of -7.4 kcal/mol (**Table7**) ranked the 2nd among other inhibitors, which explains its affinity with caspase-3, the best orientation of mol5 takes a triangular shape like Mol2 and Mol4. The pyrrole ringside was the first to approach the active site. Mol5 recorded numerous interactions with amino acids such a Gly122, Ocs163, Thr166, Leu168, Phe256 and Lys259. In addition, Phe256 and Leu168 form hydrophobic interaction type Pi-Pi T-shaped and Pi-alkyl and a hydrogen bond with Thr166 to the pyrrole ring of Mol5, Gly122 and Ocs163 form two hydrogen bonds with the imidazole ring. However, the sulfonate function forms an attractive charge interaction with Lys259. Both, Leu168and Phe256, could strongly participate in the stability of mol5 (**Figure20**). With 6 favorable interactions, three of them are formed with the pyrrole ring (main reactive function). Mol5 was centralized alongside hydrophobic amino acids as the preferred type due to its non-polarity.

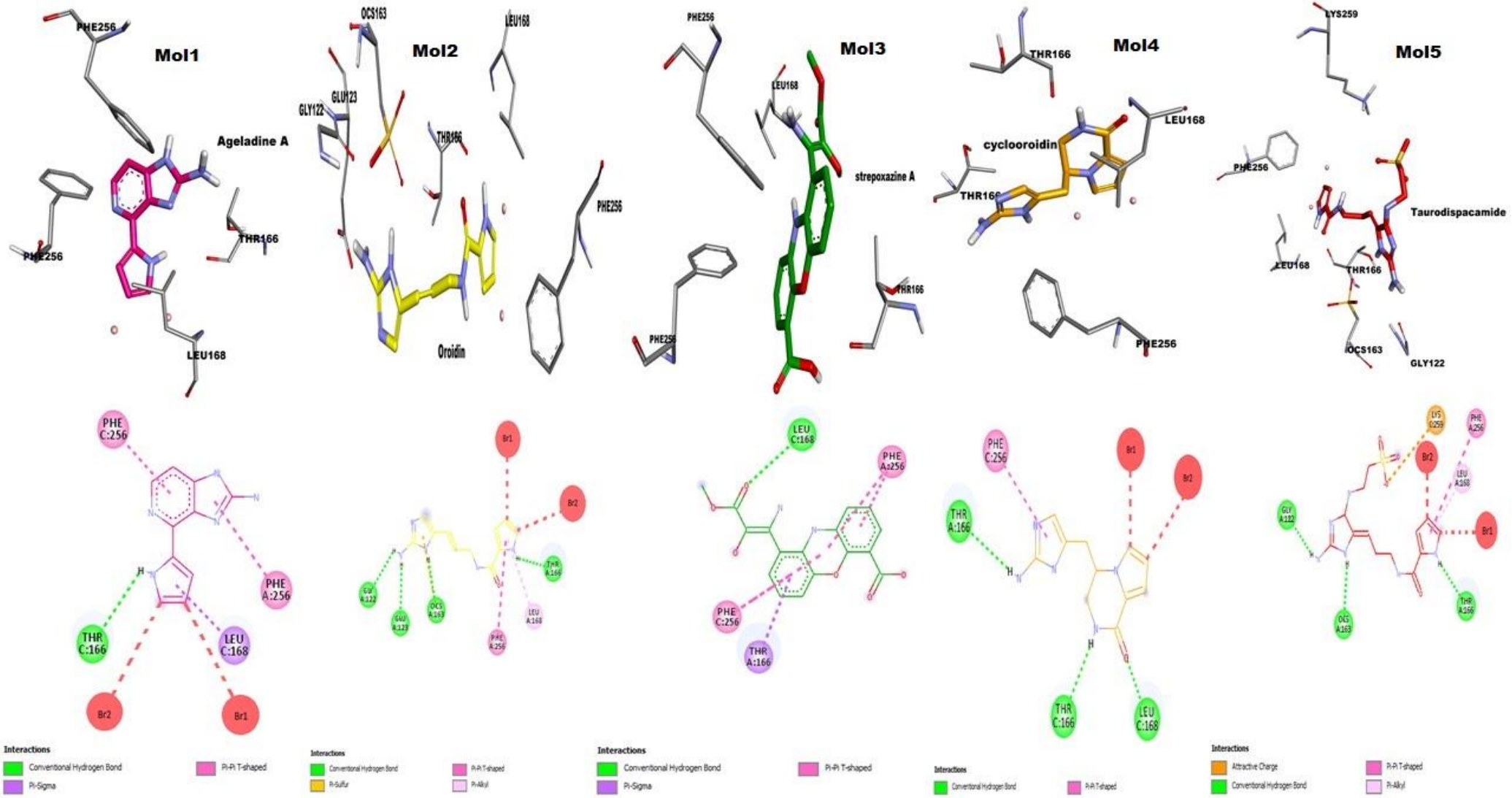

Figure 20: 2D and 3D best docking pose of the five ligands with Caspase-3 enzyme.

2.1.3. Gamma isoform of the catalytic subunit of phosphatidylinositol 4,5-bisphosphate 3-kinase (PI3K) (PDB ID: 4FA6)

- **0TA ($C_{16}H_{18}N_6O$)** named also **2-Amino-8-Cyclopentyl-4-Methyl-6-(1h-Pyrazol-4-Yl)pyrido[2,3-D]pyrimidin-7(8h)-One,** has potential therapeutic applications in the treatment of cancers and other diseases where the PI3K pathway is dysregulated or overactivated, it acts as an inhibitor of the PI3K protein. The MD results (**Table7**) show that has a 100% RR and an energy value of -9.4 Kcal/mol. 0TA is triangular in shape and is located to the upper part of the active site cavity (**Appendix4**). Specifically, the amino acids Met953, Met804, Phe961, Ile963, Ile831, Ile879, Val882, and Tyr867 are at the binding site. Along with hydrophobic types like Pi-Alkyl, Alkyl, and Pi-Sulfur interactions, it also forms two hydrogen bonds. Four of the beneficial interactions (**Figure21**), 14 in total were connected to the Pyrimidine function (main function), indicating 0TA's preference orientation for Pi3K.

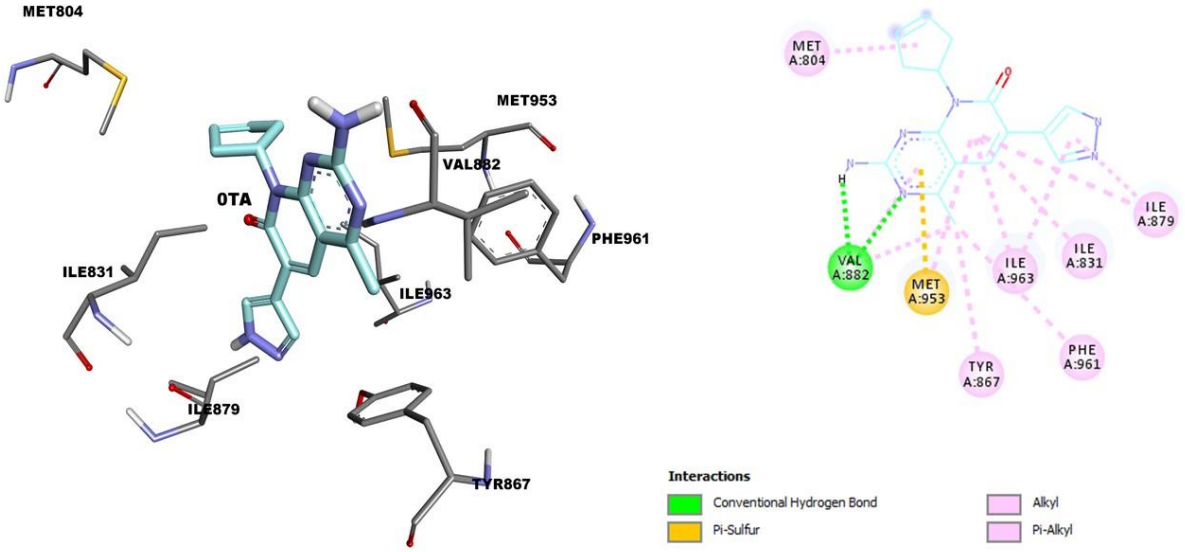

Figure 21 : Best 2D and 3D docking pose of 0TA with PI3K enzyme.

The predicted MD results show significant inhibition by the used marine alkaloids inside the active site with 70% hydrophobic interactions.

- **Mol1**

According the MD, the best pose of Mol1 takes a vertical shape and prefers the side chains of the pyrrole ring as the first to attached to the active site, which explains its affinity with an RR value of 80% and its stability with an energy of -6.6 kcal/mol (**Table7**) ranked the 4th among other inhibitors (**Table6**) compared to 0TA inhibitor. Mol1 was directed to the upper part of the active site and forms hydrogen bond and hydrophobic interactions with five different amino acids such as Ile831, Ile879, Met953, Ile963 and Asp964.

The pyrrole and pyridine form a Pi-Alkyl and Pi-Sigma interactions with amino acids such as Ile831, Ile879, Met953 and Ile963 respectively, wherein Ile831, Ile879, Met953 and Ile963 play an important role in stabilizing the pyrrole and pyridine rings. In addition, the imidazole ring forms a Pi-Alkyl interactions with the amino acids Ile879 and Ile963 and forms a conventional hydrogen bond with Asp964 (**Figure22**).

In total, 10 favorable interactions were formed. Md shows that the preferred orientation of Mol1 to caspase was close to the nonpolar amino acids.

- **Mol2**

Mol2 was docked in a triangular shape and the imidazole ring side is the first side that penetrates into the active site according to MD results, which explains its affinity for PI3K, its RR value was 80% with an energy value of -7.0 kcal/mol (**Table7**) ranked the 2nd among the other inhibitors (**Table6**) as instead to 0TA inhibitor. Mol2 forms a total of one hydrogen bond and four hydrophobic interactions with five different amino acids such as Asp841, Met804, Lys890, Ile879 and Ile963. The pyrrole ring shows two hydrophobic interactions type Pi-Sulfur and Pi-Cation with Met804 and Lys890 respectively (**Figure22**). Meanwhile, the imidazole ring shows a hydrogen bond with Asp841 and forms two Pi-alkyl interactions with Ile879 and Ile963; which increase its polarity.

A total of five favorable interactions, 3 of which are formed with the imidazole ring backbone, which was responsible for the best orientation inside the active site cavity.

- **Mol3**

MD results show that the best pose of Mol3 is vertical and the side chain of the benzene ring is the first to penetrate in the upper part of the binding site, which explains its high affinity to PI3K, its RR value was 100% and its energy was -7.7 kcal/mol. These two results are the highest among the other compounds (**Table7**) in regard to 0TA ligand. Mol3 forms a total of 10

hydrogen bond and hydrophobic interactions with amino acids namely, Val882, Ile881, Ile831, Ile963, Ile879, Met953 and Ser806.

The two benzene rings of Mol3 formed Pi-Sigma, Pi-Sulfur, Pi-Alkyl, hydrophobic interactions with amino acids such as Ile831, Ile963, Ile879 and Met953, which play an important role in stabilizing Mol3. However, the carbonyl function saved one conventional hydrogen bond with Val882 and the two hydroxyl functions formed hydrophobic interactions with Ile881 and Ser806. The piperidine ring formed Pi-Alkyl and Pi-Sigma hydrophobic interactions with Ile831, Ile879 and Ile963 respectively (**Figure22**), a total of 11 interactions were favorable, 4 of which were formed with the backbone of the benzene ring, this ring being responsible for the best preferred orientation within the active site. Therefore, Mol3 is centralized alongside Ile881, Val882, Ile831 and Met953 as the preferred type due to their nonpolar nature.

- **Mol4**

MD results show that Mol4 takes a triangular shape like Mol2 as the preferred pose and the imidazole ringside is the first to penetrate into the binding site, which explains its regular affinity for PI3K protein, its RR value was lower than all other inhibitors (60%), and its energy value was -6.7 kcal/mol (**Table7**) ranked the 3rd among other inhibitors (**Table6**).

The pyrrole ring forms three hydrophobic interactions; type Pi-Sulfur, Pi-Alkyl, and Pi-Sigma with Met804, Ile963 and Ile831 respectively. In addition, the imidazole ring of Mol4 binds to the active site by forming three hydrophobic; Pi-Alkyl type interactions with Ile879, Ile963 and an Acceptor-Acceptor interaction with Thr867. Meanwhile, it forms three hydrogen bonds with Asp964 and Asp841 (**Figure22**), the latter being essential for the stabilization and orientation of Mol4. The imidazole function is considered the most reactive function in the studied molecule; it is responsible for four of the eight favorable interactions.

- **Mol5**

MD results show a RR value of 60% same as Mol4 and an energy of -6.5 kcal/mol (**Table7**) was ranked 5th among other inhibitors (**Table6**) which explains its typical affinity with PI3K, the best orientation of mol5 takes a triangular shape like Mol2 and Mol4. Asp950 form two hydrogen bonds with the amine groups of the Mol5's imidazole ring. The pyrrole ringside was the first to approach the active site. Mol5 recorded numerous interactions with amino acids such as Lys890, Asp950, Met953 and Ile963. In addition, Ile963 and Met953 form hydrophobic interaction types Pi-Alkyl, Pi-Sigma and Pi-Sulfur with the pyrrole function of Mol5. However,

the carbonyl function forms a hydrogen bond with Lys890. Both, Ile963 and Met953, could strongly participate in the stability of Mol5 (**Figure22**). With 9 favorable interactions, three of them are formed with the pyrrole ring (main reactive function); Mol5 was centralized alongside hydrophobic amino acids as the preferred type due to its non-polarity.

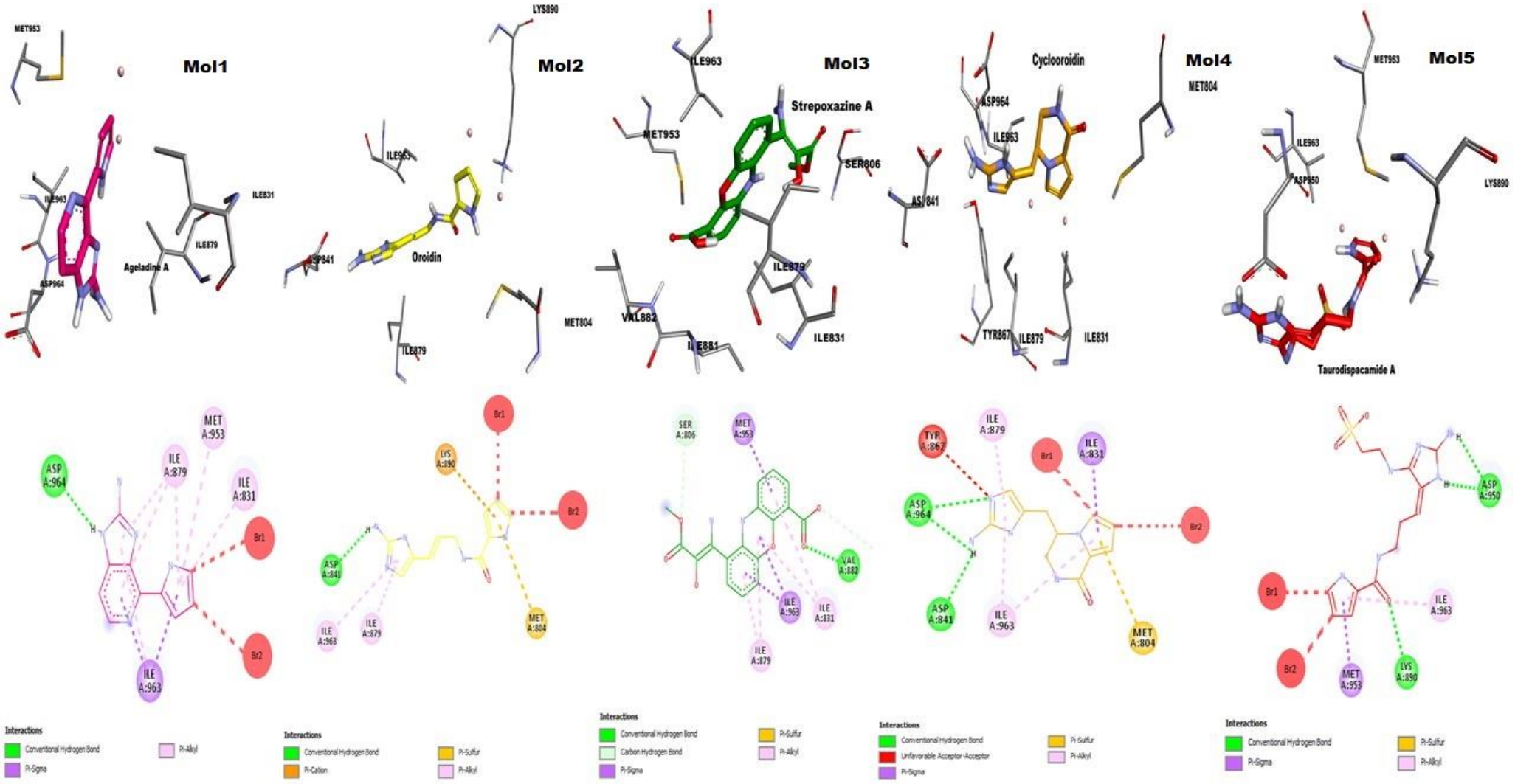

Figure 22 : 2D and 3D best docking poses of the five ligands with PI3K enzyme.

2.1.4. Telomerase reverse transcriptase (TERT) (PDB ID: 6USR)

- **G2P ($C_{11}H_{18}N_5O_{13}P_3$)** also named **Phosphomethylphosphonic acid guanylate ester,** It functions as a TERT protein inhibitor and has possible applications in the treatment of tumors and other disorders. The MD results (**Table7**) indicate that it has a 100% RR and an energy value of **-10.5 Kcal/mol** which explains its exceptional affinity to TERT enzyme. G2P is positioned in the top area of the active site cavity and has a triangular shape (**Appendix5**). The binding site is specifically occupied by the amino acids Gly309, Asp251, and Asp343, as well as certain residues like DA15, U2, and C1. In addition to hydrophobic forms like Pi-Cation, Pi-Pi T-stacked, carbon hydrogen bond and attracted charge interactions (**Figure23**). It produces six hydrogen bonds, besides the unfavorable and metal interactions. 25 out of the 36 favorable interactions had the Purine and triphosphate functions as the main ones, confirming G2P's orientation and affinity for TERT.

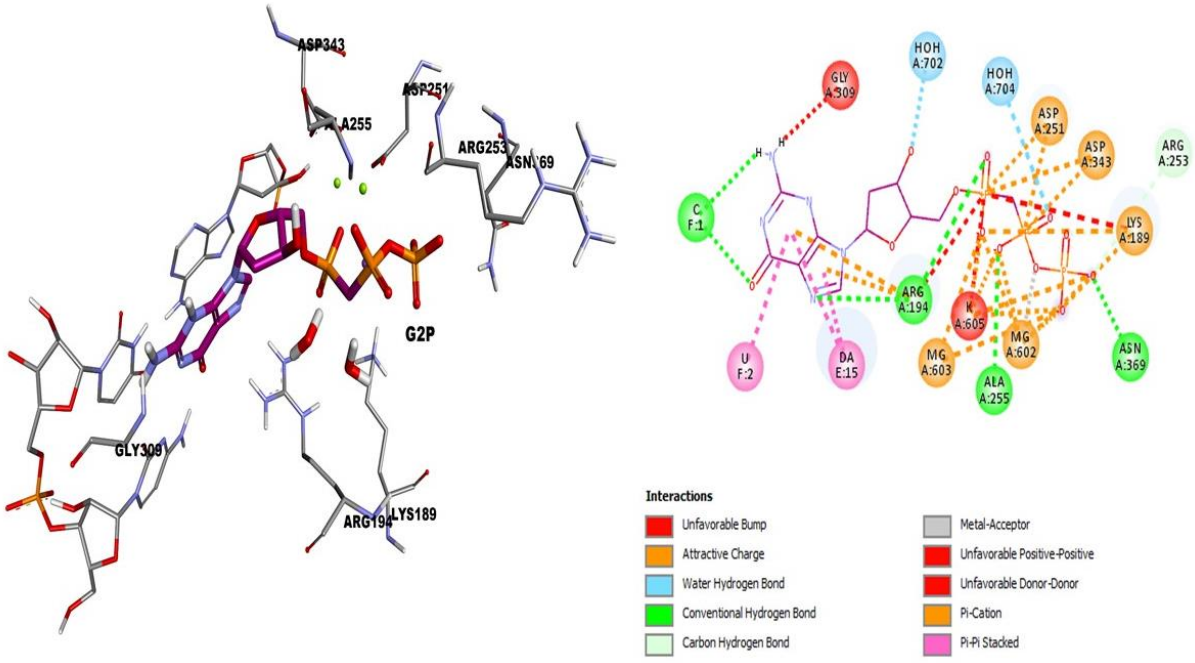

Figure 23 : Best 2D and 3D docking pose of G2P with TERT enzyme.

The predicted MD results show significant inhibition by the used marine alkaloids inside the active site with 60.6% hydrophobic interactions.

- **Mol1**

MD results show that the best pose of Mol1 takes a horizontal shape and prefers the side chains of the pyridine and imidazole rings as the first to enter deeply into the active site, which explains its affinity with an RR value of 100% and its stability with an energy of -8.3 kcal/mol (**Table7**) ranked the 2nd among other inhibitors (**Table6**) according to G2P results. Mol1 forms hydrogen bonds and hydrophobic interactions with Arg194 three different residues such as C1, U2 and DA15. The pyridine and Imidazole side chains react with the amino acid like Arg194 forming Pi-Cation and a conventional hydrogen bond and with residues of the binding site such as C1 forming two hydrogen bonds, DA15 forming two Pi-Pi- T-shaped types and U2 forming a Pi-Pi T-shaped type, wherein Arg194, DA15 and U2 play an important role in stabilizing the pyridine and pyrrole rings. In addition, pyrrole hydroxyl group react with DA15 and form a conventional hydrogen bond (**Figure24**).

In total, 10 favorable interactions were formed. MD shows that the preferred orientation of Mol1 to TERT was close to the polar amino acid.

- **Mol2**

Structurally, Mol2 was docked in a triangular shape and the pyrrole ring side is the first side that penetrates deep into the active site according to MD results, which explains its affinity for TERT, its RR value was 90% with an energy value of -7.4 kcal/mol considerably higher than mol1 (**Table7**) ranked the 4th among other inhibitors (**Table6**) compared to G2P. Mol2 forms a total of six hydrogen bonds and one hydrophobic interaction with Arg194, DA15, C1, DC14 and DT13 and a water molecule. The pyrrole ring shows two hydrophobic interactions type Pi-cation and Pi-Pi T-stacked with Arg194 and DA15 respectively, the propenyl chain forms a donor-donor interaction with C1 and a water molecule with the carbonyl function. Meanwhile, the imidazole ring shows three interactions, including a Pi-Pi T-shaped hydrophobic interaction with DC14 which forms and hydrogen bond with the amine group. DT14 forms as well a hydrogen bond with the same function (**Figure24**).

A total of eight favorable interactions, 2 of which are formed with the pyrrole ring backbone, which was responsible for the best orientation inside the active site cavity.

- **Mol3**

MD results show that the best pose of Mol3 is vertical and the side chain of the benzene ring is the first to penetrate deep into the binding site, which explains its high affinity to TERT, its RR value was 100% and its energy was -9.5 kcal/mol. These two results are the

highest in comparison to G2P, which among the various TERT inhibitors provides the best inhibition (**Table7**). Mol3 forms a total of eight hydrogen bond and hydrophobic interactions with amino acids namely, Arg194, Ala255, Tyr256, Gly309, Asp310 residues such as DA15, C1 and U2. In addition, three metal-acceptor interaction are made with Mg602, Mg603 and K605 to the benzene carbonyl function.

The benzene rings of Mol3 were directed to the lower part of the active site and formed Pi-cation, Pi-Alkyl, Pi-Pi T-shaped and Pi-Pi stacked hydrophobic interactions with amino acids such as Arg194, Ala255, DA15, Tyr256. The piperidine ring formed Pi-cation and Pi-Pi stacked hydrophobic interactions with Arg194, Tyr256 and DA15 which play an important role in stabilizing Mol3. However, the aliphatic chain's amine function formed a conventional hydrogen bond interaction with C1, and the two-hydroxyl functions formed a hydrogen bond with Tyr256 and two carbon hydrogen bonds with U2, the carbonyl group formed as well two conventional hydrogen bonds with the amino acids Gly309 and Asp310 (**Figure24**). A total of 22 interactions were favorable, 4 of which were formed with the backbone of the piperidine ring, this ring being responsible for the best preferred orientation within the active site. Therefore, Mol3 is centralized alongside Arg194, Tyr256 and DA15 as the preferred type due to their polar nature.

- **Mol4**

MD results show that Mol4 takes a triangular shape like mol2 as the preferred pose and the imidazole ringside is the first to penetrate into the binding site, which explains its affinity for TERT protein, its RR value was matching to a value of mol 2 (90%), and its energy value was -7.1 kcal/mol (**Table7**) ranked the highest among other inhibitors as compared to G2P outcomes (**Table6**).

Mol4 was directed to the lower part of the active site and the imidazole ring was bind to the active site by forming a hydrophobic; carbon hydrogen bond type interaction with DA15, a hydrogen bond with Gln308 and C1, and a Donor-Donor type with Arg194, each one of them was linked to the amine function. In addition, the piperidine ring forms a hydrogen bond with Ala255 and a metal acceptor interaction with Mg602. The pyrrole ring forms two hydrophobic interactions; type Pi-Anion with Asp343 and Pi-Pi stacked with DA15 (**Figure24**), the latter being essential for the stabilization and orientation of Mol4. The pyrrole function is considered the most reactive function in the studied molecule; it is responsible for three of the 7 favorable interactions.

- **Mol5**

MD results show a RR value of 90% and an energy of -8.3 kcal/mol (**Table7**) ranked the 3rd among other inhibitors (**Table6**) as contrasting G2P successful results, which explains its great affinity with TERT, the best orientation of mol5 takes a triangular shape like Mol2 and Mol4. The pyrrole ringside was the first to approach the active site. Mol5 is well inserted into the active site supported by many types of interactions; hydrophobic interactions, a conventional hydrogen bond, water hydrogen bonds, metal interactions, unfavorable Bump, unfavorable negative-negative…etc. (**Figure24**)

Mol5 recorded numerous interactions with amino acids such as Lys189, Arg194, Asp251 and DA15, and also with two water molecules. Three metal interactions are made with Mg603 and K605, Arg194 forms a hydrophobic interaction type Charge-Charge, Lys189 forms a conventional hydrogen bond, DA15 forms a carbon hydrogen bond interaction, in addition, three water hydrogen bond and with the sulfonate function of Mol5. Lys189 forms a carbon hydrogen bond, Asp251 and Mg602 form Pi-anion and Pi-cation interaction types with the imidazole ring. However, the amine function forms a metal-acceptor type with K605. Arg194 and DA15 form two hydrophobic interactions type Pi-Cation and Pi-Pi Stacked with the Mol5 pyrrole ring. The unfavorable bumps are considered as a barrier to the mol5 stability.

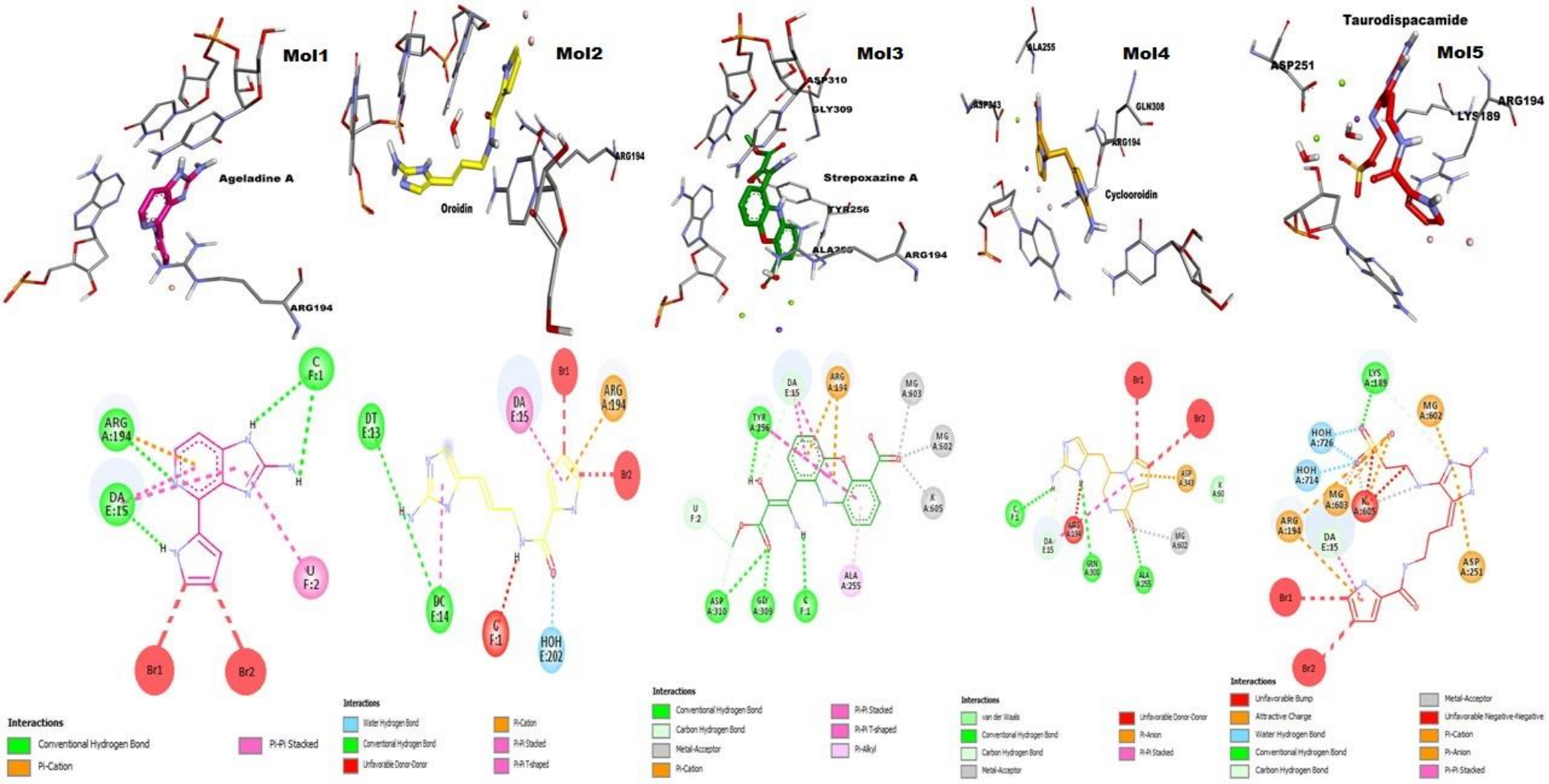

Figure 24 : 2D and 3D best docking poses of the five ligands with TERT enzyme.

2.1.5. Osm-9-like TRP channel 1 (The Transient receptor potential vanilloid) (TRPV1) (PDB ID: 7LQZ)

- **6EU ($C_{37}H_{40}O_9$)** also named **Resiniferatoxin,** it functions as the protein TRPV1's inhibitor, a treatment for cancer and other disorders, a tool for understanding the neurological system, and more. The MD results (**Table7**) show it has a 100% RR and an energy value of -8.7 Kcal/mol which leads to its excellent affinity to the enzyme. 6EU has a triangular form in the corner of the active site cavity (**Appendix6**). Leu555, Ala568, Leu576, Leu517, Tyr513, and Val520 are the specific amino acids at the binding site. A hydrogen bond was formed as well as hydrophobic types such Alkyl, Pi-Alkyl, and acceptor-acceptor interactions (**Figure25**). Eight positive interactions were found, six of which were related to the benzene rings which proved 6EU's preferential orientation to TRPV1.

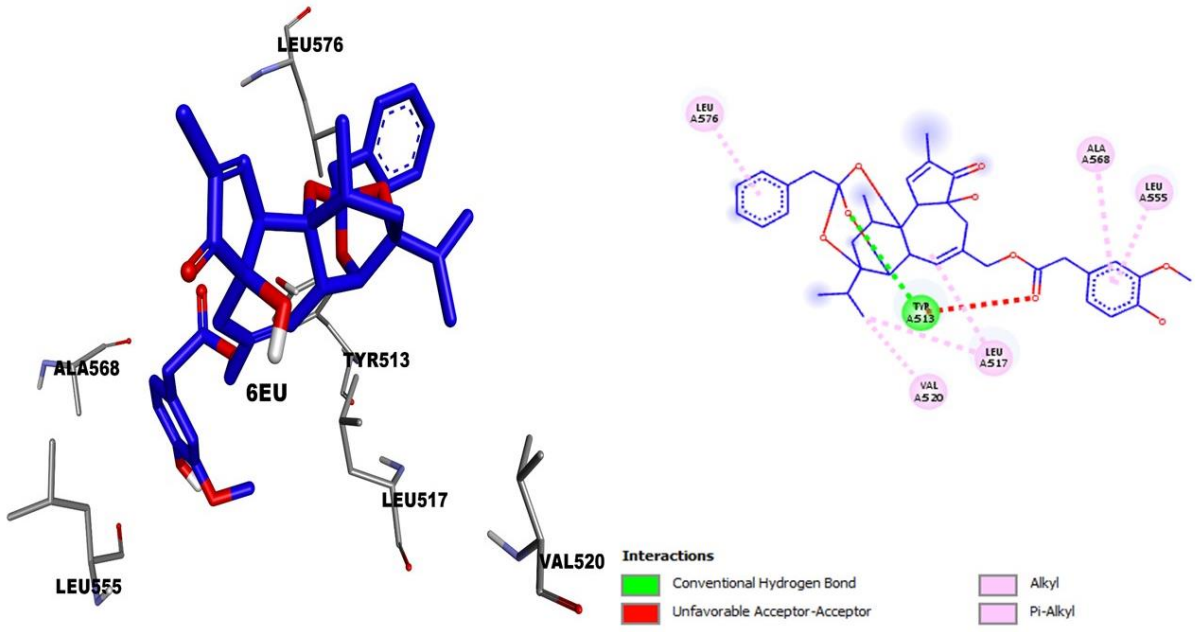

Figure 25 : Best 2D and 3D docking pose of 6EU with TRPV1 enzyme.

The predicted MD results show significant inhibition by the used marine alkaloids inside the active site with 55.26% hydrophobic interactions.

- **Mol1**

MD results show that the best pose of Mol1 takes a vertical shape and prefers the side chains of the pyridine and pyrrole rings as the first to enter deeply into the active site, which explains its affinity with an RR value of 100% and its stability with an energy of -7.1 kcal/mol (**Table7**) was ranked the best with Mol3 among all inhibitors (**Table6**) as compared to 6EU positive

outcomes. Mol1 forms hydrogen bonds and hydrophobic interactions with six different amino acids such Tyr513, Ser514, Leu517, Asn553, Leu555 and Ala568. The pyridine and pyrrole side chains react with the amino acids of the binding site such as Tyr513 and Ala568, forming Pi-Pi Stacked, Pi-Pi T-shaped and Pi-Alkyl types of hydrophobic interactions, wherein Tyr513 and Ala568 play an important role in stabilizing the pyridine and pyrrole rings. In addition, imidazole hydroxyl groups react with Ser514 and Asn553 and form conventional hydrogen bonds (**Figure26**).

In total, 10 favorable interactions were formed. MD shows that the preferred orientation of Mol1 to TRPV1 was close to nonpolar amino acids.

- **Mol2**

Mol2 was docked in a triangular shape and the pyrrole ring side is the first side that penetrates deep into the active site according to MD results, which explains its affinity for TRPV1, its RR value was 100% with an energy value of -6.2 kcal/mol considerably lower than mol1 (**Table7**) ranked the 4th among other inhibitors (**Table6**). Mol2 forms a total of seven hydrogen bonds and hydrophobic interactions with five different amino acids such as Tyr513, Ser514, Leu517, Asn553 and Ile575. The pyrrole ring shows three hydrophobic interactions type Pi-Pi T-shaped and Pi-Alkyl with Tyr513, Leu517 and Ile575 respectively, meanwhile, the imidazole ring shows four interactions, including a Pi-Alkyl hydrophobic interaction with Leu517 and three hydrogen bonds, including two with Ser514 and one with Asn553 (**Figure26**).

A total of seven favorable interactions, 3 of which are formed with the pyrrole ring backbone, which was responsible for the best orientation inside the active site cavity.

- **Mol3**

MD results show that the best pose of Mol3 is vertical and the side chain of the benzene ring is the first to penetrate deep into the binding site, which explains its high affinity to TRPV1, its RR value was 100% this shows that all positions on the active site have been located and its energy was -7.1 kcal/mol same as Mol1 (**Table7**). Mol3 forms a total of eight hydrogen bond and hydrophobic interactions with amino acids namely Tyr513, Leu517, Thr552, Asn553, Arg553 and Ile571.

The benzene ring of Mol3 was directed to the upper part of the active site and formed Pi-Sigma and Pi-Alkyl hydrophobic interactions with amino acids such as Thr552 and Ile571 which play an important role in stabilizing Mol3. The piperidine ring formed Pi-Alkyl

hydrophobic interactions with Leu517. However, the hydroxyl and oxygen groups saved three conventional hydrogen bonds with Asn553 and Tyr513. The second benzene ring located in the lower part of the active site formed as well as Pi-Alkyl type with Leu517 and a hydrogen bond with Arg559 (**Figure26**).

A total of 8 interactions were favorable, 4 of which were formed with the backbone of the benzene ring, this ring being responsible for the best preferred orientation within the active site. Therefore, Mol3 is centralized alongside, Thr552, Asn553 and Ile571 as the preferred type due to their polar nature.

- **Mol4**

MD results show that Mol4 takes a triangular shape as the preferred pose and the imidazole ringside is the first to penetrate into the binding site, which explains its affinity for TRPV1 protein, its RR value was 90% and its energy value was -6.0 kcal/mol (**Table7**) ranked the 5th among other inhibitors (**Table6**) in comparison to 6EU positive findings.

The imidazole ring of Mol4 binds to the active site by forming a hydrophobic; Pi-Sigma with Asn553, Pi-Alkyl with Leu517, carbon Hydrogen bond Tyr552 types interaction. The two amine functions saved two conventional hydrogen bonds with Ser514. In addition, the pyrrole function formed a Pi-Alkyl interaction type with Ile575 (**Figure26**).

The imidazole function is considered the most reactive function in the studied molecule; it is responsible for five of the seven favorable interactions.

The piperidine ring saved no interaction with the studied protein, same as how it was mentioned in PI3K protein.

- **Mol5**

MD results show a RR value of 100% and an energy of -8.8 kcal/mol (**Table7**) These two results are the highest among the other compounds, which explains its great affinity with TRPV1, the best orientation of mol5 takes a triangular shape like Mol2 and Mol4. The imidazole ringside was the first to approach the active site. Mol5 recorded numerous interactions with amino acids such as Tyr513, Ser514, Leu517, Met549, Asn553 and Arg559. In addition, Met549 form hydrophobic interaction type Pi-Alkyl with the pyrrole ring of Mol5, Asn553 and Ser514 form two hydrogen bonds with the amine function of the imidazole ring, however, Leu517 formed Pi-Alkyl with its skeleton. Tyr513 formed a Pi-Sulfur type, Ser514 formed a carbon hydrogen bond and Arg559 formed two interactions including Salt-Bridge and a conventional hydrogen bond with the Mol5 sulfonate function (**Figure26**). Tyr513, Ser514

and Arg559 could strongly participate in the stability of Mol5. With 16 favorable interactions, four of them are formed with the sulfonate function (main reactive function); Mol5 was centralized alongside hydrophilic amino acids as the preferred type due to its polarity.

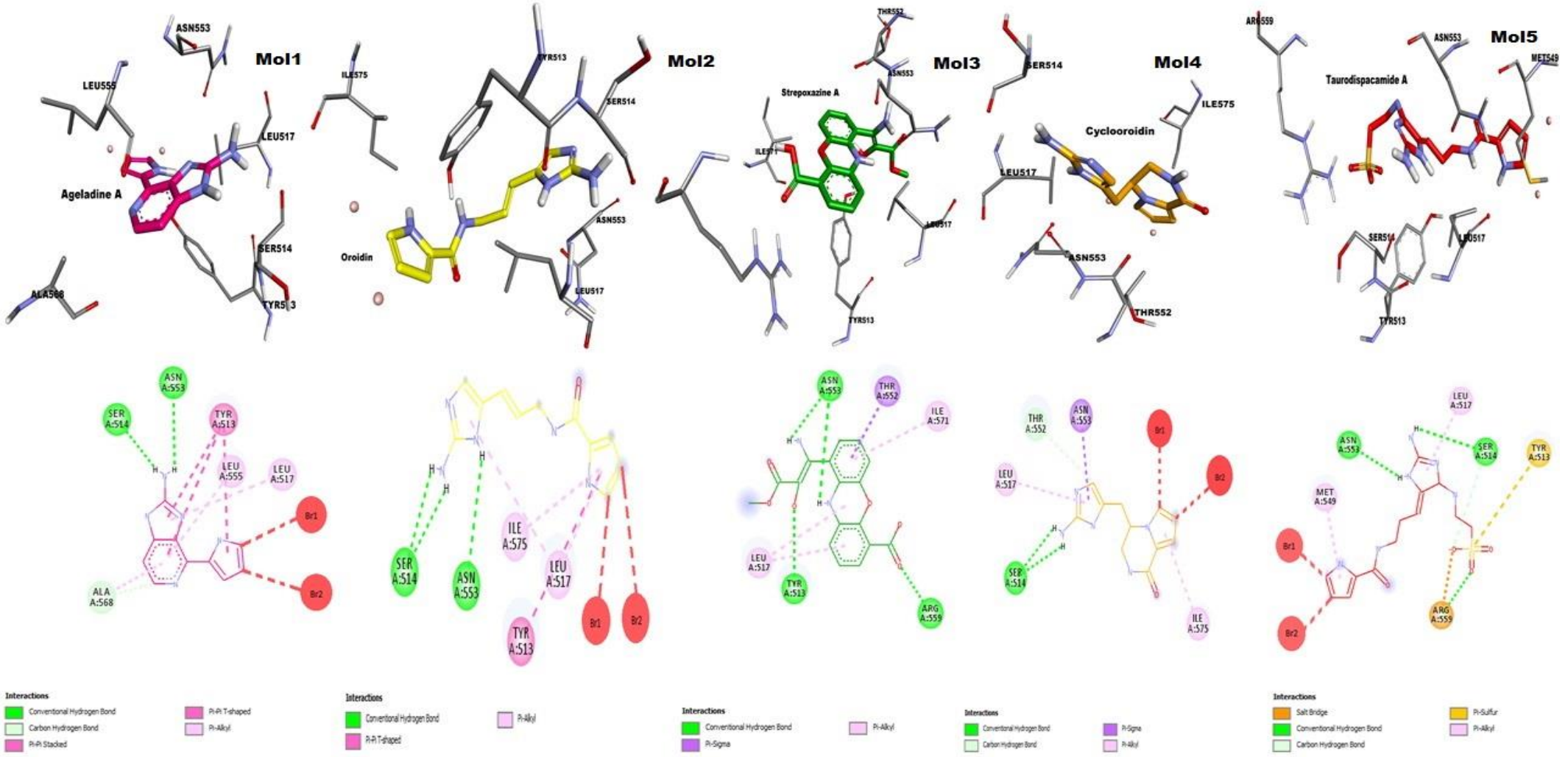

Figure 26 : 2D and 3D best docking poses of the five ligands with TRPV1 enzyme.

2.1.6. RAC-alpha serine/threonine-protein kinase (AKT1) (PDB ID: 4EKK)

- **AMP-PNP ($C_{10}H_{17}N_6O_{12}P_3$)** also named **Phosphoaminophosphonic acid-adenylate ester** or **adenylyl phosphoramidate.** This inhibitor has been investigated as a potential treatment for illnesses like cancer, cardiovascular disease, and neurological problems. It normally functions by binding to the active site of the target enzyme and inhibiting its activity. According to the MD findings (**Table7**), it has an energy value of -9.7 Kcal/mol and a 90% RR, which contribute to its strong affinity for the enzyme. Deep inside the active site cavity, AMP-PNP has a triangle shape (**Appendix7**). The particular amino acids in the binding site are Glu228, Ala230, Glu234, Lys276, Val164, Ala2177, Asp292, and Met281. Additionally, to the hydrophobic types of Pi-Alkyl, Pi-Sulfur, and Carbon hydrogen bonds, attractive charge, salt bridges, and Donnor-Donnor interactions, five hydrogen bonds were also formed (**Figure27**). In a total 23 favorable interactions, 18 of which were formed with the Purine and triphosphate functions (main functions) which show the preferred orientation of AMP-PNP to AKT1.

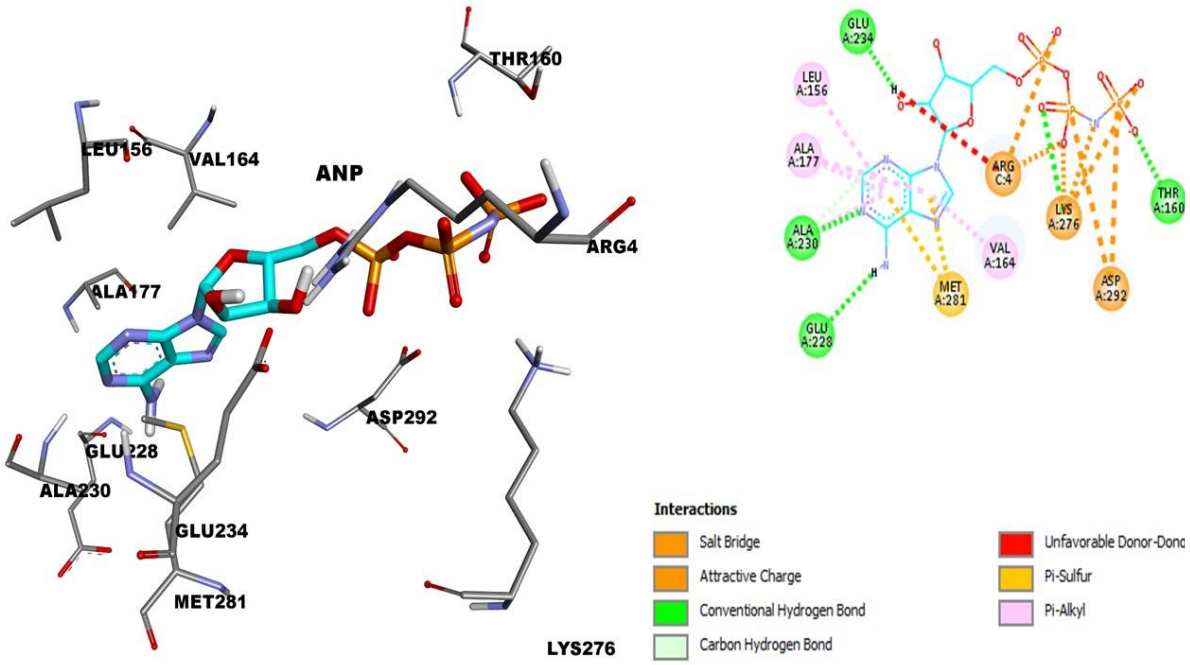

Figure 27 : Best 2D and 3D docking pose of AMP-PNP with AKT1 enzyme.

The predicted MD results show significant inhibition by the used marine alkaloids inside the active site with 44.73% hydrophobic interactions.

- **Mol1**

MD results show that the best pose of Mol1 takes a horizontal shape and prefers the side chains of the pyridine and pyrrole rings as the first to enter deeply into the active site, which explains its affinity with an RR value of 100% and its stability with an energy of -7.2 kcal/mol (**Table7**) was ranked the 5th among all inhibitors (**Table6**) compared to AMP-PNP ligand. Mol1 forms hydrogen bonds and hydrophobic interactions with five different amino acids such as Phe161, Lys179, Glu198, Asp292 and Leu295 (**Table7**). The pyrrole side chain reacts with the amino acids of the binding site such as Lys179, Asp292 forming Donor-Donor interaction, hydrogen bond with the amine function and Pi-Anion respectively, Asp292, Leu295 and Phe161 form hydrophobic interactions Pi-Anion, Pi-Alkyl and Pi-Pi T-shaped respectively, with the pyridine ring. The imidazole ring was linked to Lys179 by a hydrogen bond, Asp292 and Phe161 by hydrophobic interactions; Pi-Anion and Pi-Pi T-shaped types respectively, meanwhile Glu198 formed two types of interactions including a hydrogen bond and Pi-Anion interaction type (**Figure28**). Wherein, Phe161, Glu198, Lys179 and Asp292 play an important role in stabilizing the Imidazole ring.

In total, 11 favorable interactions were formed. MD shows that the preferred orientation of Mol1 to AKT1 was close to the polar amino acids.

- **Mol2**

Structurally, Mol2 was docked in a triangular shape and the pyrrole ring side is the first side that penetrates deep into the active site according to MD results, which explains its affinity for AKT1, its RR value was 90% with an energy value of -7.3 kcal/mol considerably lower than mol1 (**Table7**) ranked the 5th among other inhibitors (**Table6**). Mol2 forms a total of eight hydrogen bonds and hydrophobic interaction with six different amino acids such as Val164, Ala177, Met281, Thr291, Arg4 and Thr5. The pyrrole ring shows a hydrogen bond with Thr291 and three hydrophobic interactions type Pi-Sigma and Pi-Alkyl with Val164, Ala177 and Met281 respectively, the propenyl chain's carbonyl function forms as well a hydrogen bond with Thr291. Meanwhile, the imidazole ring shows three interactions, including a Pi-Cation hydrophobic interaction with Arg4 and two hydrogen bonds including Arg4 and Thr5 (**Figure28**).

A total of eight favorable interactions, 5 of which are formed with the pyrrole ring backbone, which was responsible for the best orientation inside the active site cavity.

- **Mol3**

MD results show that the best pose of Mol3 is vertical and the side chain of the benzene ring is the first to penetrate deep into the binding site, which explains its high affinity to AKT1, its RR value was 100% this shows that all positions on the active site have been located and its energy was -8.7 kcal/mol (**Table7**) ranked the 2nd among other inhibitors (**Table6**) as instead to AMP-PNP ligand. Mol3 forms a total of 13 hydrogen bond and hydrophobic interactions with amino acids namely Phe161, Lys179, Glu198, Lys276, Asp192, Arg4, Thr5 and Ser7.

The benzene ring of Mol3 was directed to the upper part of the active site and formed Pi-Anion, Pi-Cation, Pi-Pi T-shaped hydrophobic interactions and a hydrogen bond with amino acids such as Phe161, Glu198, Asp192 and Lys179 which play an important role in stabilizing Mol3. The piperidine ring formed Pi-Pi T-shaped, Pi-Anion and Pi-Cation hydrophobic interactions with Phe161, Lys179 and Asp292. However, the amine function saved a conventional hydrogen bond with Asp292. The carbonyl and hydroxyl functions formed Three conventional hydrogen bonds with the amino acids Lys276, Arg4 and Ser7. In addition, a carbon hydrogen bond with Thr5 (**Figure28**). A total of 14 interactions were favorable, 3 of which were formed with the backbone of the benzene ring, this ring being responsible for the best preferred orientation within the active site. Therefore, Mol3 is centralized alongside Phe161, Lys179, Glu198 and Asp292 as the preferred type due to their polar nature.

- **Mol4**

MD results show that Mol4 takes a triangular shape like Mol2 as the preferred pose and the imidazole ringside is the first to penetrate into the binding site, which explains its affinity for AKT1 protein, its RR value was 100%, and its energy value was -7.6 kcal/mol (**Table7**) ranked the 3rd among other inhibitors (**Table6**) as compared to AMP-PNP.

The imidazole ring of Mol4 binds to the active site by forming an unfavorable Donor-Donor interaction, which is a barrier to its stability and three conventional hydrogen bonds with Asn279 and Asp292. In addition, the piperidine ring forms two hydrogen bonds with Thr291 and Asp292. The pyrrole ring forms only a Pi-Sigma hydrophobic interaction type with Val164 (**Figure28**), the latter's being essential for the stabilization and orientation of Mol4. The pyrrole and Piperidine functions are considered the most reactive functions in the studied molecule; they are responsible for three of the seven favorable interactions.

- **Mol5**

MD results show a RR value of 100% and an energy of -8.8 kcal/mol (**Table7**) ranked the best among other inhibitors (**Table6**) according to AMP-PNP results, which is considered as an excellent inhibitor explains its affinity with AKT1, the best orientation of mol5 takes a triangular shape like Mol2 and Mol4. The pyrrole ringside was the first to approach the active site. Mol5 recorded numerous interactions with amino acids such as The160, Phe161, Val164, Lys179, Lys276, Met281, Thr291, Asp292, Arg4 and Ser7. Lys276, Arg4 and Ser7 formed an attractive charge, salt bridge and two conventional hydrogen bonds with the sulfonate function of Mol5. In addition, Phe161 and Lys179 form hydrophobic interactions types Pi-Pi T-shaped and an unfavorable Donor-Donor, Asp292, Thr160 and Ser7 formed four hydrogen bonds with the imidazole ring. However, the carbonyl function forms as well three hydrogen bonds with Lys179, Thr291 and Asp292. Val164, Met281 and Thr291 form two hydrophobic interactions type Pi-Sigma and Pi-Alkyl and a hydrogen bond with the Mol5 pyrrole ring. Both, Val164 and Met281, could strongly participate in the stability of Mol5 (**Figure28**). With 16 favorable interactions, two of them are formed with the pyrrole ring (main reactive function); Mol5 was centralized alongside hydrophobic amino acids as the preferred type due to its non-polarity.

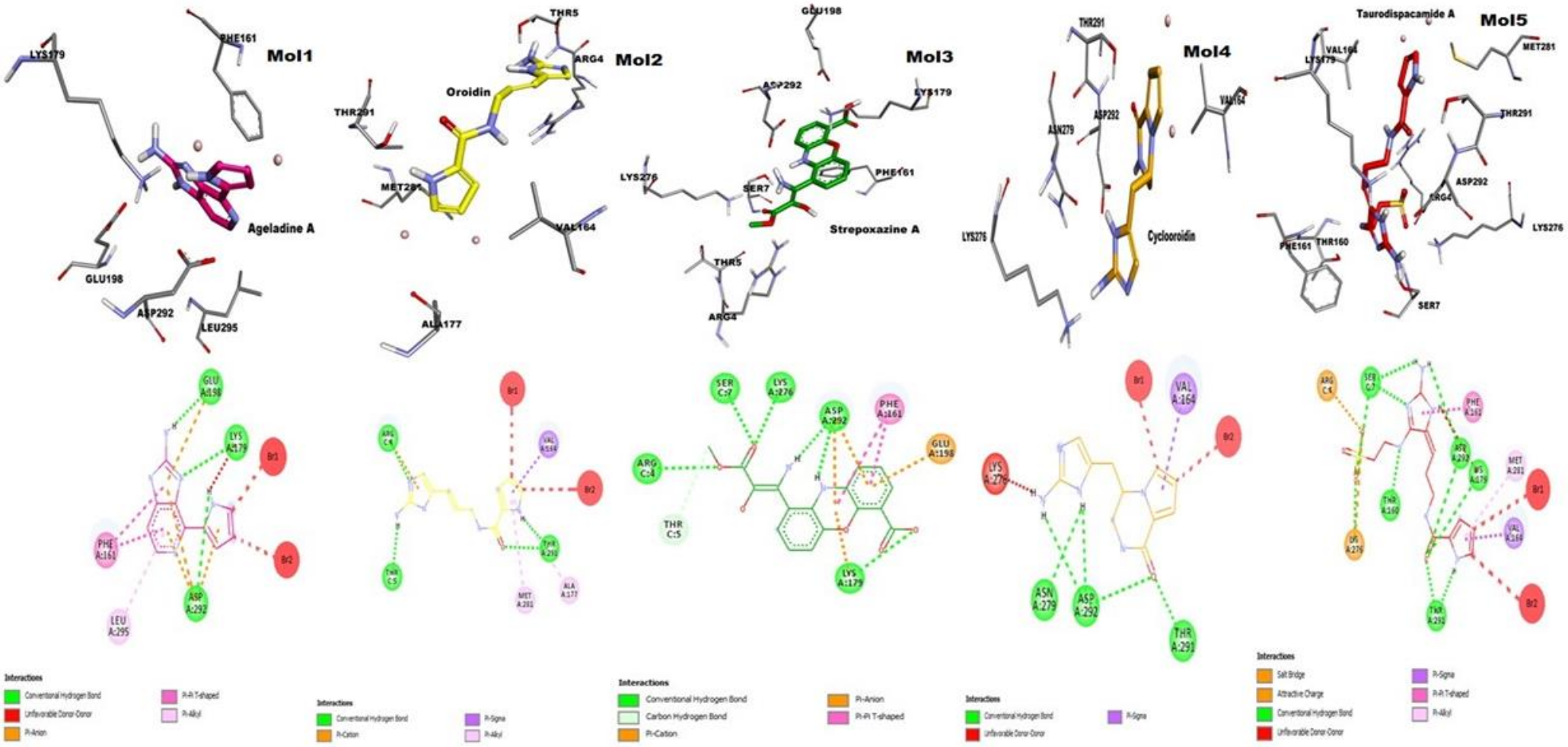

Figure 28 : 2D and 3D best docking poses of the five ligands with AKT1 enzyme.

(**Mol1** is colored with **pink**, **Mol2** is colored with **yellow**, **Mol3** is colored with **green**, **Mol4** is colored with **orange** and **Mol5** is colored with **red**)

2.2. ADMET analysis

We investigated the inhibition potential of five novel alkaloids such as Mol1 (Ageladine A), Mol2 (Oroidin), Mol3 (Strepoxazine A), Mol4 (Cyclooroidin), and Mol5 (Taurodispacamide A) on six proteins: Focal Adhesion Kinase 1 (FAK) (PDB ID: 2IJM), Caspase-3 (PDB ID: 3DEI), the gamma isoform of the catalytic subunit of phosphatidylinositol 4,5-bisphosphate 3-kinase (PI3K) (PDB ID: 4FA6), telomerase reverse transcriptase (TERT) (PDB ID: 6USR), Osm-9-like TRP channel 1 (TRPV1) (PDB ID: 7LQZ) and RAC-alpha serine/threonine-protein kinase (AKT1) (PDB ID: 4EKK), including the type of interactions and the involved amino acids.

The tested compounds were first isolated from marine sponges, such as Mol1 from *Agelas nakamurai* H. **[7]**, however, Mol2, Mol3, Mol4, and Mol5 were isolated from *Agelas oroides* S. **[73].** With the exception of Mol1, all compounds have antihistaminic activity **[74]**.

The predicted ADME parameters for all compounds show high blood-brain barrier penetration, ranging from 0.52 to 0.74 (**Table8**), indicating that they readily cross this membrane and reflecting their potential neurological action. Human intestinal absorption (HIA) of the compounds was high, ranging from 62.78% to 99.3% (**Table8**), with high water solubility. The metabolic profile showed inhibition of CYP 1A2 in multiple occasions, including Mol1, Mol2, Mol3, and Mol4. However, CYP 2D6 was only inhibited by Mol1. Finally, the metabolic profile was considered suitable because these compounds are potential substrates for other CYPs such as 2C19, 2C9 (Mol1, Mol2 and Mol3).

The toxicity of the five studied alkaloids shows similar results for mutagenicity in the Ames tests, all of which were positive, with a high risk of inhibiting the human ether-related gene channels. The toxicity profile was expected due to the toxic nature of alkaloids. Therefore, they can be dangerous for patients with chronic diseases and should be taken with caution and at minimal doses.

Conclusion and perspectives

Neuroblastoma is a type of cancer described since long time ago, but still under diagnosis, scientific progress has made it possible to establish means of diagnosis and develop new tools to treat this cancer, among them, we can cite *in silico* analysis «molecular docking», the latter is one of the potent strategies to accelerate the drug development process.

In this work, we have demonstrated for the first time the ability of five molecules belonging to pyrrole-imidazole alkaloids isolated from *Agelas sp*. to inhibit neuroblastoma targets. The results of molecular docking and the ADMET prediction are very promising, the five molecules showed considerable affinity for those targets but they differ in the binding energies, the repetition rate, the number, type of interactions and ADMET Profile. Where Strepoxazine A (**mol3**) is the best among them with the best energy and ADMET pharmacokinetics. We conclude that these molecules might become drug candidates to treat neuroblastoma.

Based on the data reported in this study, we suggest taking into account these compounds, especially Strepoxazine A to make further tests *in vitro* and *in vivo*, to examine their anticancer effect and to develop new potent drugs to prevent neuroblastoma.

Bibliographic references

[1]. Ansari, M.J., et al., Anticancer drug-loading capacity of green synthesized porous magnetic iron nanocarrier and cytotoxic effects against human cancer cell line. 2023. 34(1): p. 467-477.
[2]. Wang, Y., et al., Tumor microenvironment-responsive fenton nanocatalysts for intensified anticancer treatment. 2022. 20(1): p. 1-33.
[3]. Agostini, M., et al., Targeting lipid metabolism in cancer: neuroblastoma. 2022: p. 1-6.
[4]. Jahangiri, L.J.L., Metastasis in Neuroblastoma and Its Link to Autophagy. 2023. 13(3): p. 818.
[5]. Westermark, U.K., et al. The MYCN oncogene and differentiation in neuroblastoma. in Seminars in cancer biology. 2011. Elsevier.
[6]. Kafoud, A., et al., Potential Treatment Options for Neuroblastoma with Polyphenols through Anti-Proliferative and Apoptotic Mechanisms. 2023. 13(3): p. 563.
[7]. Magoulas, G.E.J.C., Ageladine A, a Bromopyrrole Alkaloid from the Marine Sponge Agelas nakamurai. 2023. 3(1): p. 107-121.
[8]. Varijakzhan, D., et al., Bioactive compounds from marine sponges: Fundamentals and applications. 2021. 19(5): p. 246.
[9]. Elissawy, A.M., et al., Cytotoxic alkaloids derived from marine sponges: A comprehensive review. 2021. 11(2): p. 258.
[10]. Chu, M.-J., M. Li, and Y.J.B.C. Zhao, Dimeric pyrrole-imidazole alkaloids: sources, structures, bioactivities and biosynthesis. 2022: p. 106332.
[11]. Jacobson, J.C., R.A. Clark, and D.H.J.C. Chung, High-Risk Neuroblastoma: A Surgical Perspective. 2023. 10(2): p. 388.
[12]. Pastor, E.R. and S.A.J.C.r.i.o.h. Mousa, Current management of neuroblastoma and future direction. 2019. 138: p. 38-43.
[13]. Yan, P., et al., Comparison of incidence and outcomes of neuroblastoma in children, adolescents, and adults in the United States: A surveillance, epidemiology, and end results (SEER) program population study. 2020. 26: p. e927218-1.
[14]. Van Heerden, J., et al., Neuroblastoma: The basis for cure in limited-resource settings. 2021. 68(7): p. e28923.
[15]. Okawa, S. and K.J.J.J.o.C.O. Saika, International variations in neuroblastoma incidence in children and adolescents. 2022. 52(6): p. 656-658.
[16]. Park, J.R., A. Eggert, and H.J.H.o.c.o.N.A. Caron, Neuroblastoma: biology, prognosis, and treatment. 2010. 24(1): p. 65-86.
[17]. Kholodenko, I.V., et al., Neuroblastoma origin and therapeutic targets for immunotherapy. 2018. 2018.
[18]. Erickson, A.G., P. Kameneva, and I. Adameyko. The transcriptional portraits of the neural crest at the individual cell level. in Seminars in Cell & Developmental Biology. 2023. Elsevier.
[19]. Erickson, A.G., P. Kameneva, and I. Adameyko. The transcriptional portraits of the neural crest at the individual cell level. Elsevier.
[20]. Ribatti, D., R. Tamma, and T.J.T.o. Annese, Epithelial-mesenchymal transition in cancer: a historical overview. 2020. 13(6): p. 100773.
[21]. Ji, Y., et al., Wnt signaling in neural crest ontogenesis and oncogenesis. 2019. 8(10): p. 1173.
[22]. Otte, J., et al., MYCN function in neuroblastoma development. 2021. 10: p. 624079.
[23]. Campos Cogo, S., et al., An overview of neuroblastoma cell lineage phenotypes and in vitro models. 2020. 245(18): p. 1637-1647.

[24]. Campos Cogo, S., et al., An overview of neuroblastoma cell lineage phenotypes and in vitro models. Experimental Biology and Medicine, 2020. 245(18): p. 1637-1647.
[25]. Maris, J.M.J.N.E.J.o.M., Recent advances in neuroblastoma. 2010. 362(23): p. 2202-2211.
[26]. Whittle, S.B., et al., Overview and recent advances in the treatment of neuroblastoma. 2017. 17(4): p. 369-386.
[27]. Weinstein, J.L., H.M. Katzenstein, and S.L.J.T.o. Cohn, Advances in the diagnosis and treatment of neuroblastoma. 2003. 8(3): p. 278-292.
[28]. Tolbert, V.P., K.K.J.C. Matthay, and t. research, Neuroblastoma: clinical and biological approach to risk stratification and treatment. 2018. 372: p. 195-209.
[29]. National Library Of Medicine, v.i.
[30]. Swift, C.C., et al., Updates in diagnosis, management, and treatment of neuroblastoma. 2018. 38(2): p. 566-580.
[31]. Quispe, P.A., M.J. Lavecchia, and I.E.J.D.D.T. Leon, Focal adhesion kinase inhibitors in the treatment of solid tumors: Preclinical and clinical evidence. 2022. 27(2): p. 664-674.
[32]. Wu, Y., et al., Focal adhesion kinase inhibitors, a heavy punch to cancer. 2021. 12: p. 1-15.
[33]. Miao, H., et al., Activation of EphA2 kinase suppresses integrin function and causes focal-adhesion-kinase dephosphorylation. 2000. 2(2): p. 62-69.
[34]. Chen, R., et al., Regulation of the PH-domain-containing tyrosine kinase Etk by focal adhesion kinase through the FERM domain. 2001. 3(5): p. 439-444.
[35]. Roberts, W.G., et al., Antitumor activity and pharmacology of a selective focal adhesion kinase inhibitor, PF-562,271. 2008. 68(6): p. 1935-1944.
[36]. Ayoup, M.S., et al., Nature-inspired new isoindole-based Passerini adducts as efficient tumor-selective apoptotic inducers via caspase-3/7 activation. 2023. 245: p. 114865.
[37]. Tawa, P., et al., Catalytic activity of caspase-3 is required for its degradation: stabilization of the active complex by synthetic inhibitors. 2004. 11(4): p. 439-447.
[38]. Du, J.-Q., et al., Isoquinoline-1, 3, 4-trione derivatives inactivate caspase-3 by generation of reactive oxygen species. 2008. 283(44): p. 30205-30215.
[39]. Soond, D.R., et al., PI3K p110δ regulates T-cell cytokine production during primary and secondary immune responses in mice and humans. 2010. 115(11): p. 2203-2213.
[40]. Le, P.T., et al., Design and synthesis of a novel pyrrolidinyl pyrido pyrimidinone derivative as a potent inhibitor of PI3Kα and mTOR. 2012. 22(15): p. 5098-5103.
[41]. Peng, Y., et al., PI3K/Akt/mTOR pathway and its role in cancer therapeutics: are we making headway? 2022. 12: p. 819128.
[42]. Mei, H., et al., The mTOR signaling pathway in pediatric neuroblastoma. 2013. 30(7): p. 605-615.
[43]. Meier, T.I., et al., Cloning, expression, purification, and characterization of the human Class Ia phosphoinositide 3-kinase isoforms. 2004. 35(2): p. 218-224.
[44]. Haendeler, J., et al., Antioxidants inhibit nuclear export of telomerase reverse transcriptase and delay replicative senescence of endothelial cells. 2004. 94(6): p. 768-775.
[45]. Wan, S., et al., The role of telomerase reverse transcriptase (TERT) promoter mutations in prognosis in bladder cancer. 2021. 12(1): p. 1495-1504.
[46]. Batista, L.F., et al., Telomere shortening and loss of self-renewal in dyskeratosis congenita induced pluripotent stem cells. 2011. 474(7351): p. 399-402.
[47]. Nguyen, T.H.D., et al., Cryo-EM structure of substrate-bound human telomerase holoenzyme. 2018. 557(7704): p. 190-195.

[48]. Sharma, D., R. Rana, and K. Thakur, A REVIEW ON ROLE OF TRPV CATION CHANNELS.
[49]. Hou, L., et al., A RAC-alpha serine/threonine-protein kinase (CgAKT1) involved in the synthesis of CgIFNLP in oyster Crassostrea gigas. 2022. 127: p. 129-139.
[50]. Rönnstrand, L.J.C. and M.L.S. CMLS, Signal transduction via the stem cell factor receptor/c-Kit. 2004. 61: p. 2535-2548.
[51]. Enomoto, A., et al., Akt/PKB regulates actin organization and cell motility via Girdin/APE. 2005. 9(3): p. 389-402.
[52]. Seo, G.J., et al., Akt kinase-mediated checkpoint of cGAS DNA sensing pathway. 2015. 13(2): p. 440-449.
[53]. Gomez, R.L., et al., Tumoral heterogeneity in neuroblastoma. 2022: p. 188805.
[54]. Zafar, A., et al., Molecular targeting therapies for neuroblastoma: Progress and challenges. 2021. 41(2): p. 961-1021.
[55]. Ibrahim, S.R., et al., Genus Acanthella—A Wealthy Treasure: Secondary Metabolites, Synthesis, Biosynthesis, and Bioactivities. 2023. 21(4): p. 257.
[56]. Liang, J., et al., Advances in Natural Products from the Marine-Sponge-Associated Microorganisms with Antimicrobial Activity in the Last Decade. 2023. 21(4): p. 236.
[57]. Varamogianni-Mamatsi, D., et al., A Multi-Species Investigation of Sponges' Filtering Activity towards Marine Microalgae. 2021. 20(1): p. 24.
[58]. Hentschel, U., K.M. Usher, and M.W.J.F.m.e. Taylor, Marine sponges as microbial fermenters. 2006. 55(2): p. 167-177.
[59]. Choi, C., et al., Therapeutic Potential of (−)-Agelamide D, a Diterpene Alkaloid from the Marine Sponge Agelas sp., as a Natural Radiosensitizer in Hepatocellular Carcinoma Models. 2020. 18(10): p. 500.
[60]. Di Cesare Mannelli, L., et al., Pharmacological activities of extracts and compounds isolated from mediterranean sponge sources. 2021. 14(12): p. 1329.
[61]. Chu, M.-J., et al., Secondary metabolites from marine sponges of the genus Agelas: a comprehensive update insight on structural diversity and bioactivity. 2022. 12(13): p. 7789-7820.
[62]. Alan McIntosh, J.P., Chapter 2 - Global Water Resources. Science and the Global Environment, Elsevier,, 2017: p. 113-254.
[63]. Kusama, T., et al., Agelamadins A and B, dimeric bromopyrrole alkaloids from a marine sponge Agelas sp. 2014. 16(15): p. 3916-3918.
[64]. Gribble, G.W.J.T.A.C. and Biology, Occurrence of halogenated alkaloids. 2012. 71: p. 1-165.
[65]. Zhang, H., et al., Bioactive secondary metabolites from the marine sponge genus Agelas. 2017. 15(11): p. 351.
[66]. Parra-Velandia, F.J., S. Zea, and R.W.J.Z. Van Soest, Reef sponges of the genus Agelas (Porifera: Demospongiae) from the Greater Caribbean. 2014. 3794(3): p. 301-343.
[67]. (INPN), I.N.d.P.N., Agelas sp. taxonomy. visited in 05/06/2023.
[68]. Ferretti, C., et al., Growth dynamics and bioactivity variation of the Mediterranean demosponges Agelas oroides (Agelasida, Agelasidae) and Petrosia ficiformis (Haplosclerida, Petrosiidae). 2009. 30(3): p. 327-336.
[69]. Idan, T., et al., Sponges in a changing climate: Survival of Agelas oroides in a warming Mediterranean Sea. 2020. 7: p. 603593.
[70]. Inventaire National du Partrimoine Naturel (INPN), visited in 05/06/2023.
[71]. Wang, Q., et al., A Series of New Pyrrole Alkaloids with ALR2 Inhibitory Activities from the Sponge Stylissa massa. 2022. 20(7): p. 454.

[72]. Bickmeyer, U., et al., Ageladine A, a pyrrole–imidazole alkaloid from marine sponges, is a pH sensitive membrane permeable dye. 2008. 373(3): p. 419-422.
[73]. Forte, B., et al., A submarine journey: The pyrrole-imidazole alkaloids. 2009. 7(4): p. 705-753.
[74]. Ferretti, C., et al., Effects of Agelas oroides and Petrosia ficiformis crude extracts on human neuroblastoma cell survival. 2007. 30(1): p. 161-169.
[75]. Esposito, R., et al., Marine Demospongiae: A challenging treasure of bioactive compounds. 2022. 20(4): p. 244.
[76]. Mukherjee, S., Total Synthesis Of Cyclooroidin And Studies Towards Some Oroidin Dimers. 2010.
[77]. Fattorusso, E. and O.J.T.L. Taglialatela-Scafati, Two novel pyrrole-imidazole alkaloids from the Mediterranean sponge Agelas oroides. 2000. 41(50): p. 9917-9922.
[78]. Jejurikar, B.L. and S.H. Rohane, Drug designing in discovery studio. 2021.
[79]. Pacheco, A.B. and L.J.B.R.L.S.U. Hpc, Introduction to AutoDock and AutoDock tools. 2012.
[80]. Wang, Y., et al., Pubchem bioassay: 2017 update. 2017. 45(D1): p. D955-D963.
[81]. Burley, S.K., et al., Protein Data Bank (PDB): the single global macromolecular structure archive. 2017: p. 627-641.
[82]. De Beer, T.A., et al., PDBsum additions. 2014. 42(D1): p. D292-D296.
[83]. Lamrani, M., et al., Hydroxycoumarins and some flavonoids from Pistacia atlantica Desf. as multi-targets inhibitors for Alzheimer's disease: Molecular docking and ADMET studies. 2022.
[84]. Fan, J., A. Fu, and L.J.Q.B. Zhang, Progress in molecular docking. 2019. 7: p. 83-89.
[85]. Guedes, I.A.B., A. M. S.; Marinho, and E.K. D.; Krempser, M. A.; Sperandio, O.; Dardenne, L. E.; Miteva, M. A., New Machine Learning and Physics-Based Scoring Functions for Drug Discovery. 2021(Sci Rep): p. 11 (1), 3198.
[86]. Nisha, C.M., et al., Molecular docking and in silico ADMET study reveals acylguanidine 7a as a potential inhibitor of β-secretase. 2016. 2016.
[87]. Benguechoua, M.I., et al., Quinic and Digallic acids from Pistacia atlantica Desf. Leaves Extracts as Potent Dual Effect Inhibitors against main Protease and RNA-dependent RNA Polymerase of SARS-CoV-2. 2022. 18(4): p. 307-317.
[88]. Lipinski, C.A., et al., Experimental and computational approaches to estimate solubility and permeability in drug discovery and development settings. 1997. 23(1-3): p. 3-25.
[89]. Lipinski, C.A.J.D.d.t.T., Lead-and drug-like compounds: the rule-of-five revolution. 2004. 1(4): p. 337-341.
[90]. JARGON, P., LIPINSKI'S RULE OF FIVE. visited in 01/06/2023.
[91]. Lagorce, D., et al., Computational analysis of calculated physicochemical and ADMET properties of protein-protein interaction inhibitors. 2017. 7(1): p. 46277.
[92]. Yan, A., Z. Wang, and Z.J.I.j.o.m.s. Cai, Prediction of human intestinal absorption by GA feature selection and support vector machine regression. 2008. 9(10): p. 1961-1976.
[93]. Van Breemen, R.B., Y.J.E.o.o.d.m. Li, and toxicology, Caco-2 cell permeability assays to measure drug absorption. 2005. 1(2): p. 175-185.
[94]. Keaney, J. and M.J.T.F.j. Campbell, The dynamic blood–brain barrier. 2015. 282(21): p. 4067-4079.
[95]. Hamadeh, A. and A.J.C.T. Edginton, Efficient large-scale mechanism-based computation of skin permeability. 2023: p. 100263.
[96]. Modi, S., et al., Integrated in silico approaches for the prediction of Ames test mutagenicity. 2012. 26(9): p. 1017-1033.

[97]. Kalyaanamoorthy, S. and K.H.J.M.r.r. Barakat, Development of safe drugs: the hERG challenge. 2018. 38(2): p. 525-555.
[98]. Moroy, G., et al., Toward in silico structure-based ADMET prediction in drug discovery. 2012. 17(1-2): p. 44-55.
[99]. Roussin, F. and N.J.A.P. Picard, La glycoprotéine P, une source d'interactions médicamenteuses. 2020. 59(601): p. 48-52.
[100]. Šestić, T.L., et al., In silico ADMET analysis of the A-, B-and D-modified androstane derivatives with potential anticancer effects. 2023. 189: p. 109147.
[101]. organization, A.c.c. and (ACCO), Childhood cancer rates worldwide statistics visited in 08/05/2023.

Appendices

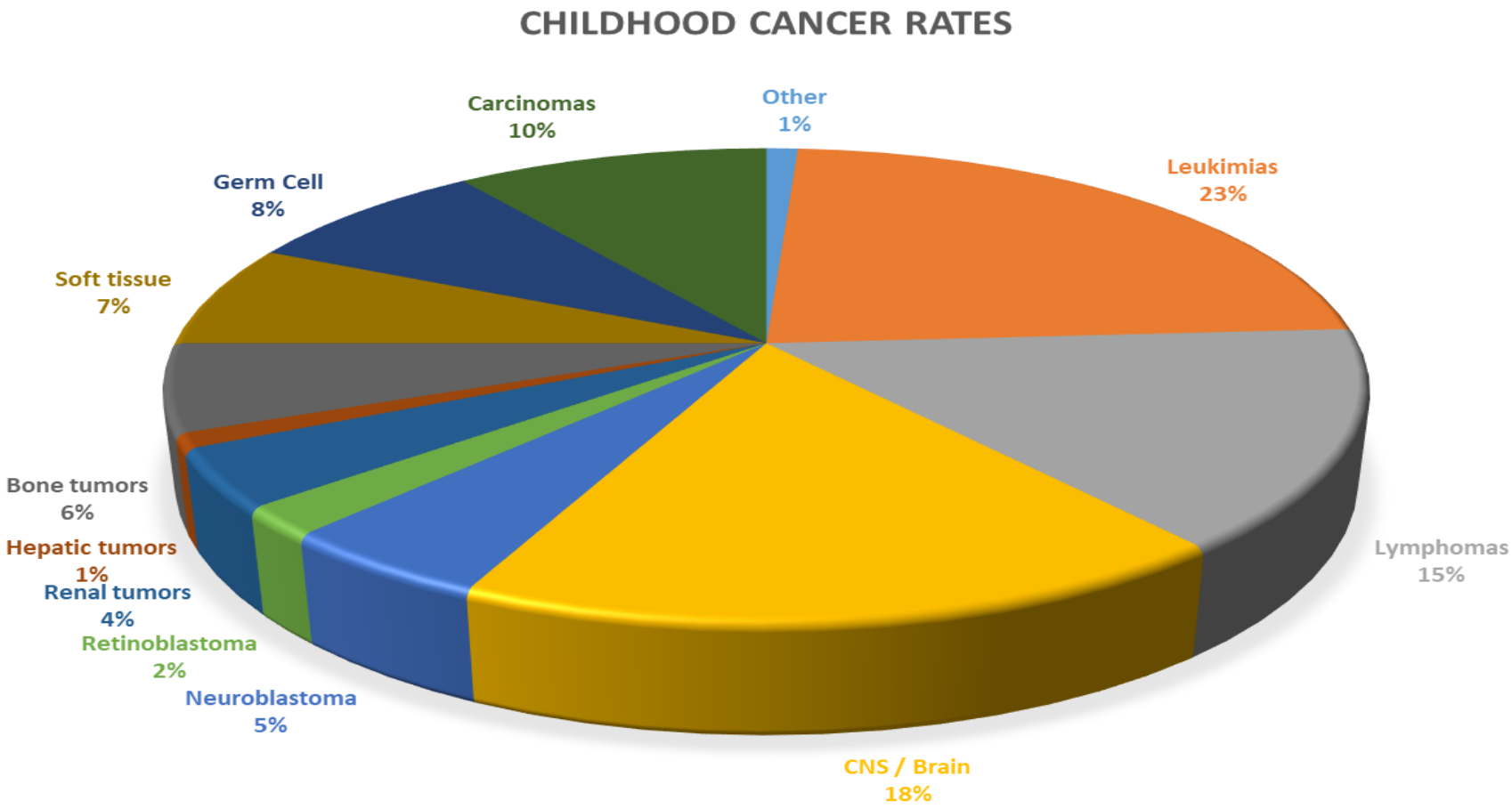

Appendix1. Childhood cancer rates worldwide statistics **[101]**.

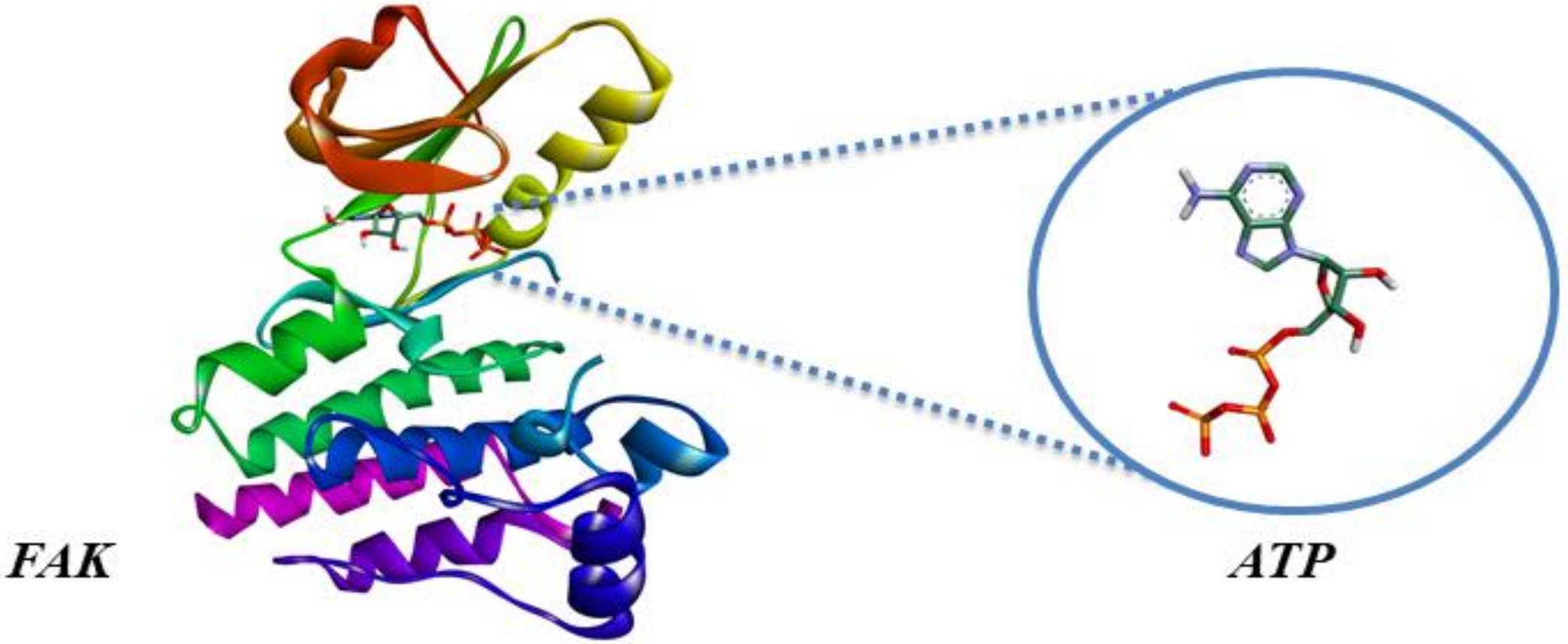

Appendix2. 3D structural representation of the FAK enzyme with its ligand ATP.

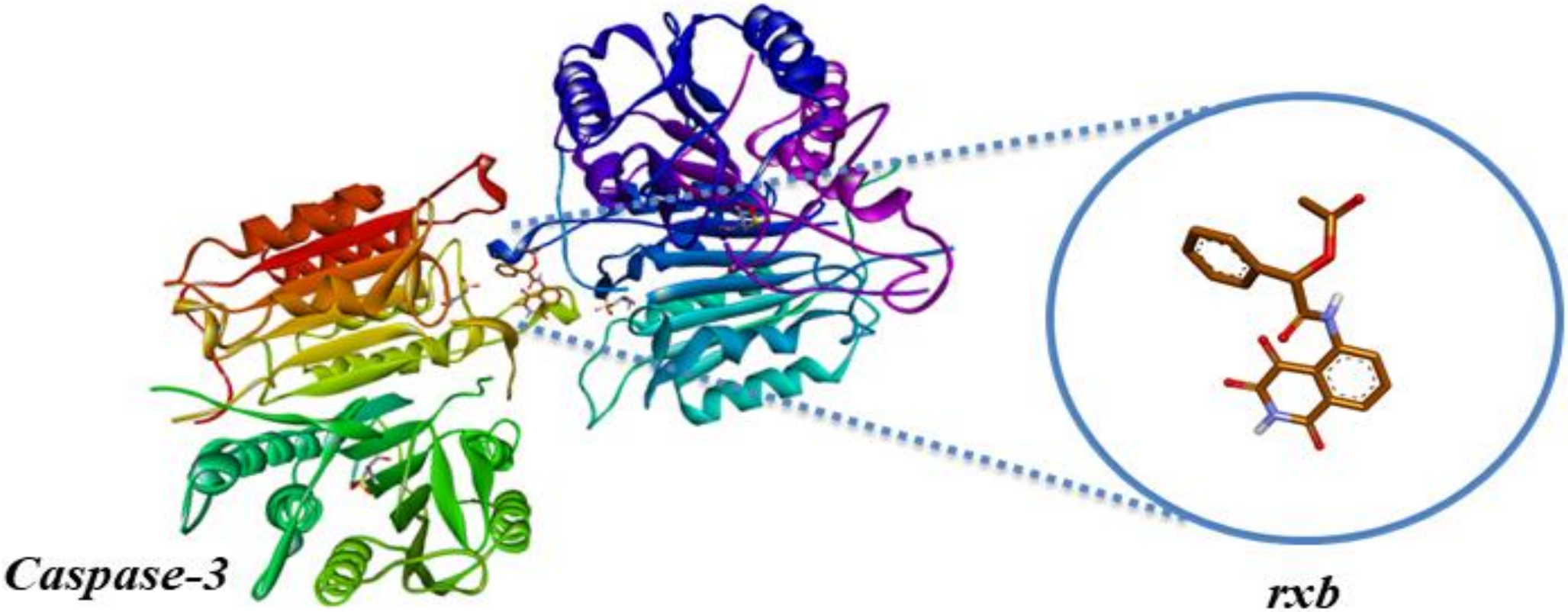

Appendix3. 3D structural representation of the Caspase-3 enzyme with its ligand rxb.

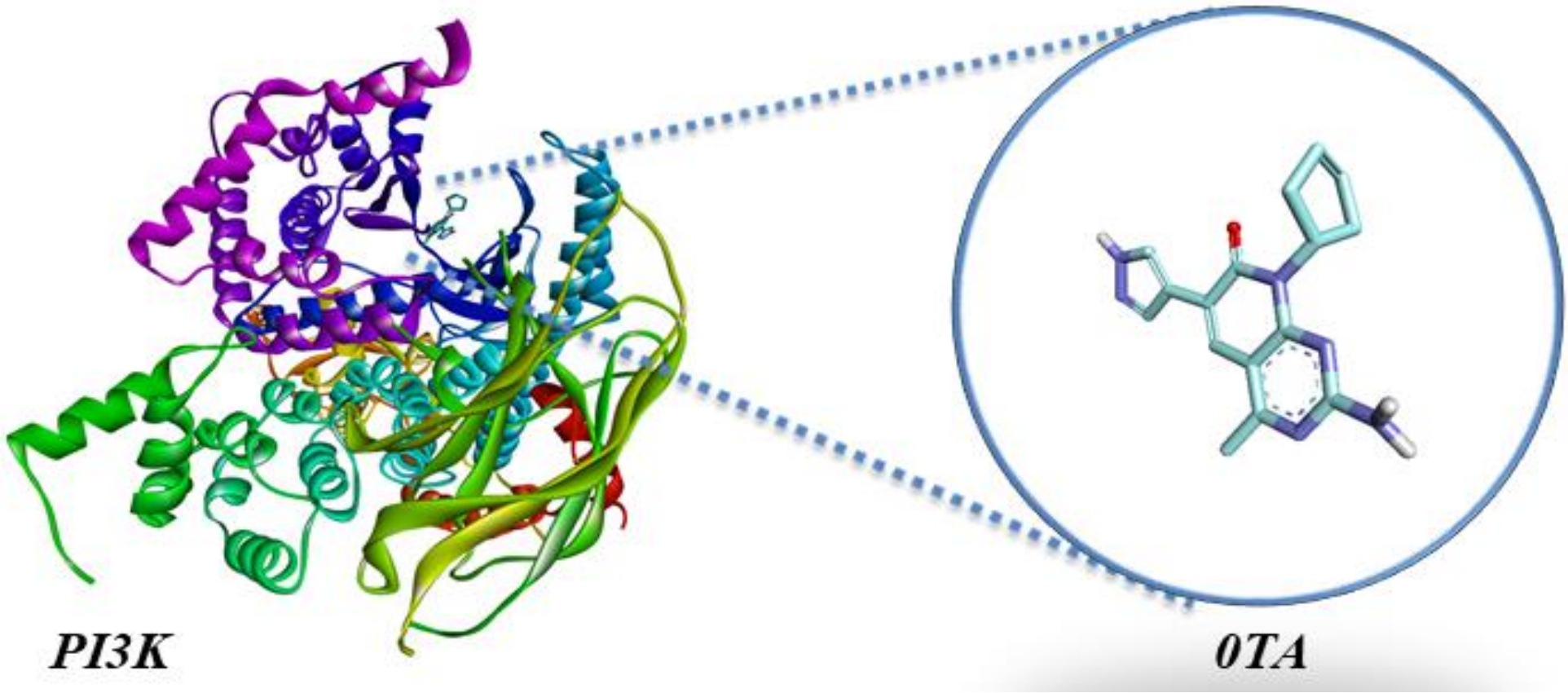

Appendix4. 3D structural representation of the PI3K enzyme with its ligand 0TA.

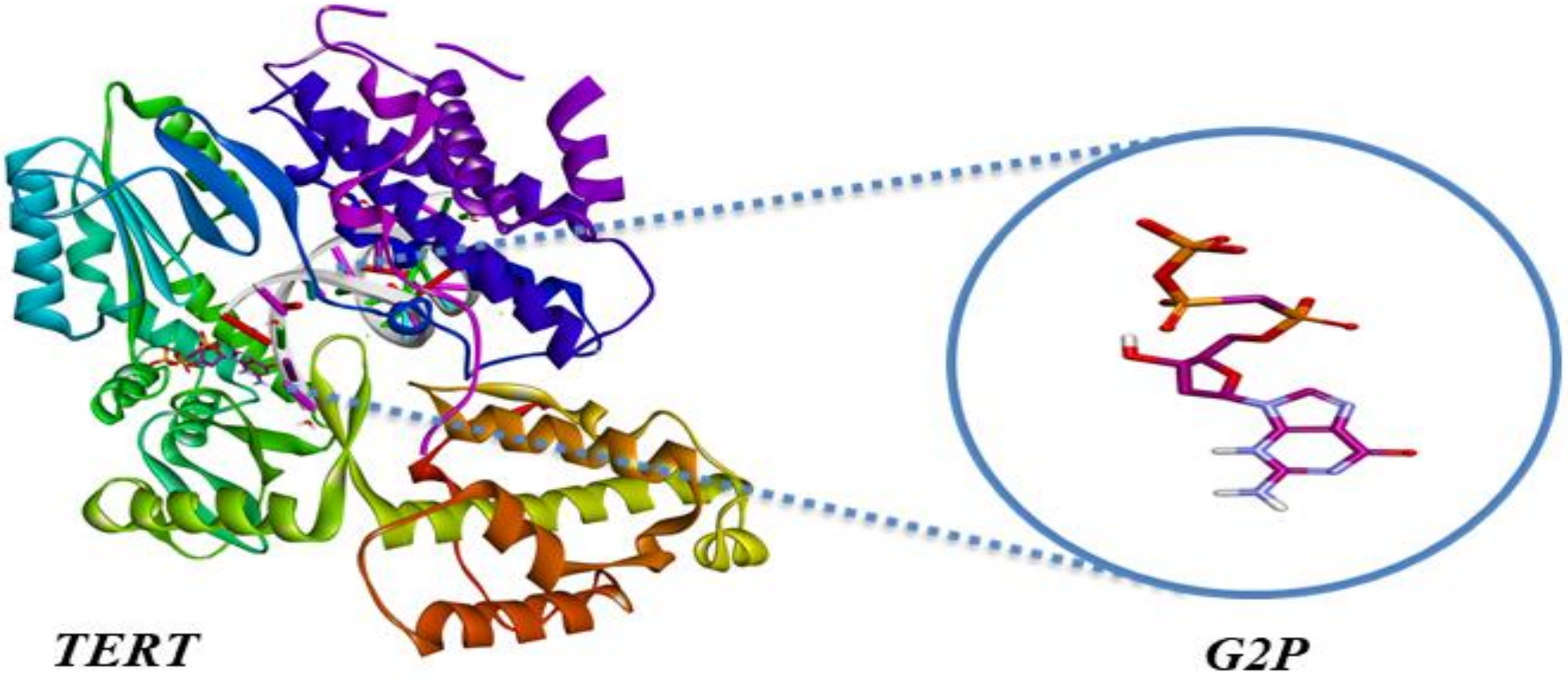

Appendix5. 3D structural representation of the TERT enzyme with its ligand G2P.

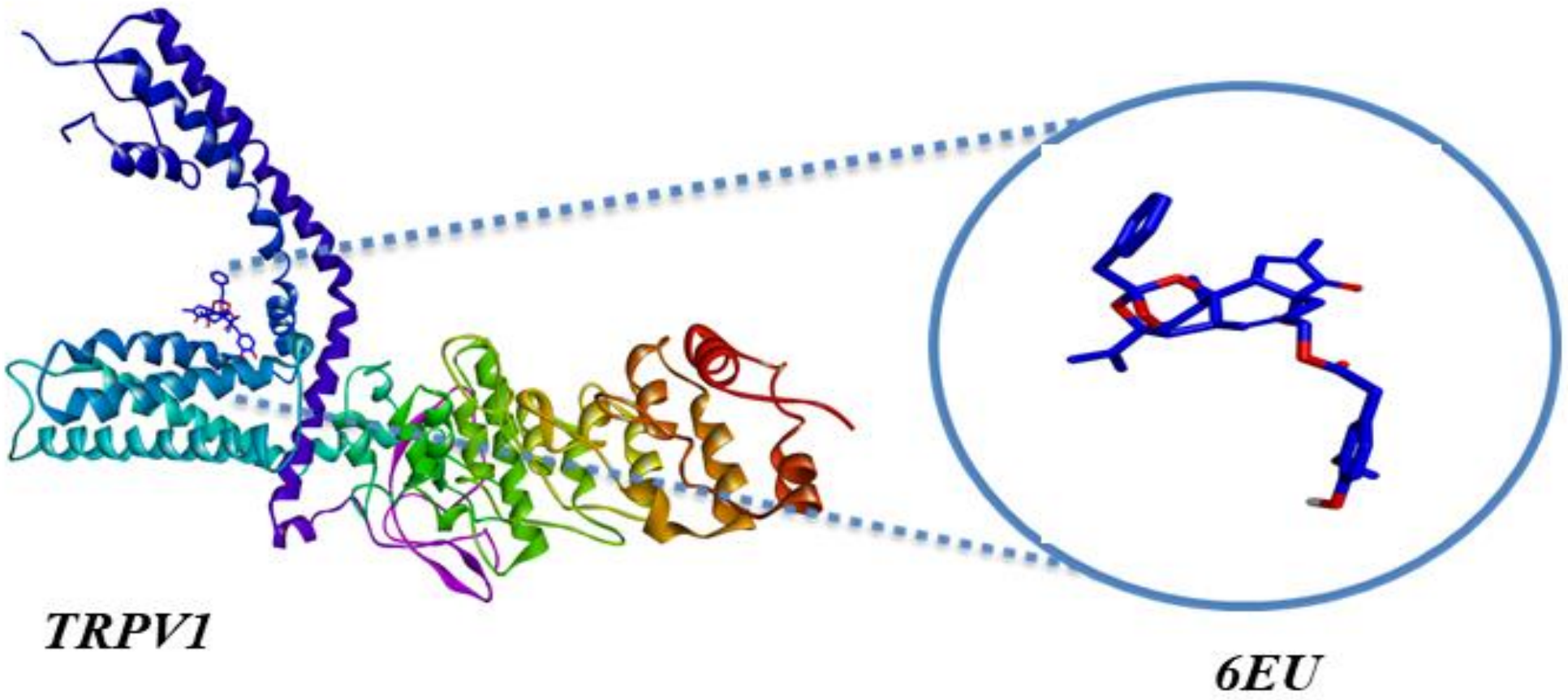

Appendix6. 3D structural representation of the TRPV1 enzyme with its ligand 6EU.

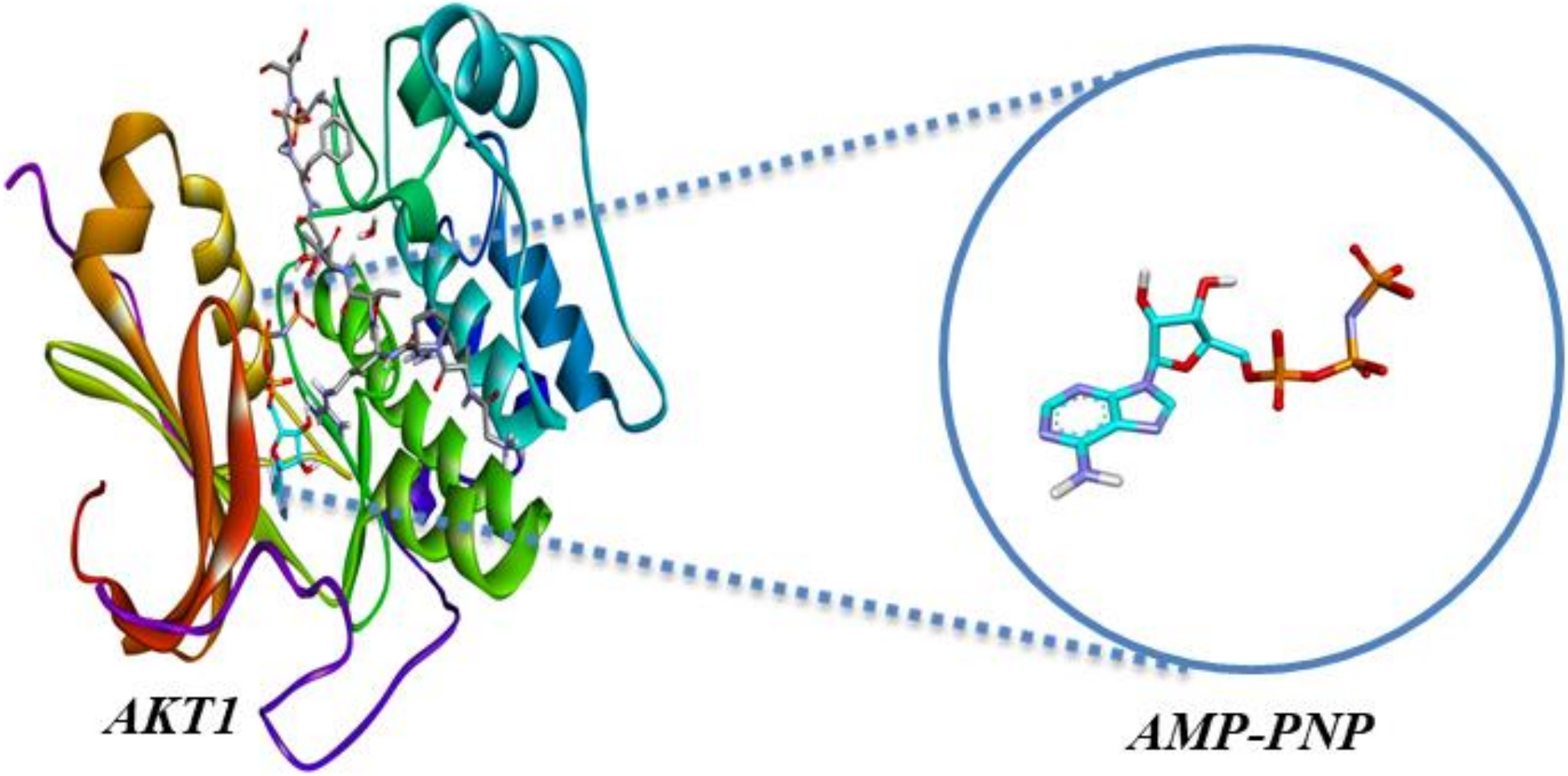

Appendix7. 3D structural representation of the AKT1 enzyme with its ligand AMP-PNP.

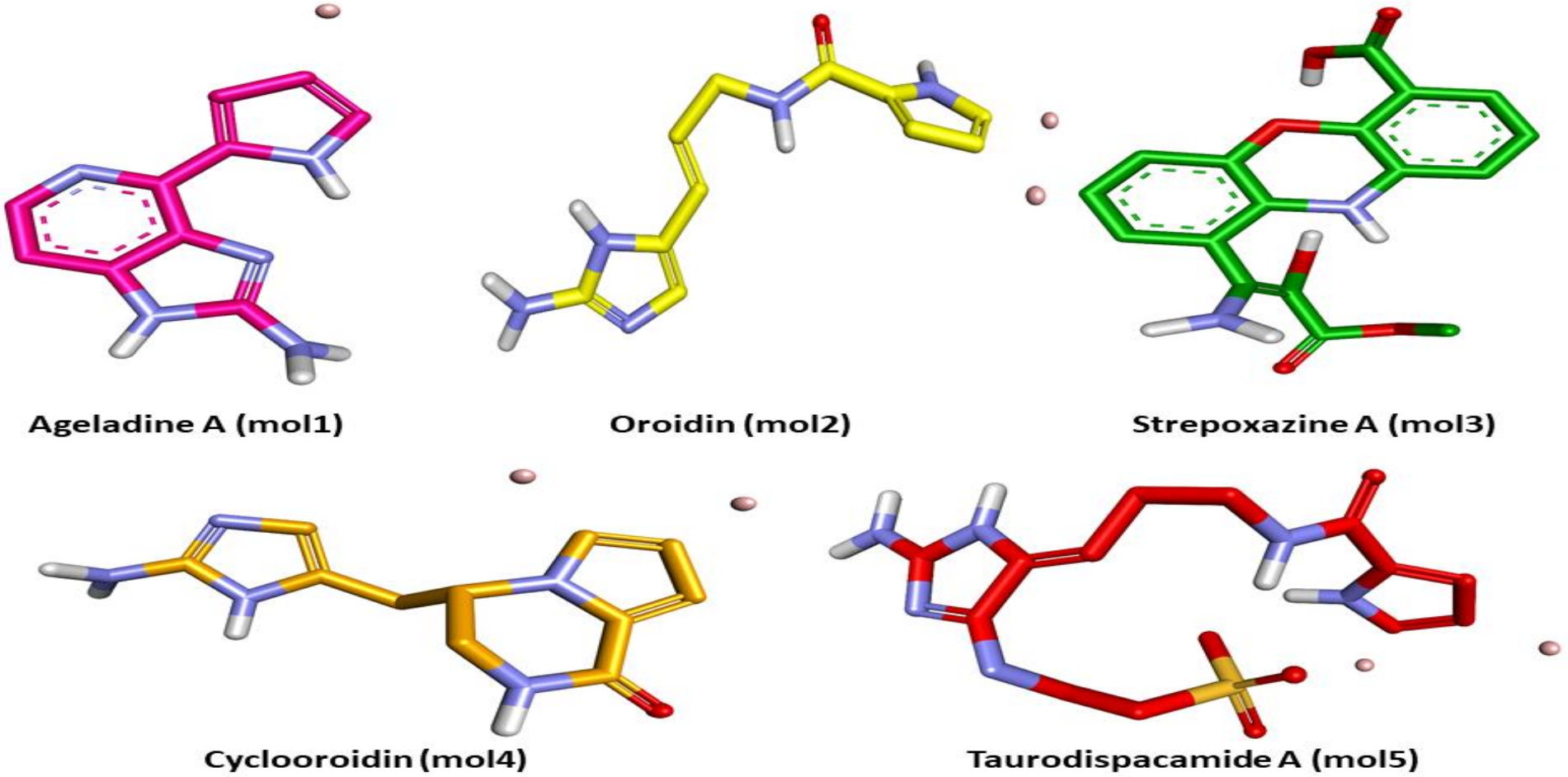

Appendix8. 3D structural representations of the five studied molecules.

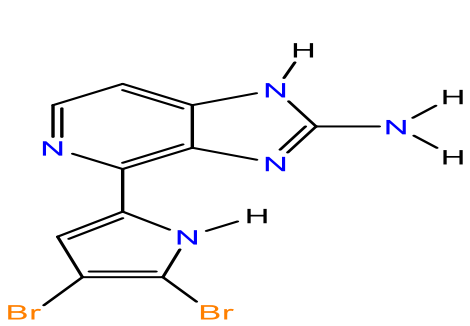

Ageladine A (mol1)

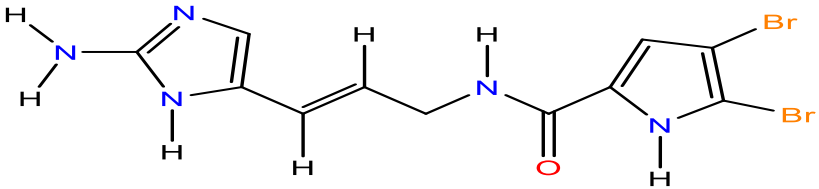

Oroidin (mol2)

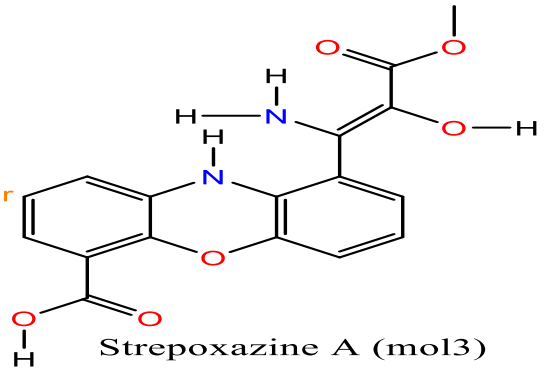

Strepoxazine A (mol3)

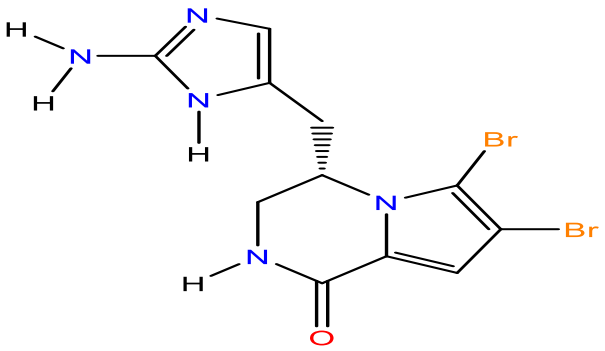

Cyclooroidin (mol4)

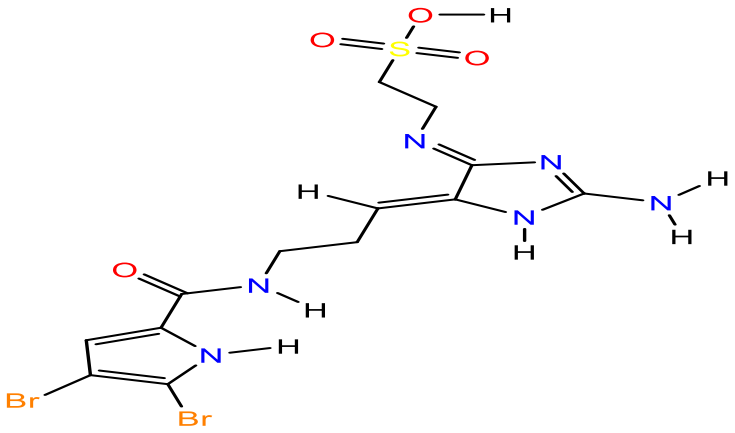

Taurodispacamide A (mol5)

.

Appendix9. 2D structural representations of the five studied ligands.

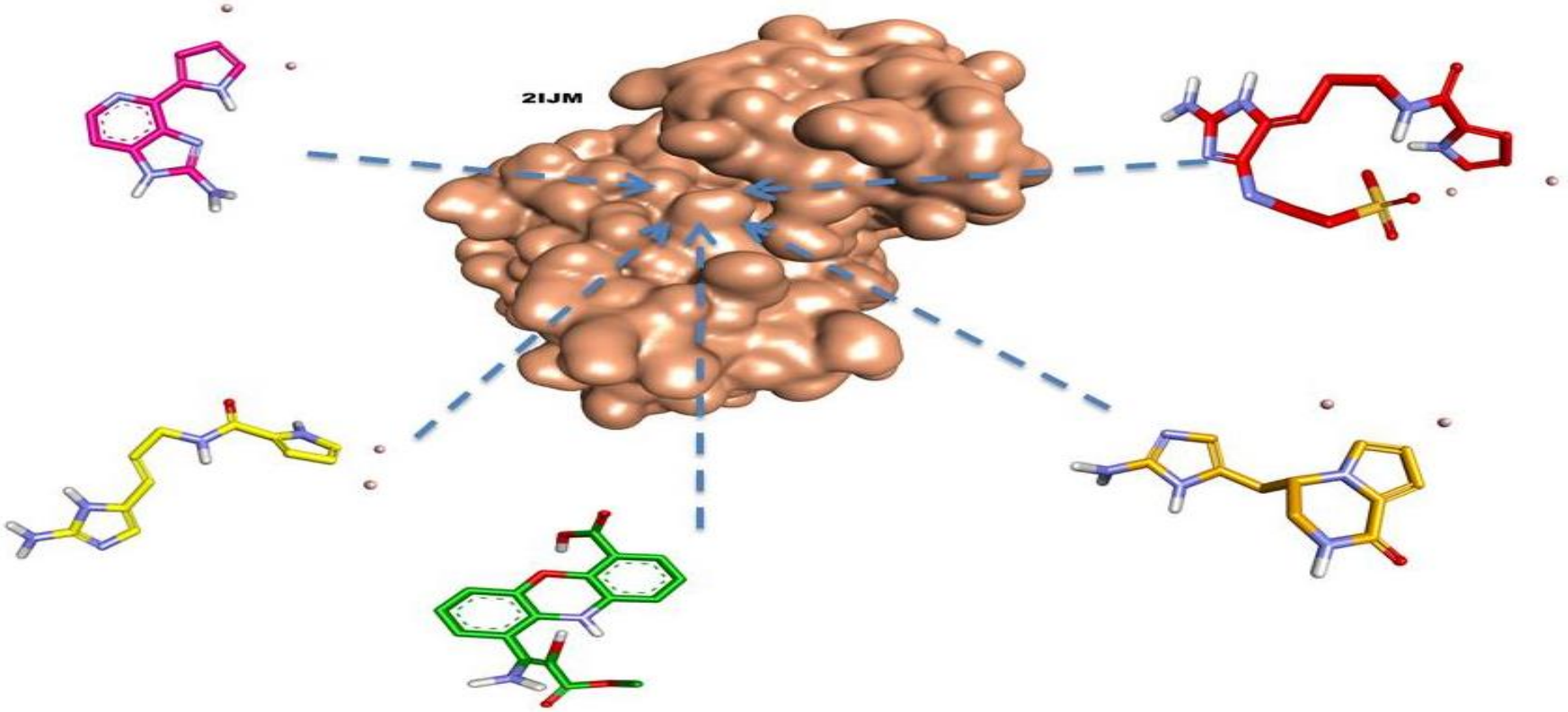

Appendix10. Representation of the enzyme 2IJM (FAK enzyme) and its active site with the 5 molecules.

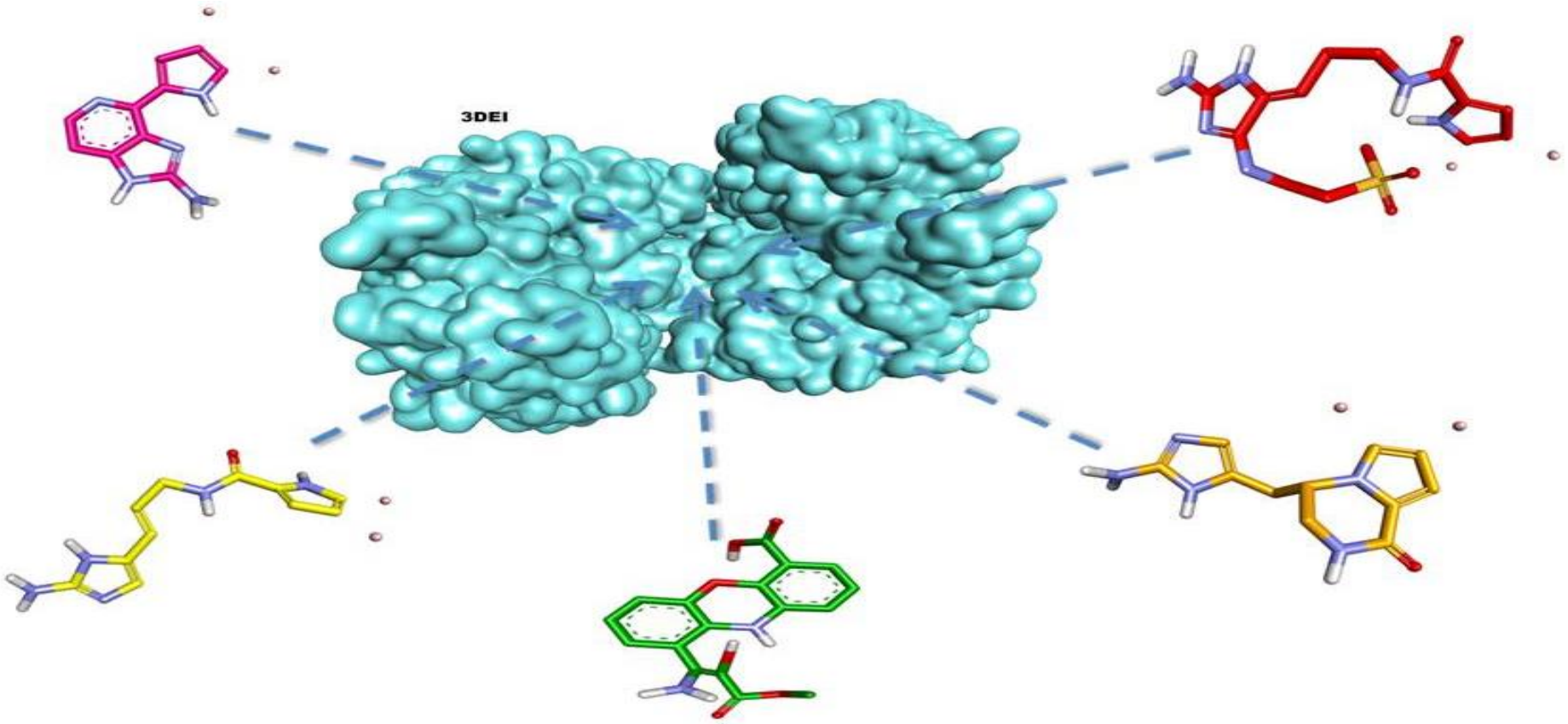

Appendix11. Representation of the enzyme 3DEI (Caspase-3 enzyme) and its active site with the 5 molecules.

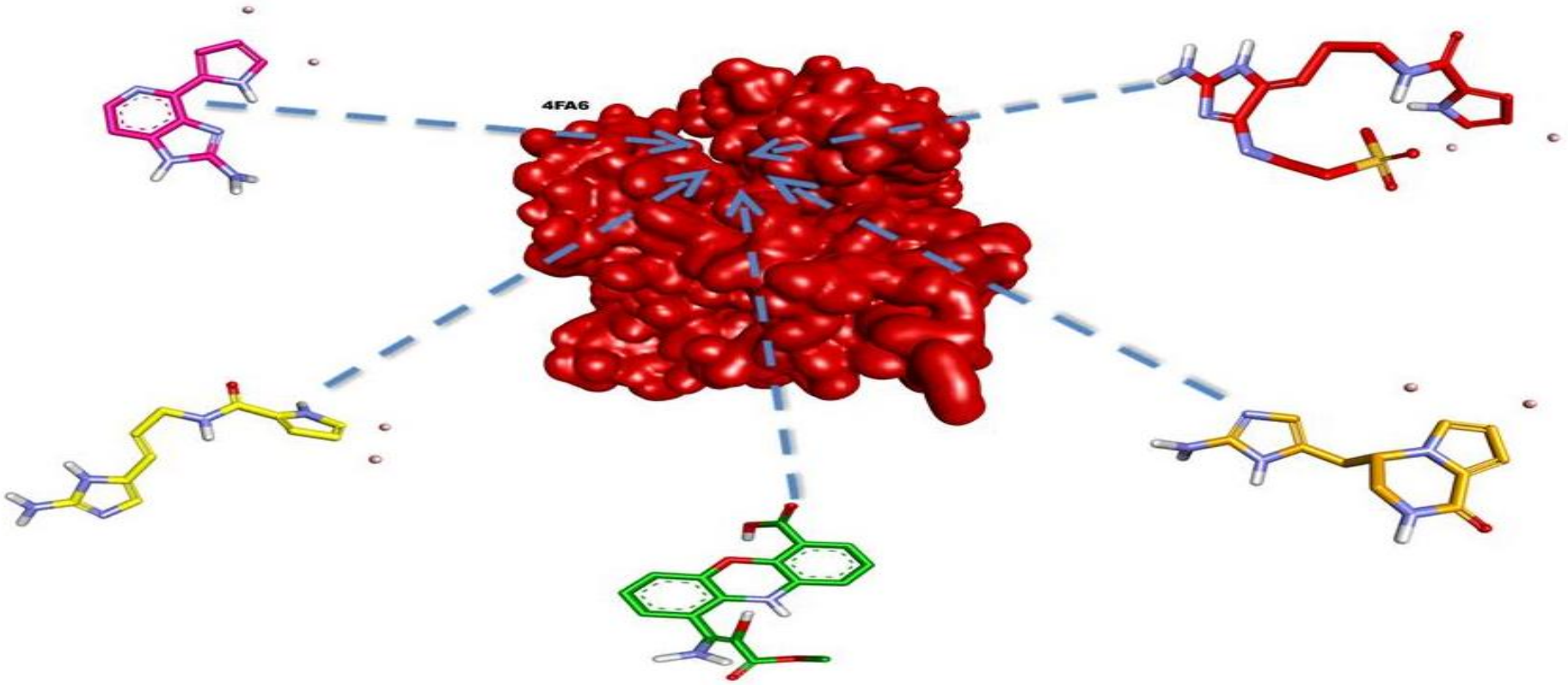

Appendix12. Representation of the enzyme 4FA6 (PI3K enzyme) and its active site with the 5 molecules.

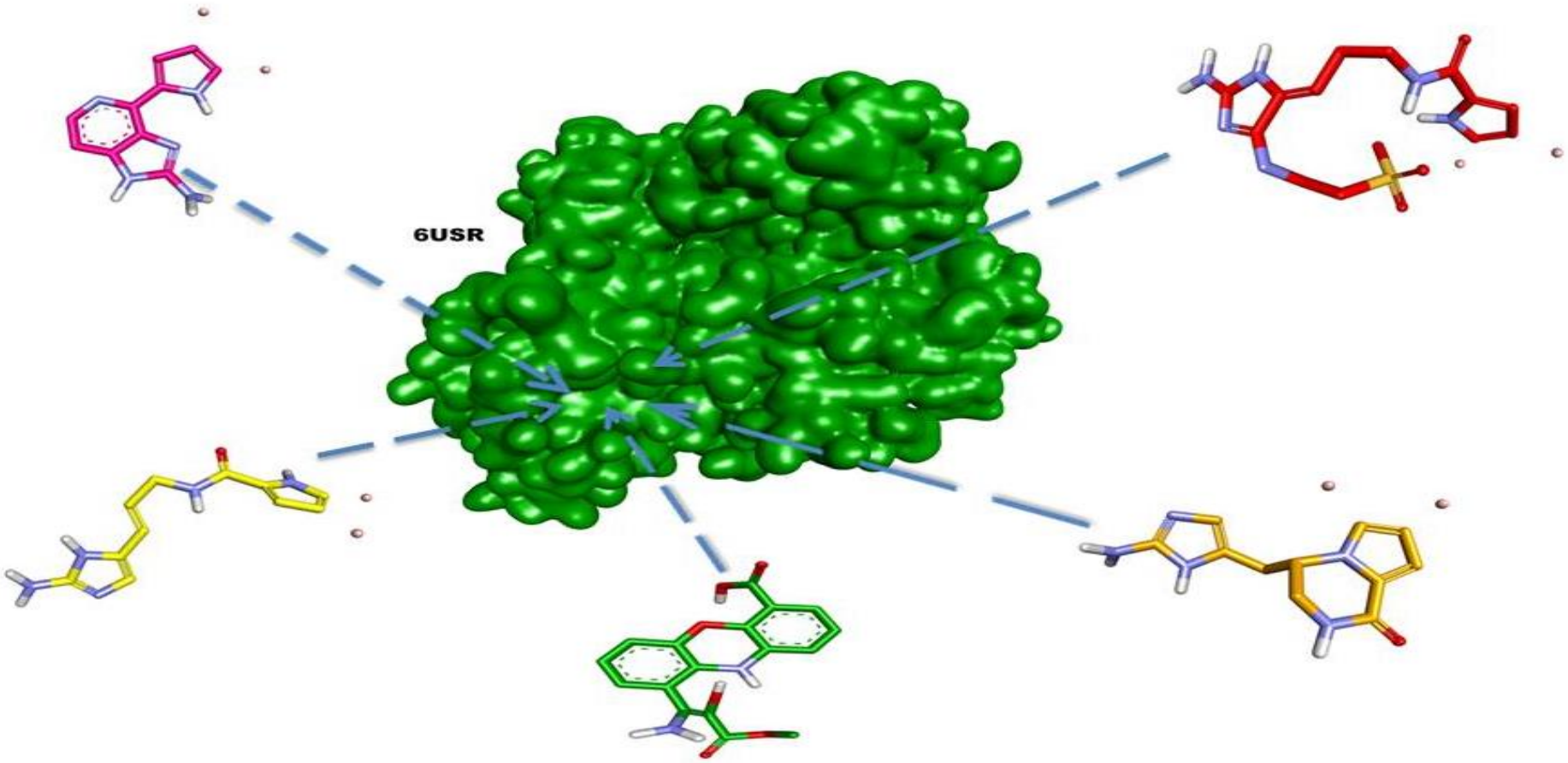

Appendix13. Representation of the enzyme 6USR (TERT enzyme) and its active site with the 5 molecules.

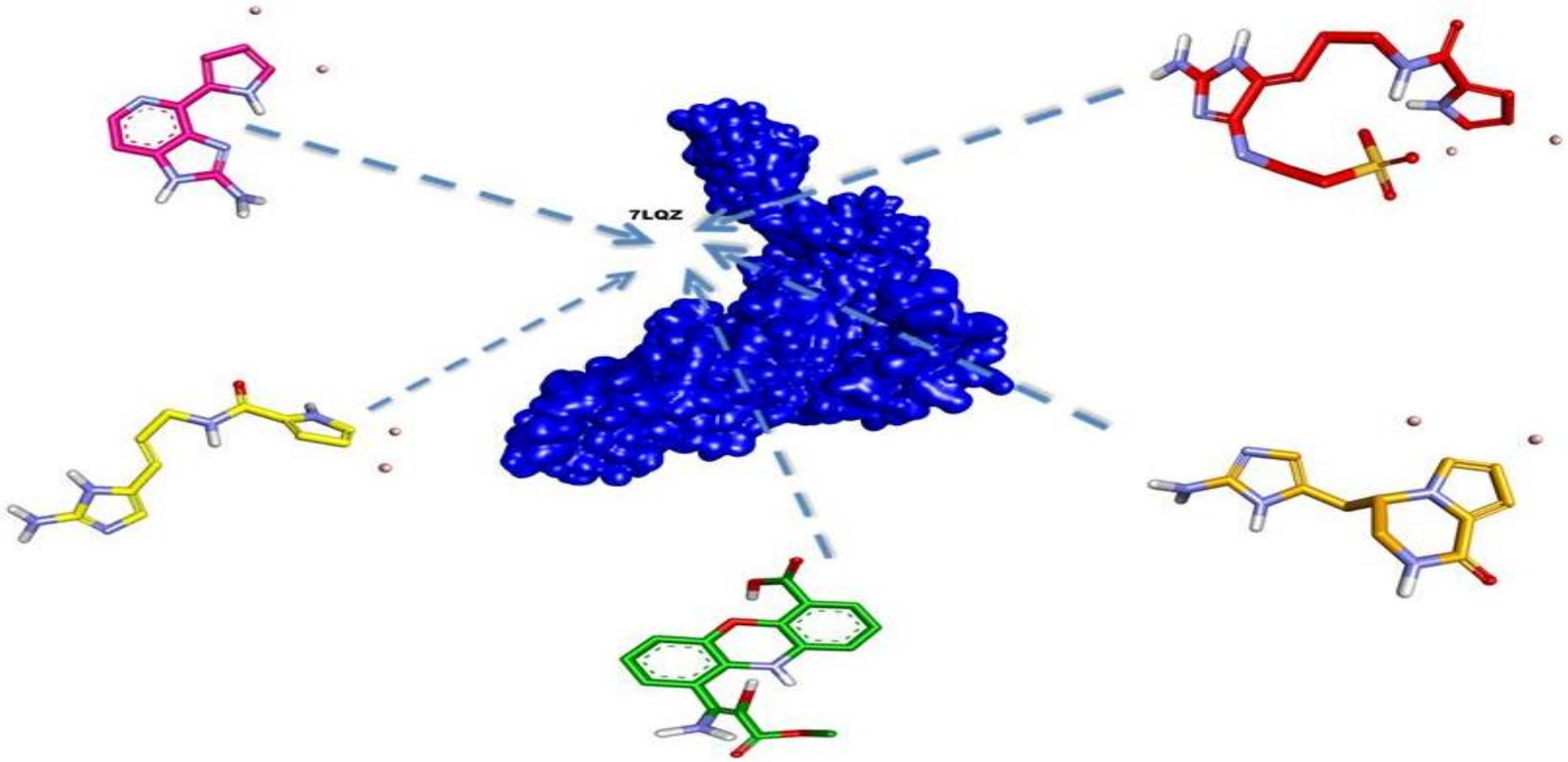

Appendix14. Representation of the enzyme 7LQZ (TRPV1 enzyme) and its active site with the 5 molecules.

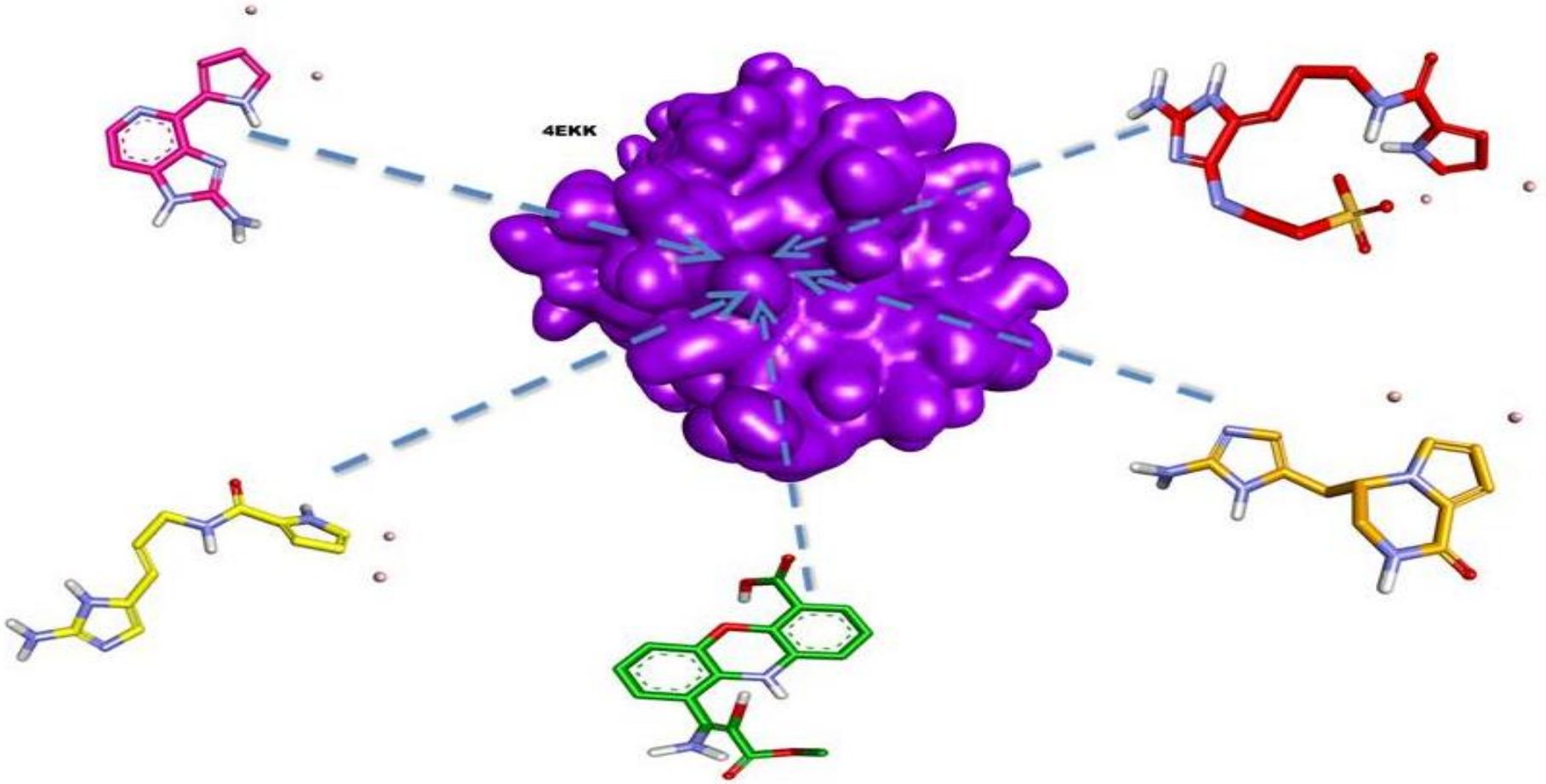

Appendix15. Representation of the enzyme 4EKK (AKT1 enzyme) and its active site with the 5 molecules.